

---

Electronic Thesis and Dissertation Repository

---

8-7-2019 10:00 AM

# Incorporation of Fluorine into Peptides and One-Bead One-Compound Libraries through Copper-free Click Chemistry for the Discovery of Radiopharmaceuticals

Emily M. Murrell, *The University of Western Ontario*

Supervisor: Luyt, Leonard G., *The University of Western Ontario*

A thesis submitted in partial fulfillment of the requirements for the Doctor of Philosophy degree in Chemistry

© Emily M. Murrell 2019

Follow this and additional works at: <https://ir.lib.uwo.ca/etd>

 Part of the [Medicinal-Pharmaceutical Chemistry Commons](#)

---

## Recommended Citation

Murrell, Emily M., "Incorporation of Fluorine into Peptides and One-Bead One-Compound Libraries through Copper-free Click Chemistry for the Discovery of Radiopharmaceuticals" (2019). *Electronic Thesis and Dissertation Repository*. 6351.  
<https://ir.lib.uwo.ca/etd/6351>

This Dissertation/Thesis is brought to you for free and open access by Scholarship@Western. It has been accepted for inclusion in Electronic Thesis and Dissertation Repository by an authorized administrator of Scholarship@Western. For more information, please contact [wlsadmin@uwo.ca](mailto:wlsadmin@uwo.ca).

## Abstract

Molecular imaging is making possible the understanding of intricate biological processes in real-time in both healthy and diseased tissues. The ability to non-invasively locate biomarkers of disease with good sensitivity and specificity affords the ability to provide accurate and early diagnoses, and patient stratification for therapy. The chemokine receptor CXCR4 is one biomarker of interest, as it is overexpressed in many cancers, yet has low expression elsewhere in normal physiology. This thesis will document a method of combinatorial chemistry to construct libraries of new potential peptide-based imaging agents for positron emission tomography (PET) imaging. It will also incorporate the study of strain-promoted alkyne-azide cycloaddition (SPAAC) as a type of copper-free click chemistry used as a method for radiofluorination of biological structures.

Chapter 2 discusses the synthesis of a library of N-terminal modified peptides created using a one-bead one-compound (OBOC) approach. Each peptide in the library contains a single fluorine atom incorporated through established SPAAC chemistry. The library of complete imaging agents was put through multiple stages of screening against CXCR4, resulting in the discovery of a peptide-based imaging agent with an  $IC_{50}$  of 138  $\mu$ M.

Chapter 3 discusses the development of a new  $^{18}F$ -labelled cyclooctyne-based prosthetic group for incorporation into azide-functionalized biological structures. This  $^{18}F$ -azadibenzocyclooctyne (ADIBO-F) was radiolabelled from its toluenesulfonate precursor in 21–35 % radiochemical yields, and subsequently incorporated into two cancer-targeting peptides through SPAAC chemistry. The result is two novel peptide-based PET imaging agents that possess high affinities for their targets, the growth hormone secretagogue receptor 1a (GHSR-1a) and gastrin-releasing peptide receptor (GRPR), with  $IC_{50}$  values of 9.7 and 0.50 nM, respectively.

Chapter 4 discusses the synthesis of an OBOC library with an imaging moiety integrated within the peptide structures. A two-pool OBOC strategy was developed to distribute the fluorine-containing amino acid throughout the peptide sequence during library synthesis. The ADIBO-F prosthetic group from Chapter 2 was employed for simple translation of peptide

hits into their radiofluorinated counterparts. An on-bead two-colour screen was performed in one step and resulted in the discovery of three CXCR4-specific peptide-based imaging agents with micromolar affinities of 28, 86 and 109  $\mu\text{M}$ .

## Keywords

Molecular Imaging, OBOC, Peptides, Fluorine-18, PET, Click Chemistry, CXCR4

## Co-Authorship Statement

Chapters 2 and 4 are manuscripts in preparation. Chapter 3 was adapted from a manuscript published in *ChemMedChem*, 2018, **13**, 1625–1628. All work and data analysis in all chapters was performed by Emily Murrell.

MALDI MS/MS was obtained by the facility manager at the UWO MALDI Mass Spectrometry Facility. HRMS was obtained by the facility manager at the Western Chemistry Mass Spectrometry facility. [<sup>18</sup>F]fluoride for these experiments was generously donated by Dr. Michael Kovacs at the Lawson Cyclotron & PET Radiochemistry Facility at St. Joseph's Hospital in London, Ontario, Canada.

The following reagents were obtained through the NIH AIDS Reagent Program, Division of AIDS, NIAID, NIH: U87.CD4.CXCR4, U87.CD4 from Dr. HongKui Deng and Dr. Dan R. Littman.

## Acknowledgments

A host of family and close friends are responsible for getting me through grad school relatively unscathed. I am so grateful to everyone for being curious about my research and making me feel so loved.

First, I want to thank my parents for instilling a love of science and math in me from a young age and encouraging me to always keep pushing and learning. They are both my strongest inspirations and greatest teachers; I would never have made it through so many years of school without their constant support, both emotionally and financially.

I am incredibly grateful to have had my sister Donna (and Brad) pave the path for me in academia. Her direction throughout life and many many years of school has been invaluable. Thank you for introducing me to the lab I've found home these past 5 years, and for always being excited to talk science and lament over grad school.

A special thank you to my best friends, Nicole and Andrew, for keeping me sane and well-fed through grad school. I know their constant distractions have come from a place of love.

I have been so lucky to work in a lab full of amazing colleagues. An enormous thank you to Mark Milne, William Turnbull and Marina Lazarakos, for being my constant sounding boards over the course of grad school. They have helped me learn, find, fix, and invent countless things; they have also definitely saved me from attempting futile experiments. Thank you to Carlie Charlton, Axie Hauser-Kawaguchi, Aagam Patel, Jordan LeSarge, and Geran Tu for being great lab friends.

I'd like to thank everyone involved in the Molecular Imaging Program. The program has expanded my horizons outside of chemistry, and I have been fortunate to be constantly exposed to so many bright minds in different fields.

Lastly, I am very thankful to my supervisor, Dr. Len Luyt, for providing me with the ability to explore so many aspects of research in the lab. He allowed me to spearhead all my own projects and explore multiple collaborations which introduced me to all sorts of new techniques I had never dreamed of learning. I'll be forever grateful for the opportunities he has given me to share my research around the world, and all the people I've been able to meet as a result.

# Table of Contents

Abstract.....	i
Co-Authorship Statement.....	iii
Acknowledgments.....	iv
Table of Contents.....	v
List of Tables.....	ix
List of Figures.....	x
List of Schemes.....	xiv
List of Abbreviations.....	xv
Chapter 1.....	1
1 Introduction.....	1
1.1 Molecular Imaging.....	1
1.2 PET and Fluorine-18.....	2
1.3 Click Chemistry.....	4
1.4 Strain-Promoted Click Chemistry.....	5
1.5 Peptides as Targeting Moieties.....	7
1.6 One-Bead One-Compound Libraries.....	8
1.7 Matrix-Assisted Laser Desorption/Ionization Mass Spectrometry.....	11
1.8 G Protein-Coupled Receptors as Biological Targets.....	14
1.9 C-X-C Chemokine Receptor 4.....	14
1.10 Summary.....	16
1.11 References.....	17
Chapter 2.....	24
2 Incorporation of Fluorine into an OBOC Peptide Library by Copper-free Click Chemistry towards the Discovery of PET Imaging Agents.....	24
2.1 Introduction.....	24

2.2	Results and Discussion .....	25
2.2.1	Design and Synthesis .....	25
2.2.2	Library Screening and Sorting .....	26
2.2.3	MALDI MS/MS Deconvolution of Hit Peptide Sequences.....	28
2.2.4	Hit Peptide Synthesis and Validation of Target Specificity .....	29
2.2.5	Hit Peptide Synthesis and Validation of Target Affinity .....	30
2.3	Conclusions.....	31
2.4	Experimental.....	31
2.4.1	General Experimental .....	31
2.4.2	Small Molecule Synthesis.....	32
2.4.3	OBOC Library Synthesis .....	35
2.4.4	Hit Peptide Synthesis .....	35
2.4.5	Cell Culture.....	37
2.4.6	Library Screening.....	37
2.4.7	MALDI MS/MS.....	39
2.4.8	Selectivity Analysis Assay.....	39
2.4.9	Competitive Binding Assays.....	40
2.5	References.....	41
Chapter 3.....		43
3	A Compact and Synthetically Accessible Fluorine-18 Labelled Cyclooctyne Prosthetic Group for Labelling of Biomolecules by Copper-free Click Chemistry.....	43
3.1	Introduction.....	43
3.2	Results and Discussion .....	45
3.2.1	Synthesis of ADIBO-F.....	45
3.2.2	Radiolabelling of a [ <sup>18</sup> F]ADIBO-F Prosthetic Group.....	47
3.2.3	Copper-Free Click Radiolabelling of Model Peptides using [ <sup>18</sup> F]ADIBO-F .....	47

3.3	Conclusions.....	50
3.4	Experimental.....	51
3.4.1	General Experimental.....	51
3.4.2	Small Molecule Synthesis.....	52
3.4.3	Peptide Synthesis.....	57
3.4.4	Radiochemistry.....	61
3.4.5	<i>In Vitro</i> Competitive Binding Assays.....	63
3.5	References.....	64
Chapter 4.....		67
4	Synthesis and Screening of a Combinatorial Library of Fluorine-Integrated Peptides for PET Imaging Agent Discovery.....	67
4.1	Introduction.....	67
4.2	Results and Discussion.....	69
4.2.1	Library Design.....	69
4.2.2	Library Synthesis.....	73
4.2.3	On-Bead Two-Colour Screen.....	74
4.2.4	MALDI MS/MS <i>De Novo</i> Sequencing of Hits.....	75
4.2.5	CXCR4 Affinity Determination of Hit Peptides.....	78
4.3	Conclusions.....	79
4.4	Experimental.....	80
4.4.1	General Experimental.....	80
4.4.2	OBOC Library Synthesis.....	80
4.4.3	Cell Culture.....	81
4.4.4	On-Bead Two-Colour Fluorescent Screening.....	82
4.4.5	Photocleavage and MALDI MS/MS.....	82
4.4.6	Hit Peptide Synthesis and Characterization.....	86



4.4.7 Radioligand Competitive Binding Assays .....	89
4.5 References .....	90
Chapter 5 .....	93
5 Conclusions .....	93
5.1 Summary and Outlook .....	93
5.2 References .....	97
Chapter 6 .....	99
6 Appendix – Additional Data for Chapter 4 .....	99
6.1 HPLC Traces for Hit Peptides .....	99
6.2 IC <sub>50</sub> Curves for Hit Peptides .....	103
6.3 MALDI MS/MS Deconvolution for Hit Peptides .....	106
Curriculum Vitae .....	113

## List of Tables

Table 2.1 Sample list of select peptide sequences resynthesized for <i>in vitro</i> validation. All are coupled to 2.3 on the N-terminal and are amidated on the C-terminal. ....	36
Table 3.1 Characterization of the <sup>18</sup> F-labelled ghrelin and bombesin peptides. ....	50
Table 4.1 Sequences and IC <sub>50</sub> values of hit peptide structures as determined by <i>de novo</i> MS/MS sequencing. Where X = lysine(cyclooctatriazole-F). Peptides have a free N-terminus and an amidated C-terminus. ....	76

## List of Figures

Figure 1.1 Design of a targeted molecular imaging agent.....	2
Figure 1.2 Representative examples of common $^{18}\text{F}$ prosthetic groups for straightforward labelling of biomolecules.....	4
Figure 1.3 Mechanism of the strain-promoted alkyne-azide cycloaddition reaction.....	5
Figure 1.4 Structures of common cyclooctynes used in SPAAC chemistry.....	6
Figure 1.5 Regioisomers produced by SPAAC of ADIBOs.....	6
Figure 1.6 A variety of $^{18}\text{F}$ prosthetic groups used in SPAAC radiochemistry. <sup>27</sup> .....	7
Figure 1.7 Scheme depicting the basic steps of Fmoc-based solid-phase peptide synthesis on an amine-functionalized resin. ....	8
Figure 1.8 Two cycles of split-and-mix in forming an OBOC library using amino acids A, C, D, E, and F. ....	10
Figure 1.9 A general hexamer peptide structure showing common fragmentation locations and examples of the fragments that are produced.....	13
Figure 1.10 CXCR4-targeting ligands with high affinities A) peptide T140 B) cyclic peptide FC131 C) AMD3100. ....	15
Figure 2.1 MALDI MS/MS deconvolution of a peptide hit from library screen; showing overlapping <i>b</i> and <i>y</i> series of fragments and demonstrating high fragmentation at $b_0$ . The isobaric amino acids lysine (K) and glutamine (Q) are both possibilities for mass fragments of ~ 128 Da. ....	28
Figure 2.2 On-bead screen of potential hits synthesized on Tentagel of the sequence F-PEG <sub>2</sub> -ADIBO-YXFXRLWP-NH <sub>2</sub> where X = Q or K. This screen allows for confirmation of 'hit' sequence when isobaric amino acids are involved and also screens for selectivity to the target. ....	30

Figure 2.3 Sample HPLC chromatogram (UV trace, 25-85% ACN/H <sub>2</sub> O with 0.1% TFA) of a purified peptide F-PEG <sub>2</sub> -ADIBO-YKFKRLWP-NH <sub>2</sub> .....	37
Figure 2.4 Screenshots of COPAS software showing A) gating selection for bead-sized objects based on size (TOF) and optical density (Ext); B) sorting selection for initial screen based on bead size and above-average green fluorescence ( $\lambda_{em} = 510\pm 23$ nm); C) sorting selection for second round with higher threshold of green fluorescence.....	38
Figure 2.5 Confocal fluorescence images of A) library pool after incubation with U87.CD4.CXCR4 cells tagged with CellTracker Green CMFDA; B) library beads after initial screen showing some hit beads with various degrees of cell coverage; C) isolated hit library bead in a well of a 96 well plate after second sorting round; D) isolated false positive bead displaying high autofluorescence. ....	39
Figure 2.6 Uncropped Images of Figure 2.2 to further display selectivity. ....	40
Figure 3.1 Structures of A) non-labelled ADIBOs where R contains an acid or amine for conjugation to a biomolecule, B) ADIBOs that have been indirectly labelled with fluorine-18 and C) ADIBOs that have been further derivatized into fluorine-18 prosthetic groups. ....	44
Figure 3.2 Overlaid analytical C18 RP-HPLC chromatograms at 25 to 80% (ACN/H <sub>2</sub> O, 0.1% TFA) over 15 minutes of purified peptide [ <sup>18</sup> F]3.12 (solid trace, radio-chromatogram) and its non-radioactive [ <sup>19</sup> F]3.12 analogue (dashed trace, UV chromatogram, $\lambda = 220$ nm). ....	49
Figure 3.3 Analytical UV chromatogram from RP-HPLC of purified 3.11 (25-80% ACN/H <sub>2</sub> O, 0.1% TFA, 10 minutes, RT = 8.69 min). ....	58
Figure 3.4 Analytical UV chromatogram from RP-HPLC of purified (D-Phe <sup>6</sup> , $\beta$ -Ala <sup>11</sup> ,Phe <sup>13</sup> ,Nle <sup>14</sup> )-Bombesin(6-14)-PEG <sub>8</sub> (N <sub>3</sub> ) (30-85% ACN/H <sub>2</sub> O, 0.1% TFA, 10 minutes, RT = 9.30 min).....	58
Figure 3.5 Analytical UV chromatogram from RP-HPLC of purified [ <sup>19</sup> F]3.12 (25-80% ACN/H <sub>2</sub> O, 0.1% TFA, 10 minutes, RT = 9.15 min). ....	59

Figure 3.6 Analytical UV chromatogram from RP-HPLC of purified (D-Phe <sup>6</sup> ,β-Ala <sup>11</sup> ,Phe <sup>13</sup> ,Nle <sup>14</sup> )-Bombesin(6-14)-PEG <sub>8</sub> (triazole-ADIBO-F) (35-80% ACN/H <sub>2</sub> O, 0.1% TFA, 10 minutes, RT = 9.22 min). .....	60
Figure 3.7 Overlaid analytical RP-HPLC UV chromatogram at 220 nm of [ <sup>19</sup> F]3.10 (dashed) and radio-chromatogram of [ <sup>18</sup> F]3.10 (solid) (50% ACN/H <sub>2</sub> O 0.1% TFA). .....	61
Figure 3.8 Overlaid analytical RP-HPLC UV chromatogram at 220 nm of standard (D-Phe <sup>6</sup> ,β-Ala <sup>11</sup> ,Phe <sup>13</sup> ,Nle <sup>14</sup> )-Bombesin(6-14)-PEG <sub>8</sub> (triazole-ADIBO-F) (dashed) and radio-chromatogram of [ <sup>18</sup> F](D-Phe <sup>6</sup> ,β-Ala <sup>11</sup> ,Phe <sup>13</sup> ,Nle <sup>14</sup> )-Bombesin(6-14)-PEG <sub>8</sub> (triazole-ADIBO-F) (solid) (25 to 80% ACN/H <sub>2</sub> O, 0.1% TFA). .....	62
Figure 3.9 Binding curve for the competitive binding assay of [ <sup>19</sup> F]3.12 in HEK293-GHSR-1a cells. The IC <sub>50</sub> value determined was 9.7 nM. ....	64
Figure 3.10 Binding curves for the competitive binding assay of standard (D-Phe <sup>6</sup> ,β-Ala <sup>11</sup> ,Phe <sup>13</sup> ,Nle <sup>14</sup> )-bombesin(6-14) (red), and of (D-Phe <sup>6</sup> ,β-Ala <sup>11</sup> ,Phe <sup>13</sup> ,Nle <sup>14</sup> )-bombesin(6-14)PEG <sub>8</sub> (triazole-ADIBO-F) (black) with PC3 cells. The IC <sub>50</sub> values determined were 0.70 and 0.50 nM, respectively. ....	64
Figure 4.1 Incorporation of an <sup>18/19</sup> F-ADIBO-F into a lysine-azide residue in a peptide.....	70
Figure 4.2 Synthesis cascade showing two-pool split-and-mix SPPS steps to incorporate a lysine-azide into a library of octapeptides in single random position. This allows a fluorine-containing cyclooctyne (ADIBO-F) to be globally clicked to the library to produce a library of on-bead imaging agents. ....	72
Figure 4.3 Sample MS and MS/MS spectra demonstrating presence of an ion fragment resulting from loss of 61 Da from the parent peptide <i>m/z</i> to confirm inclusion of imaging component cyclooctatriazole-F. ....	74
Figure 4.4 Representative confocal fluorescence microscopy images of library Tentagel beads during two-colour screening depicting A) bulk beads B) isolated beads showing affinity for CXCR4 C) individual bead showing specificity to CXCR4. ....	75

Figure 4.5 MALDI MS/MS deconvolution of hit peptide imaging agent 4.3 showing a full <i>y</i> series of ions and some <i>b</i> series ions. ....	76
Figure 4.6 MALDI MS/MS showing insufficient fragmentation to deconvolute entire peptide sequence when the Lys(cyclooctatriazole) residue is centered in the peptide sequence. ....	78
Figure 4.7 Sample <i>de novo</i> sequencing of a random library peptide of 1177 Da showing almost complete coverage of <i>b</i> and <i>y</i> ion series.....	83
Figure 4.8 MALDI mass spectra for hit peptides demonstrating A) MS with no ions present in the mass range of interest for our library, B) MS with multiple ion peaks, and C) MS with a single parent ion present (and its sodium adduct).....	85

## List of Schemes

Scheme 2.1 Synthesis of an octamer library on Tentagel resin using ADIBO-COOH 2.1 and a PEG-based azide-containing fluoride 2.2. X is any natural amino acid excluding cysteine, methionine, and isoleucine.....	26
Scheme 2.2 Scheme for synthesis of 2.2.....	33
Scheme 3.1 Branching synthesis of both ADIBO-OTs 3.8 and [ <sup>19</sup> F]ADIBO-F 3.10 standard via modifications to the Popik synthesis <sup>22-23</sup> of ADIBOs.....	46
Scheme 3.2 Radiosynthesis of [ <sup>18</sup> F]ADIBO-F [ <sup>18</sup> F]3.10.....	47
Scheme 3.3 Strain-promoted alkyne-azide cycloaddition of [ <sup>18</sup> F]ADIBO-F prosthetic group [ <sup>18</sup> F]3.10 with an azide-modified ghrelin peptide 3.11. Only one regioisomer of [ <sup>18</sup> F]3.12 is shown for simplicity. ....	48

## List of Abbreviations

$\beta^+$	positron
$\delta$	chemical shift
$\lambda_{\text{ex}}$	wavelength of excitation
$\lambda_{\text{em}}$	wavelength of emission
$\mu\text{L}$	microlitre
$\mu\text{M}$	micromolar
$\mu\text{mol}$	micromole
ACN	acetonitrile
ADIBO	azadibenzocyclooctyne
Alloc	allyloxycarbonyl
ANP	3-amino-3-(2-nitro-phenyl)propionic acid
AU	arbitrary units
AUC	area under the curve
BARAC	biarylazacyclooctyne
BCN	bicyclononyne
BSA	bovine serum albumin
CD4	cluster of differentiation 4
CHCA	$\alpha$ -cyano-4-hydroxycinnamic acid
CI	chemical ionization
CMFDA	5-chloromethylfluorescein diacetate
CMPX	4-({[4-(chloromethyl)phenyl]carbonyl}amino)-2-(1,2,2,4,8,10,10,11-octamethyl-10,11-dihydro-2 <i>H</i> -pyrano[3,2- <i>g</i> :5,6- <i>g'</i> ]diquinolin-1-ium-6-yl)benzoate
COPAS	complex object parametric analyzer and sorter
cpm	counts per minute
CT	computed tomography
CuAAC	copper(I)-catalyzed alkyne-azide cycloaddition
CXCL12	C-X-C motif chemokine 12
CXCR4	C-X-C chemokine receptor 4
d	doublet
Da	Dalton
DCM	dichloromethane
dd	doublet of doublets
ddd	doublet of doublet of doublets
DFS	double-focusing sector
DIFO	difluorinated cyclooctyne
DIPEA	<i>N,N</i> -diisopropylethylamine
DMEM	Dulbecco's modified Eagle's medium
DMF	dimethylformamide
Dpr	diaminopropionic acid
dt	doublet of triplets
EDTA	ethylenediaminetetraacetic acid
EI	electron ionization
eq	equivalents
ESI	electrospray ionization
EtOAc	ethyl acetate



EtOH	ethanol
Ext	optical extinction
FDA	food and drug administration
Fmoc	fluorenylmethyloxycarbonyl
GBq	gigabequerel
GHSR-1a	growth hormone secretagogue receptor-1a
GPCR	G protein-coupled receptor
GRPR	gastrin-releasing peptide receptor
h	hour
HATU	1-[bis(dimethylamino)methylene]-1 <i>H</i> -1,2,3-triazolo[4,5- <i>b</i> ]pyridinium 3-oxid hexafluorophosphate
HCTU	O-(1 <i>H</i> -6-chlorobenzotriazole-1-yl)-1,1,3,3-tetramethyluronium hexafluorophosphate
HEPES	4-(2-hydroxyethyl)piperazine-1-ethanesulfonic acid
HIV	human immunodeficiency virus
HPLC	high-performance liquid chromatography
HRMS	high resolution mass spectrometry
HTS	high-throughput screening
Hz	hertz
IC <sub>50</sub>	half maximal inhibitory concentration
iEDDA	inverse electron demand Diels-Alder
<i>J</i>	spin-spin coupling constant
K <sub>222</sub>	Kryptofix 222
keV	kiloelectronvolt
LUMO	lowest unoccupied molecular orbital
m	multiplet
M	molar
MALDI	matrix-assisted laser desorption/ionization
MBHA	methylbenzhydryl amine
MBq	megabequerel
MeOH	methanol
MHz	megahertz
min	minute
mg	milligram
mL	millilitre
mM	millimolar
MRI	magnetic resonance imaging
MS	mass spectrometry
MS/MS	tandem mass spectrometry
<i>m/z</i>	mass-to-charge ratio
NEt <sub>3</sub>	triethylamine
Nle	norleucine
nm	nanometer
nM	nanomolar
NMP	<i>N</i> -methyl-2-pyrrolidone
NMR	nuclear magnetic resonance
OBOC	one-bead one-compound
OBTC	one-bead two-compound

PBS	phosphate-buffered saline
PEG	polyethylene glycol
PET	positron emission tomography
RBCs	red blood cells
RFID	radio-frequency identification
RP	reverse phase
rpm	rotations per minute
s	singlet
SDF-1	stromal cell-derived factor 1
SPAAC	strain-promoted alkyne-azide cycloaddition
SPECT	single-photon emission computed tomography
SPPS	solid-phase peptide synthesis
t	triplet
TBAF	tetra- <i>n</i> -butylammonium fluoride
TBME	<i>tert</i> -butyl methyl ether
<i>t</i> Bu	<i>tert</i> -butoxy
<i>t</i> -BuOH	<i>tert</i> -butanol
TFA	trifluoroacetic acid
THF	tetrahydrofuran
TIPS	triisopropyl silane
TOF	time of flight
Ts	tosyl
UV	ultraviolet
W	watt

## Chapter 1

### 1 Introduction

#### 1.1 Molecular Imaging

Molecular imaging is a technique that combines molecular biology with non-invasive medical imaging and can be used to visualize and diagnose a large range of biological events and pathologies. It is routinely employed in the clinic to give a real-time image of the presence of important biomarkers or cell processes which allows for early diagnoses and monitoring of disease progression or treatment efficacy. Preclinical development of targeted therapeutics and understanding of the role of biomarkers in disease states can also be guided via molecular imaging.<sup>1</sup> Many modalities of molecular imaging, such as magnetic resonance imaging (MRI) or computed tomography (CT), can rely on inherent biological contrast to give images with good resolution and specificity. However, some modalities require the administration of an external agent to provide the information that is detectable by the instrument of choice. This is particularly important in positron emission tomography (PET) and single photon emission computed tomography (SPECT) imaging, where the presence of a radioisotope in the form of a radiopharmaceutical is essential to the imaging process. Furthermore, the specificity of molecular imaging agents can be improved by incorporating a targeting portion in addition to the imaging component. Targeted agents are often designed to bind to cell surface receptors or to be incorporated into enzymatic processes in the cell (Figure 1.1). The targeting moiety is most often a small molecule, a peptide, or an antibody, depending on the necessary pharmacokinetics and distribution for the intended imaging modality.

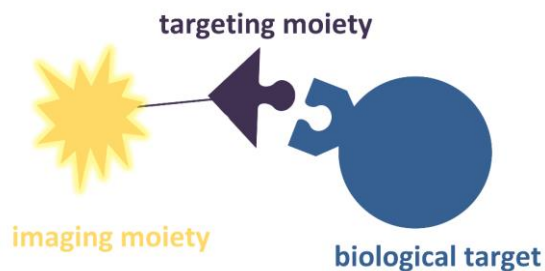


**Figure 1.1** Design of a targeted molecular imaging agent.

## 1.2 PET and Fluorine-18

PET imaging is used for diagnostic imaging applications including oncology and neurology. It is a vital imaging technique as it offers a limitless depth of penetration, has high sensitivity, and gives a 3D image wherein the amount of radioactivity can be quantified using standard uptake values.

As stated, PET imaging requires the presence of a radioactive atom to provide signal. PET affords us with excellent sensitivity as an imaging modality, as only a small dose of the radiopharmaceutical is required to give a detectable signal ( $10^{-11}$  -  $10^{-12}$  M). Specifically, PET imaging requires a radionuclide that emits a positron; nuclei that are commonly used for PET imaging include  $^{11}\text{C}$ ,  $^{13}\text{N}$ ,  $^{15}\text{O}$ ,  $^{18}\text{F}$ ,  $^{64}\text{Cu}$ , and  $^{68}\text{Ga}$  because they decay by positron emission, also known as  $\beta^+$  decay. All of these radionuclides contain an excess of protons and decay by converting the extra proton into a neutron (p, n), releasing a positron and a neutrino. The positron then travels some short distance until it undergoes electron annihilation and creates two 511 keV gamma-ray photons that are released  $180^\circ$  apart from one another. PET cameras are set up so that the detectors are ringed around the subject in order to capture incidences of photons  $180^\circ$  apart. Lines of coincidence are recorded and a three-dimensional tomographic image with quantitative information can be constructed based on annihilation locations of coincident photon events.

As previously discussed, there are multiple options of radioisotopes for PET, however fluorine-18 has chemical and physical characteristics that make it a preferred radioisotope for PET imaging. Fluorine-18 is routinely produced in a cyclotron by bombarding  $^{18}\text{O}$ -enriched water with high-energy protons, making it comparatively easily accessible and

inexpensive to produce. Compared to other organic radioisotopes,  $^{18}\text{F}$  has a longer half-life of 109.8 minutes, which is generally sufficient to provide time for synthesis, delivery, and imaging without significant decay. Fluorine-18 also decays almost entirely by  $\beta^+$  decay (97%), making it an ideal isotope for PET imaging because the high quantity of annihilation events allows for high molar activities. Beyond the physical properties of fluorine-18, there are chemical properties that are considered beneficial over metallic radioisotopes that require chelation systems for incorporation into biomolecules. Fluorine is relatively small; this makes it a superior option in applications with small molecules in order to reduce steric bulk. Moreover, fluorine is most often introduced into molecules in the form of a stable carbon-fluorine bond which makes it more stable *in vivo* leading to low potential of radioactive accumulation in off-target tissues. An important consideration is the rapidity of incorporating the fluoride so that radiolabelling is facile and time-considerate. The synthetic conditions required to directly fluorinate targeting entities with [ $^{18}\text{F}$ ]fluoride are often too harsh for biomolecule-based targeting moieties. A few notable exceptions include non-canonical  $^{18}\text{F}$ -labelling strategies involving isotope exchange reactions from fluorine-19 precursors, and aluminum fluoride constructs, which can all be achieved under mild conditions.<sup>87-89</sup> Another common route is to incorporate  $^{18}\text{F}$  through a small molecule prosthetic group which is radiolabelled first and then attached to the biomolecule through milder reaction conditions. The radiochemical reactions to attach the prosthetic group must be rapid and involve minimal or simple purification steps. These include nucleophilic substitution ( $\text{S}_{\text{N}}2$ ) reactions, Michael additions, or click chemistry. Some common fluorine-18 prosthetic groups are shown in Figure 1.2.<sup>2</sup>

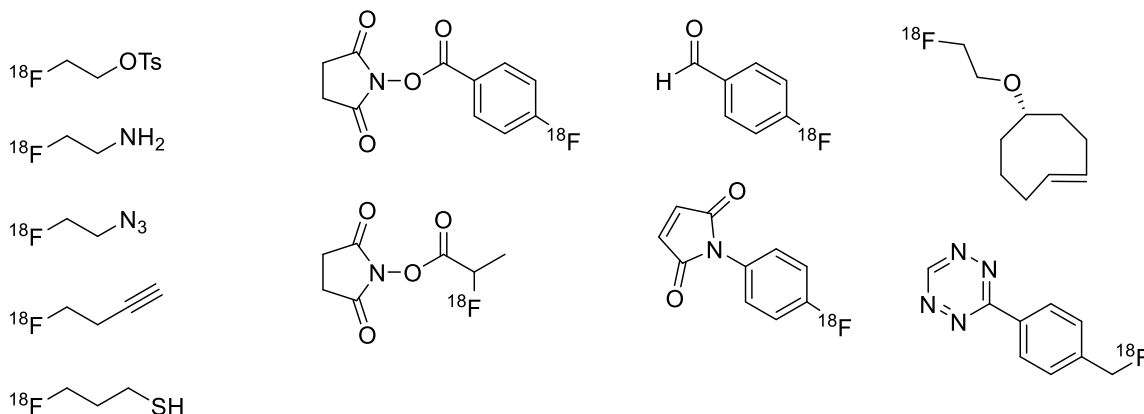


**Figure 1.2** Representative examples of common  $^{18}\text{F}$  prosthetic groups for straightforward labelling of biomolecules.

### 1.3 Click Chemistry

Click chemistry is a recently explored family of reactions, where the reaction method is rapid, bioorthogonal, produces no or harmless by-products, and can be conducted in physiologically friendly reaction conditions (physiological pH, room temperature, aqueous solution). The classic click chemistry reaction first introduced by Sharpless is the copper-catalyzed Huisgen cycloaddition of an alkyne and an azide to produce a 1,4-triazole.<sup>3</sup> This reaction is extensively used in radiolabelling and imaging because of its fast reaction rates. Additionally, amino acids with an azido or alkyne side chain are often incorporated into peptides and antibodies for easy modification with complementarily functionalized imaging entities – generally fluorescent dyes. However, the cytotoxicity of residual copper is a concern in bio-applications,<sup>4</sup> leading to research into copper-free click chemistry.

The most prominent developments for copper-free click chemistry include Bertozzi's Staudinger ligation,<sup>5</sup> strain-promoted alkyne-azide cycloaddition (SPAAC),<sup>6,7</sup> and inverse electron demand Diels-Alder (IEDDA).<sup>8,9</sup> All of these reactions are used mostly for biological applications with nuclear imaging being an especially important area of research because the mild reaction conditions are desirable for radiolabelling. Of these copper-free click techniques, we chose to invest in SPAAC chemistry, as the reaction rates favour radiolabelling strategies and the components could be easily modified to suit our needs.

## 1.4 Strain-Promoted Click Chemistry

SPAAC enlists the help of a strained alkyne in order to lower activation energy requirements of the click reaction and increase the rate constant. The reaction typically takes place between a strained alkyne and an organic azide (Figure 1.3). The  $160^\circ$  angle introduced to the *sp*-hybridized carbons of the alkyne by constraining it into an eight-membered ring induces sufficient polarization for it to react without a copper catalyst, unlike a terminal alkyne. Additionally, electron-withdrawing groups can be added to the cyclooctyne to further lower the energy of the LUMO (lowest unoccupied molecular orbital).<sup>10,11</sup>

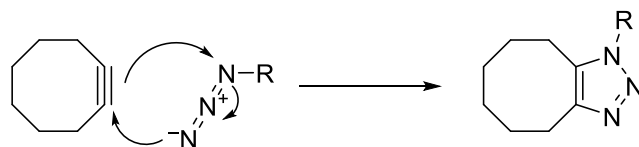


**Figure 1.3** Mechanism of the strain-promoted alkyne-azide cycloaddition reaction.

SPAAC has rate constants of around  $0.076 \text{ M}^{-1} \text{ s}^{-1}$  (difluorinated cyclooctyne, DIFO)<sup>11</sup> to  $0.96 \text{ M}^{-1} \text{ s}^{-1}$  (biarylazacyclooctyne, BARAC)<sup>12</sup> for different cyclooctynes (Figure 1.4), generally measured with the standard of benzyl azide in  $\text{CD}_3\text{OD}$  or  $\text{CD}_3\text{CN}$ . These numbers average out to be lower compared to those of iEDDA and normal copper-catalyzed click reactions, but higher than those of the Staudinger ligation. Some cyclooctynes employed in SPAAC increase strain through a fused cyclopropyl ring at the base, such as in bicyclononyne (BCN).<sup>13</sup> The highest rate constants come from further strained cyclooctynes, such as those with benzene fused to either side of the eight-membered ring. BARAC is one of these alkynes – with the quickest rate constant reported to date of  $0.96 \text{ M}^{-1} \text{ s}^{-1}$ .<sup>12</sup> However this also comes with a loss of stability; rearrangement often occurs in these structures over time.<sup>14</sup> Azadibenzocyclooctynes (ADIBO or DIBAC) have a less ideal rate constant of around  $0.31 \text{ M}^{-1} \text{ s}^{-1}$  but comes with much better shelf and solution stability.<sup>15</sup> Variations on the structure of ADIBO, in which more electron-withdrawing groups have been added, are also seen to improve rate constants.<sup>16</sup> Unfortunately, these modifications introduce synthetic complexity, which limits their availability. An acid or

amine handle incorporated into the R group in ADIBO provides a mode of bioconjugation for peptides and other biologically relevant structures.

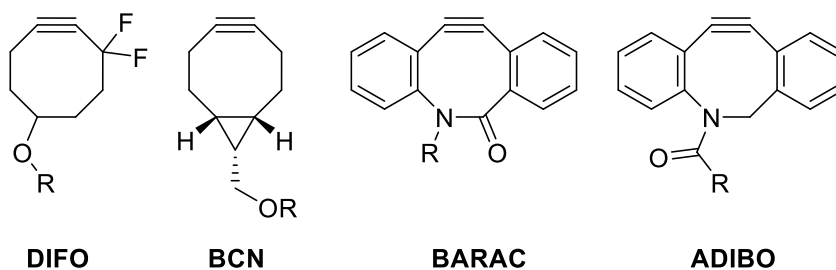


**Figure 1.4** Structures of common cyclooctynes used in SPAAC chemistry.

An inherent fault in SPAAC reactions using ADIBO and most other cyclooctynes is that two regioisomers are produced that are difficult to separate (Figure 1.5). For radiochemistry applications, the lengthy separation especially becomes an issue with the need for short syntheses to prevent radioactive decay. Some cyclooctynes, like BCN, do not form regioisomers but can create equally undesirable diastereomers or enantiomers.<sup>13</sup> Some work has been done with various cyclooctynes in which bulky functional groups are selectively placed near one side of the alkyne in order to favour one regioisomeric product due to steric bulk limitations.<sup>17,18</sup> Similarly, Gröst and Berg reported a cyclooctyne that offers a single product with no isomers, although its reaction kinetics are not particularly impressive.<sup>19</sup>

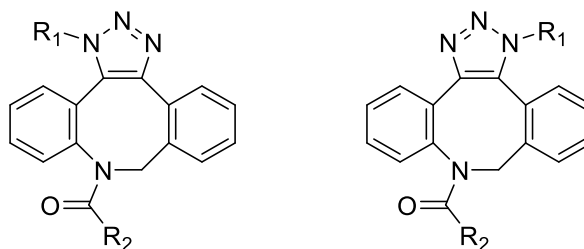


**Figure 1.5** Regioisomers produced by SPAAC of ADIBOs.

Nonetheless, SPAAC employing ADIBO has seen use for radiolabelled and biological applications. In a few cases, <sup>18</sup>F is integrated into a cyclooctyne structure over multiple steps to produce a <sup>18</sup>F-cyclooctyne prosthetic group (Figure 1.6A), to which an azide-



containing targeting entity is then clicked.<sup>20–24</sup> More commonly, the  $^{18}\text{F}$  is incorporated into an azide functionalized small molecule (Figure 1.6B), followed by a click reaction with an ADIBO-functionalized biological entity.<sup>25,26</sup>

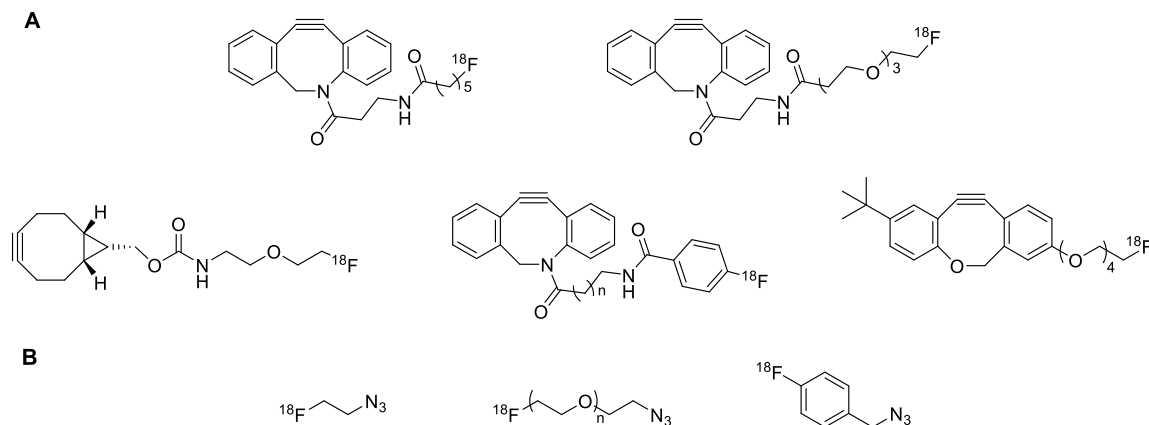


**Figure 1.6** A variety of  $^{18}\text{F}$  prosthetic groups used in SPAAC radiochemistry.<sup>27</sup>

## 1.5 Peptides as Targeting Moieties

Peptides are especially useful as targeting components of radiopharmaceutical imaging agents.<sup>28</sup> Their size and connectivity give them relatively short biological half lives that match the radioactive half lives of isotopes used. Because they circulate and clear quickly, this results in lower background levels of signal in PET or SPECT imaging. In addition, peptides are often highly selective and specific for their target. Peptide ligands for targeting can be discovered through rational design, where the side chains of the peptide sequence can be chosen based on the desired interactions with the known microenvironment in a binding pocket of a biological target. For targets of high complexity or with an unknown microenvironment, combinatorial methods are also used to discover novel peptide sequences. Although peptides are not usually very stable in biological conditions due to proteolysis, simple modifications to make the structures less like those of natural peptides are often employed, including amidation or acetylation of the C- and N-terminals, and incorporation of D-amino acids, unnatural amino acids or non-amino acid components. Many prosthetic groups are amenable to incorporation into peptides via coupling of free amines or carboxylic acids in the peptide structure.

Solid-phase peptide synthesis (SPPS) allows for straightforward synthesis and simple modifications of peptide structures. The approach uses an orthogonal protecting group strategy in order to couple amino acids one at a time onto a growing peptide chain built on resin from the C- to N- terminus. The fluorenylmethyloxycarbonyl protecting group (Fmoc) is base-labile and used to protect backbone amino groups on amino acids introduced. Various acid-labile protecting groups are used to protect side chain functional groups. Each amino acid is successively coupled to the amino-terminal of the growing peptide using a coupling reagent to form an active ester of the amino acid being introduced. Fmoc-removal using piperidine is then performed to generate a free amine for the next coupling step. Because the peptide is built on-resin, unused reagents and byproducts are washed away between steps. Final cleavage from the resin and side-chain protecting group removal can be afforded under acidic conditions (Figure 1.7).

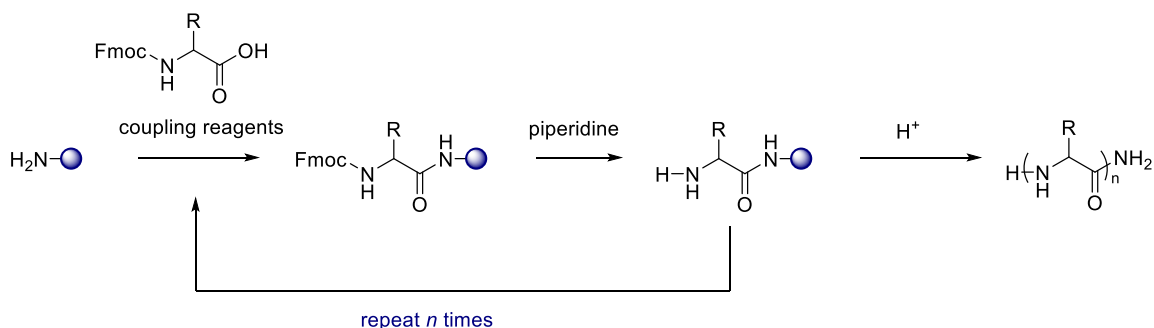


**Figure 1.7** Scheme depicting the basic steps of Fmoc-based solid-phase peptide synthesis on an amine-functionalized resin.

## 1.6 One-Bead One-Compound Libraries

One-bead one-compound (OBOC) libraries and phage-display libraries are both combinatorial methods which allow the high-throughput screening of a diverse population of peptides against a target.<sup>29</sup> These biologically active peptides can then later be conjugated to an imaging moiety to form a targeted imaging agent.<sup>30</sup> OBOC libraries are a combinatorial method in which SPPS is used to produce a large number of chemically unique peptides each formed in multiple copies on a single resin bead. The process was developed by Kit Lam in 1991 as a method to rapidly chemically synthesize a large library of randomized peptides for screening for biological activity.<sup>31</sup> Importantly, unlike many

other options to synthesize large libraries of peptides, such as phage display, OBOC can easily incorporate D-amino acids, unnatural amino acids, other small molecular weight components, and can overcome other limitations inherent of biological selection bias.

Although OBOC libraries have been employed to discover new peptides that target cancer, among other diseases,<sup>29,32–39</sup> there are relatively few reports of these peptides successfully modified into imaging agents.<sup>30,33,40–45</sup> For direct identification of potential imaging agents, the integration of an imaging surrogate before screening for biological activity should be performed. This process would allow the imaging portion of the agent to be incorporated into the binding pocket of the target protein during solid-phase affinity studies. Peptide sequences where the imaging portion would prevent binding are excluded before further synthesis and complex binding assays. Conversely, peptides that bind better with the imaging portion present compared to the unmodified peptide would now be included in further studies. Whereas, when using the classic approach where the imaging moiety is added post-screening, these unmodified peptides may not have been included after the initial screen. To our knowledge, only three examples have been reported in the literature of such an approach, whereby the OBOC library consisted of imaging agents. In two cases, the design of such libraries was described: an N-terminally modified  $\text{Re}(\text{CO})_3$  organometallic peptide library was developed in our lab for the discovery of  $^{99\text{m}}\text{Tc}$  SPECT imaging agents;<sup>46</sup> and the synthesis of a peptoid DOTA-containing OBOC library for different metal chelates was described towards application for PET or MRI imaging.<sup>47</sup> A recent publication describes the creation and on-bead screening of a focused OBOC peptide library containing the  $\alpha_v\beta_6$ -targeting motif and a C-terminal 4-fluorobenzoyl group, which had some success in the discovery of lead peptides towards new  $^{18}\text{F}$  imaging agents.<sup>48</sup>

An OBOC library is created by splitting the resin into  $n$  equal portions in  $n$  wells. To each well a different Fmoc-protected amino acid is added, along with the necessary coupling reagents. After coupling is achieved, the resin from all of the wells are combined, Fmoc-deprotected, and split back into  $n$  wells. Subsequent coupling and deprotecting is performed and this process is repeated until the desired length of peptide is obtained (Figure 1.8). By splitting the resin in this way, the possibility for a bead to host a mixture of peptides is eliminated, and so each bead contains solely multiple copies of a single entity.

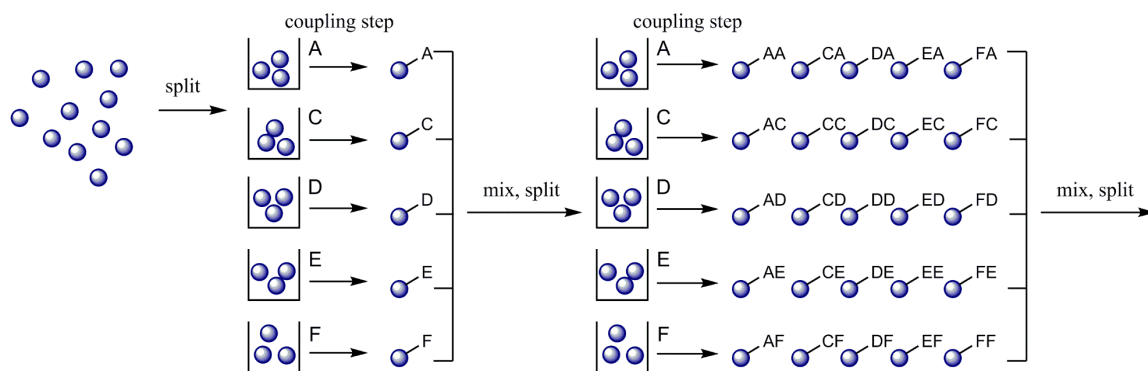


**Figure 1.8** Two cycles of split-and-mix in forming an OBOC library using amino acids A, C, D, E, and F.

This split-and-mix technique allows the diversity of the library to grow exponentially with each coupling step. For example, a library of octamers created from 17 different amino acids would result in a theoretical diversity of  $17^8$  – around 7 billion possible unique peptide sequences. Since the amount of resin typically used is only 1 g (around 1.5 million TentaGel beads), less than 0.1% of possible peptides are expressed. This suggests that there is likely no redundancy in the library. Generally, some amino acids such as cysteine are excluded from those employed in the library so as to avoid complications such as cross-linking. Likewise, methionine is also often not used because of its ability to easily become oxidized. Once the library has been synthesized, all remaining amino acid side-chain protecting groups are cleaved by an acidic solution, while the peptide stays attached to the resin through some linker. These linkers can be stable, or cleaved orthogonally through chemistries such as photolabile or disulfide linkers.<sup>49,50</sup>

To screen the millions of peptides created from an OBOC library, the beads holding the peptides are combined with a biological entity of interest. A known target is not necessary, as often phenotypic screens are performed on cells. Specific targets can be used by either isolating a protein or by overexpressing the target in a cell line. The protein or cell line is generally fluorescently labelled in order to have the ability to detect the peptide beads that have binding interactions. Unbound cells or protein are washed away and beads are sorted based on affinity to the target. Alternatively, a protein linked to a magnetic bead could also

be used for screening and sorted from unbound library beads by a magnet in a “beads on a bead” approach.<sup>51,52</sup>

Several approaches for sequence deconvolution of peptide hits exist, although it still remains the most laborious and challenging part of the OBOC screening process. Classical techniques included Edman degradation which is costly, time-consuming and is limited for peptides without N-terminal modifications or unnatural modifications in the peptide backbone. Matrix-assisted laser desorption/ionization (MALDI) tandem mass spectrometry (MS/MS) has emerged as a more rapid and cost-effective method to determine peptide sequences, and has no limits based on modifications, but has its own limitations based on fragmentation and ionization efficiency (Chapter 1.7). New technology has allowed for other emerging methods of deconvolution. One-bead two-compound (OBTC) bilayer approaches to chemically encoding beads involves parallel synthesis of small amounts of another molecule with the peptide<sup>53,54</sup>; these can even be oligonucleotides that can later be amplified by PCR and used to relate the DNA sequence to the corresponding amino acids used in the peptide construction.<sup>55</sup> Ladder-synthesis approaches cap small amounts of peptide after each coupling, which leaves behind partial sequences that are more reliably observed in MS than peptide fragments via MS/MS.<sup>56,57</sup> Perhaps the most exciting recent advance in the field is the development of RFID-tagged chips that can be followed through each split-and-mix step for immediate and reliable identification of hit sequences, although this capability is still limited to smaller sized libraries.<sup>58</sup>

## 1.7 Matrix-Assisted Laser Desorption/Ionization Mass Spectrometry

MALDI is a frequently used tool for *de novo* sequencing of unknown peptides in either an on-bead process developed previously in our lab,<sup>50</sup> or once the peptide has been photocleaved from the peptide into solution. This technique is often used over techniques like Edman degradation or OBTC because it is fast, cheap, and consistent. It also allows the recovery of small quantities of the peptide once completed. Cruikshank *et al.* reported the ability to sequence N-terminally modified Re-complexed peptides by MALDI MS/MS at single bead quantities of peptide.<sup>46</sup>

Tandem mass spectrometry is performed by selecting for the complete peptide at a determined parent ion  $m/z$ , fragmenting the peptide in the collision cell, and then collecting a complete mass spectrum of the fragments produced. In peptides, the location of the most common cleavage in low energy collisions is at the amide bonds between amino acids. Since almost each amino acid has a specific mass to charge ratio ( $m/z$ ) for their residue, the mass difference between fragment peaks can be used to determine the amino acid sequence. Because this fragmentation produces both ionized fragments containing the N-terminus of the peptide or containing the C-terminus, it results in two series of peptide fragments detectable by MS/MS. The  $y$  ion series describes the result of amino acid loss from the N-terminus. This means that all the fragments retain the original C-terminus of the peptide and the fragments have a charged N-terminus. Similarly, the  $b$  ion series reflects the result of amino acid cleavage from the C-terminus. All fragments in the  $b$  series retain the N-terminus of the peptide and contain a charged C-terminus. An extension of the  $b$  series is also sometimes seen in lower incidence than  $b$  or  $y$  ions, wherein further fragmentation of the  $b$  series ions has occurred through the loss of a carbonyl; this is called the  $a$  ion series (Figure 1.9).<sup>59</sup>

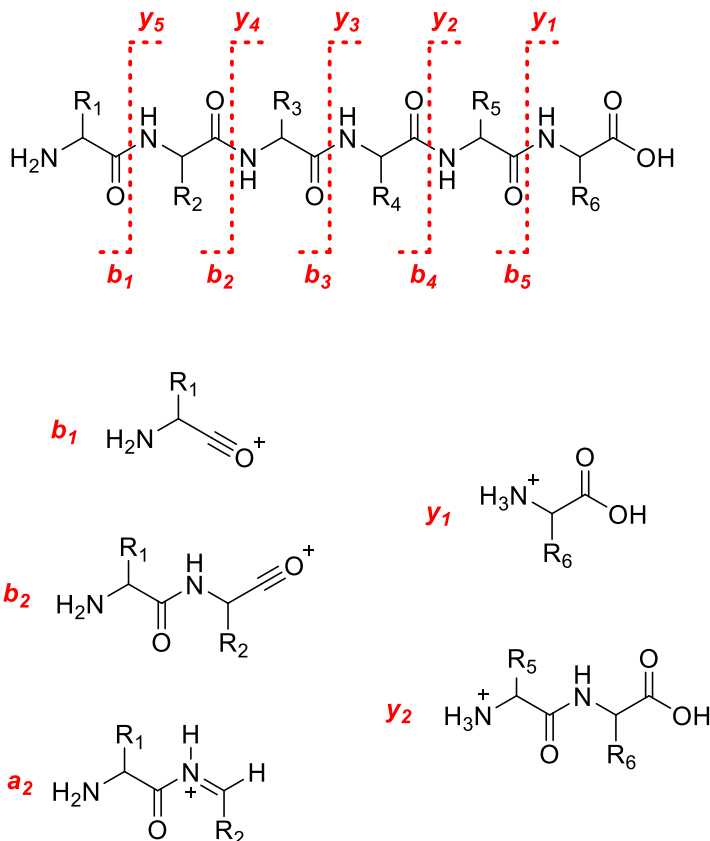


**Figure 1.9** A general hexamer peptide structure showing common fragmentation locations and examples of the fragments that are produced.

Because this fragmentation occurs randomly within the peptide, some fragments may not appear in the MS/MS spectra with significant intensity. Because of this, sequencing by MALDI often has a low success rate. However, as long as there is sufficient overlap between the two series, full sequence deconvolution of the peptide is possible.

Another difficulty encountered in sequencing by MS/MS lies in isobaric amino acids (those with similar masses such as leucine and isoleucine, or glutamine and lysine). Often, only one of the two matching amino acids are employed in the library. This unfortunately limits the structural diversity in peptides that could be generated in the library. Alternatively, peptides hits that include these mass residues can be resynthesized using either amino acid in the location of question and further screening can be performed with both options of which the sequences are now known.

## 1.8 G Protein-Coupled Receptors as Biological Targets

G protein-coupled receptors (GPCRs) are a class of proteins with seven transmembrane domains. Because they are cell-surface receptors they are designed to detect extracellular molecules to start signal transductions within the cell, which makes them well-suited as biological targets for imaging agents. Their cell surface binding site allows for easy accessibility of the targeting entity which means imaging agents do not need to be cell permeable. Internalization through the receptor can occur, which often does lead to increased uptake of the tracer. Because GPCRs are such a large class of proteins, almost 34% of FDA approved drugs target GPCRs, which means many are well-characterized and their roles in disease states have been explored.<sup>60</sup> An important GPCR studied in cancer imaging is the gastrin-releasing peptide receptor (GRPR, also known as BB<sub>2</sub>) due to its high levels of overexpression in various cancers. The peptide bombesin has been found to bind to GRPR with high affinity and has been derivatized and used in multiple nuclear imaging applications.<sup>26,61-63</sup> Our lab has also explored the growth hormone secretagogue receptor (GHSR-1a) as a target due to its differential expression in prostate cancer over benign prostate tissues.<sup>64</sup> The endogenous ligand for GHSR-1a is the peptide ghrelin, and previous efforts in our lab have established ghrelin peptide analogues that can be modified with fluorescent dyes or radioligands for imaging.<sup>65-67</sup>

## 1.9 C-X-C Chemokine Receptor 4

The chemokine receptor CXCR4 is a GPCR that was first identified as a route of entry for HIV infection into CD4<sup>+</sup> cells. Its natural ligand is CXCL12 (also known as SDF-1 $\alpha$ ), and together they are involved in various cellular pathways including chemotaxis, angiogenesis and proliferation. Although this receptor has relatively low expression in normal tissues, it is expressed in over 23 types of cancers including breast and prostate cancer and melanomas.<sup>68</sup> The expression of CXCR4 has been linked to metastatic forms of cancer due to its role in chemotactic pathways and homing to lymph nodes and bone marrow. It was determined in clinical prostate cancer biopsies that although the expression of CXCR4 is not significantly associated with Gleason score, frequency of CXCR4 expression is 35 times higher in prostate cancer than non-malignant prostate tissue.<sup>69</sup> Imaging of CXCR4 is



therefore an exciting target that could prove to be important for diagnoses and stratification of malignant and metastatic cancers.

All forays into imaging CXCR4 have stemmed from research into anti-HIV-1 drugs. Antimicrobial self-defense peptide polyphemusin II was identified from the extracts of horseshoe crab (*Tachypleus tridentatus*) hemocytes.<sup>70</sup> This peptide and its derivatives were found to be effective at inhibiting HIV-1 entry into cells via CXCR4.<sup>71</sup> The peptide is 18 amino acids in length, contains two disulfide bonds to form a beta-hairpin structure, and is amidated at the C-terminus. Initial structure-activity studies in order to improve potency and reduce cytotoxicity identified a peptide termed T22 (Tyr<sup>5,12</sup>, Lys<sup>7</sup>).<sup>72</sup> Efforts to shorten the peptide and maintain potency eventually resulted in T140, a 14 amino acid peptide with a carboxylic acid C-terminus and a single disulfide bridge that retains high CXCR4 affinity (Figure 1.10a).<sup>73</sup> FC131 is a cyclic pentapeptide which is the result of structure-activity studies to determine the main binding residues of T140; the N-terminal arginine, naphthylalanine, and tyrosine were found to be important for CXCR4 affinity (Figure 1.10b).<sup>74</sup> In addition, small molecule AMD3100 (Plerixafor) was also explored for its use as an HIV inhibitor as it is known to block the CXCR4 receptor but has since been used to treat cancer patients by mobilizing hematopoietic stem cells for transplantation (Figure 1.10c).<sup>75,76</sup>

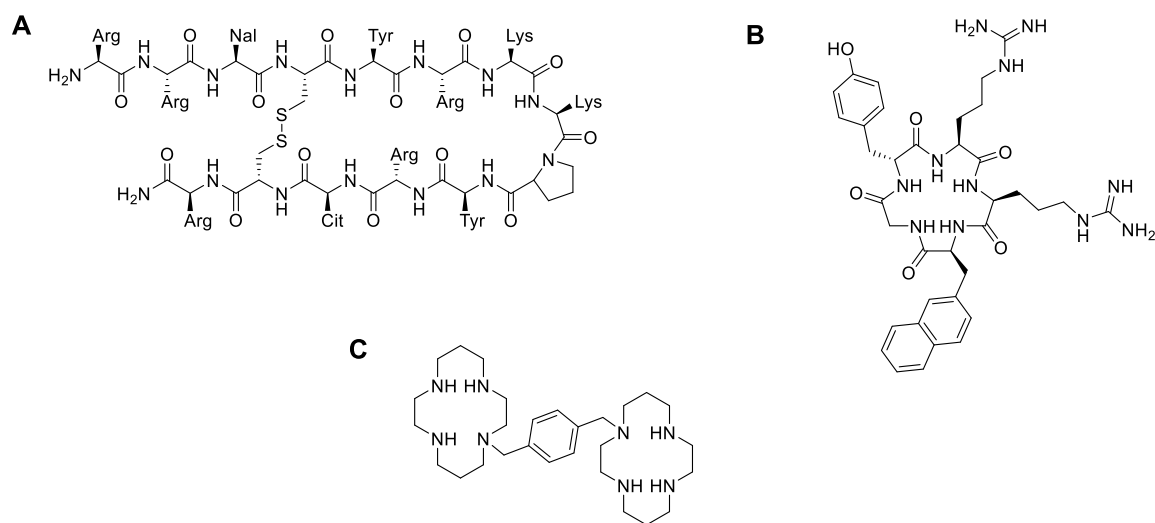


**Figure 1.10** CXCR4-targeting ligands with high affinities A) peptide T140 B) cyclic peptide FC131 C) AMD3100.

Of the PET imaging agents developed for CXCR4, T140 has been most often used as the scaffold of choice. In the first attempts to create a CXCR4 imaging agent, T140 was labelled on the N-terminus with various prosthetic groups. The use of [ $^{18}\text{F}$ ]4-fluorobenzoyl resulted in extremely high non-CXCR4 specific binding to red blood cells (RBCs) which proved not useful for imaging.<sup>77</sup> Modifications of T140 with DOTA or NOTA for  $^{68}\text{Ga}$ ,  $^{64}\text{Cu}$ , and [ $^{18}\text{F}$ ]AlF incorporation lowered binding to RBCs but had significant liver and kidney uptake (up to 30% ID/g) and a decreased CXCR4 affinity.<sup>78–80</sup> N-terminal acetylated T140 derivatives were also labelled on the Lys<sup>7</sup> residue with [ $^{18}\text{F}$ ]2-fluoropropionyl or [ $^{18}\text{F}$ ]4-fluorobenzoyl groups, showing lower blood retention, good CXCR4 affinity, but still high liver and kidney retention.<sup>81</sup> Co-injection with excess cold tracer was shown to decrease liver uptake, which proves that the uptake is receptor-specific, but this strategy is not realistic for imaging purposes. FC131 has been modified to contain a DOTA chelator which was radiolabelled with  $^{68}\text{Ga}$  while retaining excellent CXCR4 affinity.<sup>82</sup> This radiopharmaceutical, called Pentixafor, is now being used in humans to image a variety of CXCR4-expressing cancers.<sup>83,84</sup> A fluorine-18 labelled analogue utilizing [ $^{18}\text{F}$ ]AlF chemistry is being evaluated as an alternative.<sup>90</sup> FC131 has also been labelled via a click reaction on a side chain with [ $^{18}\text{F}$ ]fluoroethylazide, which resulted in a poorer CXCR4 binder than FC131 on its own, and has not yet been explored for *in vivo* biodistribution or imaging.<sup>85</sup> AMD3100 labelled with  $^{64}\text{Cu}$  has also shown promise as a PET imaging agent targeting CXCR4, but also has high liver uptake due to its positively charged nature, as well as issues with tumour to background ratios from plasma protein binding and potential transchelation of the metal.<sup>86</sup>

Unfortunately, many of these peptide-based imaging agents, especially those employing fluorine-18, display poor pharmacokinetics and biodistribution *in vivo* which can likely be attributed to being based on the same peptide structure which carries through the physicochemical profile. New CXCR4-binding peptide-based imaging agents could be discovered through combinatorial methods and would likely result in a different pharmacokinetic profile.

## 1.10 Summary

The discovery of new peptide-based ligands for cancer targeting is important for the

development of the field of molecular imaging. OBOC libraries are often employed to discover such ligands. However, the addition of an imaging component to the peptide can often be detrimental to the binding affinity of the peptide sequence. To overcome this obstacle, we propose to integrate the imaging surrogate in the library prior to screening. We can discover new peptide-based imaging agents by screening a fluorine-containing OBOC library against a target of choice, wherein the imaging component of the molecule is essential to the binding affinity. Fluorine-18 radiochemistry is often performed through the use of click chemistry such that radiolabelling is fast, clean and simple. OBOC peptide libraries containing a clicked cyclooctatriazole moiety will be prepared so that a  $^{18}\text{F}$ -labelled version would be easily prepared through SPAAC. The target of interest for this project is CXCR4, which has been implicated as a receptor highly expressed in various solid cancers. Although some CXCR4 imaging agents have been developed, they all stem from the same natural peptide structure which has resulted in a poor biodistribution profile common amongst all designs. An OBOC library of imaging agents could be used to screen for new CXCR4-targeting ligands. This will lead to the discovery of new fluorine-18 PET imaging probes for CXCR4-expressing cancers.

## 1.11 References

- 1 M. L. James and S. S. Gambhir, *Physiol. Rev.*, 2012, **92**, 897–965.
- 2 R. Schirmacher, B. Wängler, J. Bailey, V. Bernard-Gauthier, E. Schirmacher and C. Wängler, *Semin. Nucl. Med.*, 2017, **47**, 474–492.
- 3 H. C. Kolb, M. G. Finn and K. B. Sharpless, *Angew. Chem. Int. Ed.*, 2001, **40**, 2004–2021.
- 4 G. J. Brewer, *Chem. Res. Toxicol.*, 2010, **23**, 319–326.
- 5 E. Saxon and C. R. Bertozzi, *Science*, 2000, **287**, 2007–2010.
- 6 G. Wittig and A. Krebs, *Chem. Ber.*, 1961, **94**, 3260–3275.
- 7 N. J. Agard, J. A. Prescher and C. R. Bertozzi, *J. Am. Chem. Soc.*, 2005, **127**, 11196–11196.
- 8 R. A. Carboni and R. V Lindsey, *J. Am. Chem. Soc.*, 1959, **81**, 4342–4346.
- 9 M. L. Blackman, M. Royzen and J. M. Fox, *J Am Chem Soc*, 2008, **130**, 13518–

- 13519.
- 10 N. J. Agard, J. M. Baskin, J. A. Prescher, A. Lo and C. R. Bertozzi, *ACS Chem. Biol.*, 2006, **1**, 644–648.
  - 11 J. M. Baskin, J. A. Prescher, S. T. Laughlin, N. J. Agard, P. V Chang, I. A. Miller, A. Lo, J. A. Codelli and C. R. Bertozzi, *Proc. Natl. Acad. Sci.*, 2007, **104**, 16793–16797.
  - 12 C. G. Gordon, J. L. Mackey, J. C. Jewett, E. M. Sletten, K. N. Houk and C. R. Bertozzi, *J. Am. Chem. Soc.*, 2012, **134**, 9199–9208.
  - 13 J. Dommerholt, S. Schmidt, R. Temming, L. J. A. Hendriks, F. P. J. T. Rutjes, J. C. M. Van Hest, D. J. Lefeber, P. Friedl and F. L. Van Delft, *Angew. Chem. Int. Ed.*, 2010, **49**, 9422–9425.
  - 14 M. Chigrinova, C. S. McKay, L. P. B. Beaulieu, K. A. Udachin, A. M. Beauchemin and J. P. Pezacki, *Org. Biomol. Chem.*, 2013, **11**, 3436–3441.
  - 15 M. F. Debets, S. S. Van Berkel, S. Schoffelen, F. P. J. T. Rutjes, J. C. M. Van Hest and F. L. Van Delft, *Chem. Commun.*, 2010, **46**, 97–99.
  - 16 M. F. Debets, J. S. Prins, D. Merckx, S. S. Van Berkel, F. L. Van Delft, J. C. M. Van Hest and F. P. J. T. Rutjes, *Org. Biomol. Chem.*, 2014, **12**, 5031–5037.
  - 17 F. Starke, M. Walther and H. J. Pietzsch, *Arkivoc*, 2010, **2010**, 350–359.
  - 18 C. D. McNitt and V. V Popik, *Org. Biomol. Chem.*, 2012, **10**, 8200–8202.
  - 19 C. Gröst and T. Berg, *Org. Biomol. Chem.*, 2015, **13**, 3866–3870.
  - 20 K. Kettenbach and T. L. Ross, *MedChemComm*, 2016, **7**, 654–657.
  - 21 V. Bouvet, M. Wuest and F. Wuest, *Org. Biomol. Chem.*, 2011, **9**, 7393–7399.
  - 22 S. Arumugam, J. Chin, R. Schirmacher, V. V. Popik and A. P. Kostikov, *Bioorganic Med. Chem. Lett.*, 2011, **21**, 6987–6991.
  - 23 R. D. Carpenter, S. H. Hausner and J. L. Sutcliffe, *ACS Med. Chem. Lett.*, 2011, **2**, 885–889.
  - 24 M. Boudjemeline, C. D. McNitt, T. A. Singleton, V. V. Popik and A. P. Kostikov, *Org. Biomol. Chem.*, 2018, **16**, 363–366.
  - 25 S. T. Lim, E.-M. Kim, V. H. Jadhav, S. B. Lee, H.-J. Jeong, D. W. Kim, K. Sachin, H. L. Kim and M.-H. Sohn, *Bioconjug. Chem.*, 2012, **23**, 1680–1686.
  - 26 L. S. Campbell-Verduyn, L. Mirfeizi, A. K. Schoonen, R. A. Dierckx, P. H. Elsinga and B. L. Feringa, *Angew. Chem. Int. Ed.*, 2011, **50**, 11117–11120.

- 27 J. P. Meyer, P. Adumeau, J. S. Lewis and B. M. Zeglis, *Bioconjug. Chem.*, 2016, **27**, 2791–2807.
- 28 C. L. Charron, J. L. Hickey, T. K. Nsiama, D. R. Cruickshank, W. L. Turnbull and L. G. Luyt, *Nat. Prod. Rep.*, 2016, **33**, 761–800.
- 29 O. H. Aina, R. Liu, J. L. Sutcliffe, J. Marik, C. X. Pan and K. S. Lam, *Mol. Pharm.*, 2007, **4**, 631–651.
- 30 L. Y. Hu, K. A. Kelly and J. L. Sutcliffe, *Mol. Imaging Biol.*, 2017, **19**, 163–182.
- 31 K. S. Lam, S. E. Salmon, E. M. Hersh, V. J. Hruby, W. M. Kazmierski and R. J. Knapp, *Nature*, 1991, **354**, 82–84.
- 32 Y. Gao, S. Amar, S. Pahwa, G. Fields and T. Kodadek, *ACS Comb. Sci.*, 2015, **17**, 49–59.
- 33 L. Peng, R. Liu, J. Marik, X. Wang, Y. Takada and K. S. Lam, *Nat. Chem. Biol.*, 2006, **2**, 381–389.
- 34 I. B. DeRoock, M. E. Pennington, T. C. Sroka, K. S. Lam, G. T. Bowden, E. L. Bair and A. E. Cress, *Cancer Res.*, 2001, **61**, 3308–3313.
- 35 N. Yao, W. Xiao, X. Wang, J. Marik, S. H. Park, Y. Takada and K. S. Lam, *J. Med. Chem.*, 2009, **52**, 126–133.
- 36 W. Wang, Z. Wei, D. Zhang, H. Ma, Z. Wang, X. Bu, M. Li, L. Geng, C. Lausted, L. Hood, Q. Fang, H. Wang and Z. Hu, *Anal. Chem.*, 2014, **86**, 11854–11859.
- 37 K. S. Lam, Q. Lou, Z.-G. Zhao, J. Smith, M. Chem, E. Pleshko and S. E. Salmon, *Biomed. Pept. Proteins Nucleic Acids*, 1995, **1**, 205–210.
- 38 W. Xiao, Y. Wang, E. Y. Lau, J. Luo, N. Yao, C. Shi, L. Meza, H. Tseng, Y. Maeda, P. Kumaresan, R. Liu, F. C. Lightstone, Y. Takada and K. S. Lam, *Mol. Cancer Ther.*, 2010, **9**, 2714–2723.
- 39 S. I. Park, M. Renil, B. Vikstrom, N. Amro, L. Song, B. Xu and K. S. Lam, *Lett. Pept. Sci.*, 2001, **8**, 171–178.
- 40 D. Walker, Y. Li, Á. Roxin, P. Schaffer, M. J. Adam and D. M. Perrin, *Bioorg. Med. Chem. Lett.*, 2016, **26**, 5126–5131.
- 41 O. H. Aina, J. Marik, R. Gandour-Edwards and K. S. Lam, *Mol. Imaging*, 2005, **4**, 439–447.
- 42 M. Jiang, R. Ferdani, M. Shokeen and C. J. Anderson, *Nucl. Med. Biol.*, 2013, **40**, 245–251.
- 43 M. K. J. Gagnon, S. H. Hausner, J. Marik, C. K. Abbey, J. F. Marshall and J. L.

- Sutcliffe, *Proc. Natl. Acad. Sci.*, 2009, **106**, 17904–17909.
- 44 W. Xiao, T. Li, F. C. Bononi, D. Lac, I. A. Kekessie, Y. Liu, E. Sanchez, A. Mazloom, A.-H. Ma, J. Lin, J. Tran, K. Yang, K. S. Lam and R. Liu, *EJNMMI Res.*, 2016, **6**, 18.
- 45 W. Beaino, J. R. Nedrow and C. J. Anderson, *Mol. Pharm.*, 2015, **12**, 1929–1938.
- 46 D. R. Cruickshank and L. G. Luyt, *Can. J. Chem.*, 2014, **93**, 234–243.
- 47 J. Singh, D. Lopes and D. Gomika Udugamasooriya, *Biopolymers*, 2016, **106**, 673–684.
- 48 Y. S. C. Tang, R. A. Davis, T. Ganguly and J. L. Sutcliffe, *Molecules*, 2019, **24**, 309.
- 49 F. Shaheen, R. Liu and K. Lam, *J. Comb. Chem.*, 2010, **12**, 700–712.
- 50 G. A. Amadei, I. F. Cho, J. D. Lewis and L. G. Luyt, *J. Mass Spectrom.*, 2010, **45**, 241–251.
- 51 V. V. Komnatnyy, T. E. Nielsen and K. Qvortrup, *Chem. Commun.*, 2018, **54**, 6759–6771.
- 52 C. F. Cho, G. A. Amadei, D. Breadner, L. G. Luyt and J. D. Lewis, *Nano Lett.*, 2012, **12**, 5957–5965.
- 53 X. Wang, L. Peng, R. Liu, S. S. Gill and K. S. Lam, *J. Comb. Chem.*, 2005, **7**, 197–209.
- 54 R. Liu, J. Marik and K. S. Lam, *J. Am. Chem. Soc.*, 2002, **124**, 7678–7680.
- 55 A. B. MacConnell, P. J. McEnaney, V. J. Cavett and B. M. Paegel, *ACS Comb. Sci.*, 2015, **17**, 518–534.
- 56 B. T. Chait, R. Wang, R. C. Beavis and S. B. Kent, *Science*, 1993, **262**, 89–92.
- 57 R. S. Youngquist, G. R. Fuentes, M. P. Lacey and T. Keough, *J. Am. Chem. Soc.*, 1995, **117**, 3900–3906.
- 58 J. Vastl, T. Wang, T. B. Trinh and D. A. Spiegel, *ACS Comb. Sci.*, 2017, **19**, 255–261.
- 59 B. Palzs and S. Suhal, *Mass Spectrom. Rev.*, 2005, **24**, 508–548.
- 60 A. S. Hauser, S. Chavali, I. Masuho, L. J. Jahn, K. A. Martemyanov, D. E. Gloriam and M. M. Babu, *Cell*, 2018, **172**, 41–54.
- 61 T. K. Pradhan, T. Katsuno, J. E. Taylor, S. H. Kim, R. R. Ryan, S. A. Mantey, P. J.

- Donohue, H. C. Weber, E. Sainz, J. F. Battey, D. H. Coy and R. T. Jensen, *Eur. J. Pharmacol.*, 1998, **343**, 275–287.
- 62 R. Alberto, R. Schibli, A. Egli, A. P. Schubiger, U. Abram and T. A. Kaden, *J. Am. Chem. Soc.*, 1998, **120**, 7987–7988.
- 63 L. Bella, E. Garcia-Garayoa, Bähler, P. Bläuenstein, R. Schibli, P. Conrath, D. Tourwé and P. A. Schubiger, *Bioconjug. Chem.*, 2002, **13**, 599–604.
- 64 C. Lu, M. S. McFarland, R. L. Nesbitt, A. K. Williams, S. Chan, J. Gomez-Lemus, A. M. Autran-Gomez, A. Al-Zahrani, J. L. Chin, J. I. Izawa, L. G. Luyt and J. D. Lewis, *Prostate*, 2012, **72**, 825–833.
- 65 G. A. F. Douglas, R. McGirr, C. L. Charlton, D. B. Kagan, L. M. Hoffman, L. G. Luyt and S. Dhanvantari, *Peptides*, 2014, **54**, 81–88.
- 66 R. McGirr, M. S. McFarland, J. McTavish, L. G. Luyt and S. Dhanvantari, *Regul. Pept.*, 2011, **172**, 69–76.
- 67 C. L. Charron, M. S. McFarland, S. Dhanvantari and L. G. Luyt, *Med. Chem. Commun.*, 2018, **9**, 1761–1767.
- 68 F. Balkwill, *Semin. Cancer Biol.*, 2004, **14**, 171–179.
- 69 G. L. Gravina, A. Mancini, P. Muzi, L. Ventura, L. Biordi, E. Ricevuto, S. Pompili, C. Mattei, E. Di Cesare, E. A. Jannini and C. Festuccia, *Prostate*, 2015, **75**, 1227–1246.
- 70 K. Yoshikawa, T. Yoneya, T. Miyata, S. Iwanaga, F. Tokunaga, M. Niwa, T. Takao and Y. Shimonishi, *J. Biochem.*, 1989, **106**, 663–668.
- 71 T. Murakami, T. Nakajima, Y. Koyanagi, K. Tachibana, N. Fujii, H. Tamamura, N. Yoshida, M. Waki, A. Matsumoto, O. Yoshie, T. Kishimoto, N. Yamamoto and T. Nagasawa, *J. Exp. Med.*, 1997, **186**, 1389–1393.
- 72 M. Masuda, H. Nakashima, T. Ueda, H. Naba, R. Ikoma, A. Otaka, Y. Terakawa, H. Tamamura, T. Ibuka, T. Murakami, Y. Koyanagi, M. Waki, A. Matsumoto, N. Yamamoto, S. Funakoshi and N. Fujii, *Biochem. Biophys. Res. Commun.*, 1992, **189**, 845–850.
- 73 H. Tamamura, Y. Xu, T. Hattori, X. Zhang, R. Arakaki, K. Kanbara, A. Omagari, A. Otaka, T. Ibuka, N. Yamamoto, H. Nakashima and N. Fujii, *Biochem. Biophys. Res. Commun.*, 1998, **253**, 877–882.
- 74 N. Fujii, S. Oishi, K. Hiramatsu, T. Araki, S. Ueda, H. Tamamura, A. Otaka, S. Kusano, S. Terakubo, H. Nakashima, J. A. Broach, J. O. Trent, Z. Wang and S. C. Peiper, *Angew. Chem. Int. Ed.*, 2003, **42**, 3251–3253.

- 75 E. De Clercq, N. Yamamoto, R. Pauwels, J. Balzarini, M. Witvrouw, K. De Vreese, Z. Debyser, B. Rosenwirth, P. Peichl and R. Datema, *Antimicrob. Agents Chemother.*, 1994, **38**, 668–674.
- 76 E. De Clercq, *Biochem. Pharmacol.*, 2009, **77**, 1655–1664.
- 77 O. Jacobson, I. D. Weiss, D. O. Kiesewetter, J. M. Farber and X. Chen, *J. Nucl. Med.*, 2010, **51**, 1796–1804.
- 78 X. Yan, G. Niu, Z. Wang, X. Yang, D. O. Kiesewetter, O. Jacobson, B. Shen and X. Chen, *Mol. Imaging Biol.*, 2016, **18**, 135–142.
- 79 O. Jacobson, I. D. Weiss, L. P. Szajek, G. Niu, Y. Ma, D. O. Kiesewetter, J. M. Farber and X. Chen, *Theranostics*, 2011, **1**, 251–262.
- 80 U. Hennrich, L. Seyler, M. Schäfer, U. Bauder-Wüst, M. Eisenhut, W. Semmler and T. Bäuerle, *Bioorganic Med. Chem.*, 2012, **20**, 1502–1510.
- 81 X.-X. Zhang, Z. Sun, J. Guo, Z. Wang, C. Wu, G. Niu, Y. Ma, D. O. Kiesewetter and X. Chen, *Mol. Imaging Biol.*, 2013, **15**, 758–767.
- 82 O. Demmer, E. Gourni, U. Schumacher, H. Kessler and H.-J. Wester, *ChemMedChem*, 2011, **6**, 1789–1791.
- 83 T. Vag, C. Gerngross, P. Herhaus, M. Eiber, K. Philipp-Abbrederis, F.-P. Graner, J. Ettl, U. Keller, H.-J. Wester and M. Schwaiger, *J. Nucl. Med.*, 2016, **57**, 741–746.
- 84 K. Philipp-Abbrederis, K. Herrmann, S. Knop, M. Schottelius, M. Eiber, K. Lückerrath, E. Pietschmann, S. Habringer, C. Gerngroß, K. Franke, M. Rudelius, A. Schirbel, C. Lapa, K. Schwamborn, S. Steidle, E. Hartmann, A. Rosenwald, S. Kropf, A. J. Beer, C. Peschel, H. Einsele, A. K. Buck, M. Schwaiger, K. Götze, H.-J. Wester and U. Keller, *EMBO Mol. Med.*, 2015, **7**, 477–487.
- 85 G. P. C. George, F. Pisaneschi, E. Stevens, Q. D. Nguyen, O. Åberg, A. C. Spivey and E. O. Aboagye, *J. Label. Compd. Radiopharm.*, 2013, **56**, 679–685.
- 86 S. Nimmagadda, M. Pullambhatla, K. Stone, G. Green, Z. M. Bhujwalla and M. G. Pomper, *Cancer Res.*, 2010, **70**, 3935–3944.
- 87 R. Ting, M. J. Adam, T. J. Ruth and D. M. Perrin, *J. Am. Chem. Soc.*, 2005, **127**, 13094–13095.
- 88 R. Schirmacher, G. Bradtmöller, E. Schirmacher, O. Thews, J. Tillmanns, T. Siessmeier, H. G. Buchholz, P. Bartenstein, B. Wängler, C. M. Niemeyer and K. Jurkschat, *Angew. Chemie - Int. Ed.*, 2006, **45**, 6047–6050.
- 89 W. J. McBride, R. M. Sharkey, H. Karacay, C. A. D. Souza, E. A. Rossi, P. Laverman, C. Chang, O. C. Boerman and D. M. Goldenberg, *J. Nucl. Med.*, 2009,



**50**, 991–998.

- 90 A. Poschenrieder, T. Osl, M. Schottelius, F. Hoffmann, M. Wirtz, M. Schwaiger and H. Wester, *Tomography*, 2016, **2**, 85–93.

## Chapter 2

# 2 Incorporation of Fluorine into an OBOC Peptide Library by Copper-free Click Chemistry towards the Discovery of PET Imaging Agents

## 2.1 Introduction

New peptide-based imaging agents can be developed by rational design from known target-specific peptides or through combinatorial methods. The synthesis of one-bead one-compound (OBOC) libraries is a combinatorial method introduced by Lam *et al.* in 1991<sup>1</sup> which involves split-and-mix synthesis to create millions of candidates from which peptide-receptor interactions can be discovered. Although the screening of classic OBOC libraries produces target-specific peptides,<sup>2-6</sup> post-identification modification of these peptides to convert them into imaging agents often decreases binding affinity and creates the necessity for further modifications.<sup>7-11</sup> However, few ventures have been made into making OBOC libraries of imaging agents.<sup>12-14</sup>

Fluorine-18 is a preferred radioisotope for positron emission tomography (PET) imaging due to its half-life and availability; as such, incorporating a <sup>19</sup>F-moiety into each entity of an OBOC library would create a library of complete imaging agents. This allows the imaging portion of the agent to be incorporated into the binding pocket of the target protein during affinity studies. Peptide sequences where the imaging portion would prevent binding would be excluded before further synthesis and complex binding assays. Conversely, peptides that bind better with the imaging portion present compared to the unmodified peptide are now included in further studies. This enables high-throughput screening of millions of potential imaging agents. Tang *et al.* recently created a focused OBOC peptide library containing the  $\alpha_v\beta_6$ -targeting motif and with a C-terminal 4-fluorobenzoyl group and had some success in the discovery of lead peptides towards new <sup>18</sup>F imaging agents.<sup>14</sup>

In this work, we aimed to develop an entirely randomized OBOC library containing an N-terminal functionalized fluoride-containing moiety in hopes of producing imaging agents where the imaging portion is involved in receptor binding itself. Copper-free click

chemistry by strain-promoted alkyne-azide cycloaddition (SPAAC)<sup>15</sup> is an increasingly popular technique for incorporating radioisotopes into biomolecular targeting agents due to its quick and mild reaction conditions.<sup>16-18</sup> By using cyclooctyne-modified peptides and an azide-containing <sup>19</sup>F-prosthetic group, this would allow for efficient and simple radiolabelling to produce the eventual <sup>18</sup>F-imaging agent for PET imaging.

The chemokine receptor CXCR4 has been implicated as a receptor of interest in a wide variety of cancers, especially in advanced and metastatic stages.<sup>19</sup> Current peptide-based <sup>18</sup>F PET imaging agents that target CXCR4 have been based on the CXCR4-antagonist peptide T140, which was developed from the natural peptide polyphemusin II.<sup>20</sup> Unfortunately, many of these imaging agents display poor pharmacokinetics and biodistribution *in vivo*.<sup>21-24</sup> New CXCR4-binding peptide-based imaging agents could be discovered through combinatorial methods.

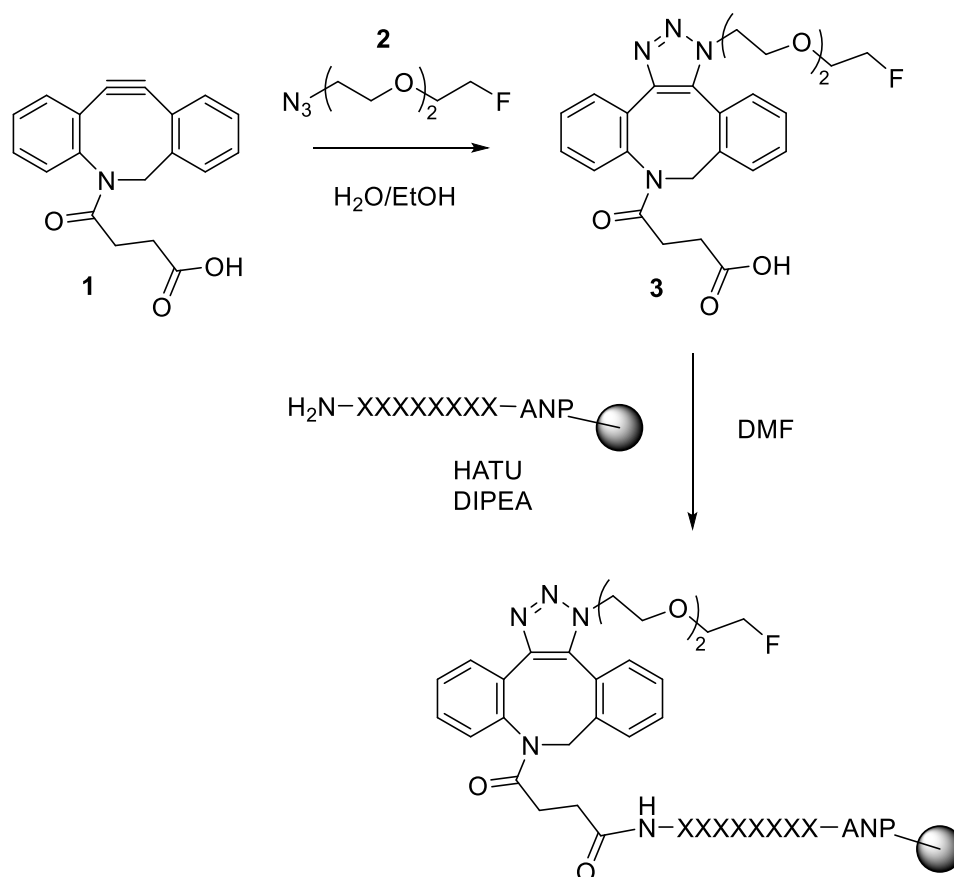
Our unique combinatorial library was screened on-resin against a U87 cell line that highly expresses CXCR4; beads that showed binding to the cells were isolated, and the sequences of the respective peptide portions were identified by MALDI tandem mass spectrometry (MS/MS). This demonstrates a methodology where novel fluorine-containing peptide-based imaging agents can be discovered with straightforward translation into <sup>18</sup>F PET imaging agents of CXCR4-expressing cancer.

## 2.2 Results and Discussion

### 2.2.1 Design and Synthesis

The cyclooctyne moiety chosen for the construction of our library was azadibenzocyclooctyne-acid (ADIBO-COOH) **2.1** and was synthesized according to the methods of Chadwick *et al.*<sup>25</sup> We chose to employ a PEG-based azide-containing <sup>18</sup>F prosthetic group in order to offer some hydrophilicity to balance the large hydrophobic cyclooctyne. The fluorine-19 analogue **2.2** was synthesized and used in the construction of our library. An entirely randomized octamer OBOC library was synthesized on one gram of Tentagel S resin equipped with a photocleavable linker ((3-amino-3-(2-nitrophenyl)propionic acid) (ANP)). This allows protecting groups to be removed while the peptides stay attached to the resin beads; yet, the peptides can be later removed from resin

for sequencing. Seventeen natural amino acids (excluding cysteine, methionine, and isoleucine) were used in the split-and-mix process, after which the “clicked” portion **2.3** was coupled onto the N-terminal of the combined library (Scheme 2.1). The result is a pool of about 1.5 million potential imaging agent candidates in which there is likely no redundancy of peptide sequences (less than 0.1% of potential diversity explored).



**Scheme 2.1** Synthesis of an octamer library on Tentagel resin using ADIBO-COOH **2.1** and a PEG-based azide-containing fluoride **2.2**. X is any natural amino acid excluding cysteine, methionine, and isoleucine.

### 2.2.2 Library Screening and Sorting

The deprotected library beads were subjected to screening against U87.CD4.CXCR4<sup>26</sup> cells that had been pre-incubated with a green Cell Tracker dye (ThermoFisher) to afford a way to visualize and sort the beads. In multiple wells the entire library was screened; approximately 500,000 cells were incubated with 20,000 beads in 3 mL of media per well

for one hour at 37 °C. After incubation, some wells were visualized under fluorescence microscopy to confirm interactions between the cells and beads. Receptor-peptide interactions between the cells and beads were fixed with 4% paraformaldehyde, excess was quenched with 2 M glycine. Library beads were then recombined, media was decanted, and the beads were resuspended in PBS.

Beads were sorted in aliquots using a Complex Object Parametric Analyzer and Sorter (COPAS, Union Biometrica)<sup>27</sup> through two screening steps. Initially, all beads were collected that expressed any threshold of green fluorescence (dye  $\lambda_{\text{ex/em}} = 492/517$  nm) which resulted in narrowing the library hits to approximately 2,500 beads. This pool, however, can include false positive beads that exhibit autofluorescence of the Tentagel bead. These beads were then subjected to a second round of sorting by the COPAS with the green fluorescence threshold set to a higher limit (Figure 2.4). Hit beads during this step were sorted individually into 96 well plates and around 200 beads were collected. Visualization of the wells was performed under fluorescence microscopy to remove any remaining false positive results that were incorrectly identified as hits during the automated COPAS sort due to high levels of bead autofluorescence (Figure 2.5). Remaining beads were swollen in water and placed under a UV lamp for two hours in order to cleave peptides off the beads. The supernatant was then subjected to MALDI MS/MS for peptide sequence deconvolution (Figure 2.1).

## 2.2.3 MALDI MS/MS Deconvolution of Hit Peptide Sequences

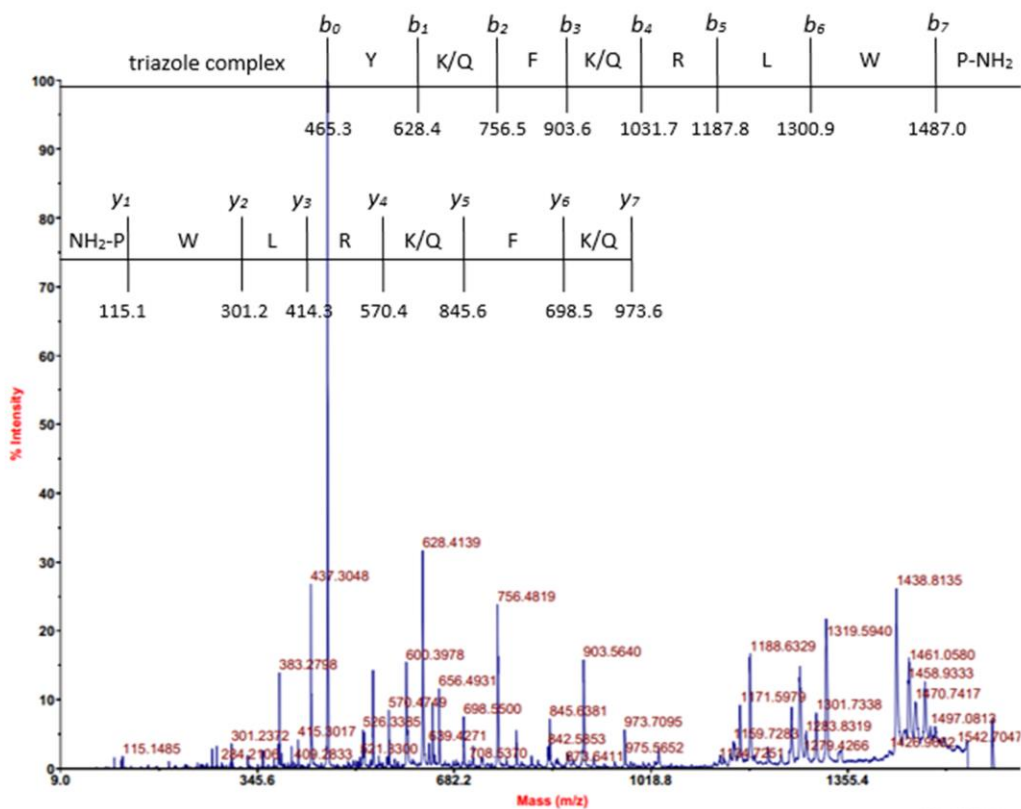


**Figure 2.1** MALDI MS/MS deconvolution of a peptide hit from library screen; showing overlapping *b* and *y* series of fragments and demonstrating high fragmentation at  $b_0$ . The isobaric amino acids lysine (K) and glutamine (Q) are both possibilities for mass fragments of ~ 128 Da.

This step of the process proved challenging where some wells produced no observable MS product (possibly due to insolubility, incomplete cleavage from bead, etc.), or incomplete fragmentation in MS/MS leading to unsolvable sequences (a known issue in this deconvolution technique).<sup>28–30</sup> In addition, the isobaric amino acids lysine and glutamine were both used in this library to promote diversity, but the corresponding residue mass was often observed in MS/MS spectra, which lead to multiple possible iterations of the hit from a single bead. An unexpected issue that arose was the high frequency of fragmentation

between the N-terminal amino acid and the imaging portion (at  $b_0$ ), causing less intense fragmentation patterns along the rest of the peptide backbone.

#### 2.2.4 Hit Peptide Synthesis and Validation of Target Specificity

In the end, hit sequences that could be fully identified (Table 2.1) were resynthesized on Tentagel resin, including all possible combinations with Lys/Gln. Evaluation of each hit sequence using bulk beads allowed for a final determination of which peptide sequence iteration was legitimately a sequence that interacts with CXCR4. Peptides on resin were incubated with a single sequence in individual wells with either fluorescently-tagged U87.CXCR4.CD4 cells or U87.CD4 cells to serve as a control. Wells were imaged by fluorescent microscopy to re-confirm CXCR4 affinity and to select for peptides with CXCR4 selectivity. This step serves to remove any remaining false positives and to identify peptides that had off-target binding to the cells. Figure 2.2 displays an example where the four possible iterations of the ‘hit’ sequence shown in Figure 2.1 were synthesized separately on Tentagel resin. Of the combinations, only one (-YKFKRLWP-) shows good affinity to the CXCR4-expressing cells as well as strong selectivity for CXCR4 compared to the control cell line (cells in the top right image are in the background and not adherent to the beads). The other sequences show either low affinity, poor selectivity, or both.

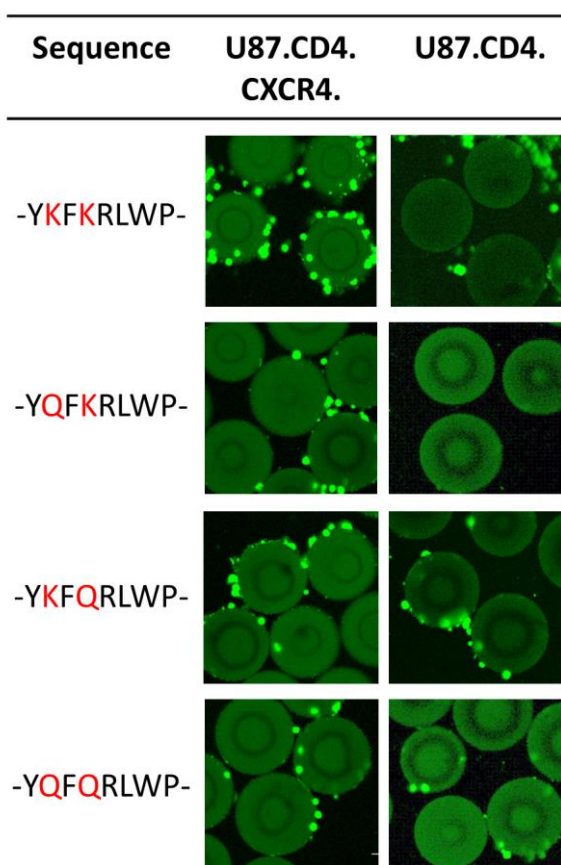


**Figure 2.2** On-bead screen of potential hits synthesized on Tentagel of the sequence F-PEG<sub>2</sub>-ADIBO-YXFXRLWP-NH<sub>2</sub> where X = Q or K. This screen allows for confirmation of ‘hit’ sequence when isobaric amino acids are involved and also screens for selectivity to the target.

### 2.2.5 Hit Peptide Synthesis and Validation of Target Affinity

CXCR4-selective peptides were then resynthesized on Rink-amide resin and purified as the C-terminal amide. These peptides were subjected to a competitive binding assay using U87.CD4.CXCR4 cells and [<sup>125</sup>I]-SDF-1 $\alpha$  as the radioligand. The lead compound from this target affinity assay was identified as F-PEG<sub>2</sub>-ADIBO-YKFKRLWP-NH<sub>2</sub> and has an IC<sub>50</sub> of 138  $\mu$ M. While other <sup>18</sup>F peptide-based imaging agents for CXCR4 have higher affinities, they are primarily based on the same polyphemusin peptide sequence and often have comparable drawbacks when it comes to *in vivo* behaviour.<sup>21–24</sup> This OBOC library



produced a new sequence that can serve as a starting point for further development towards novel CXCR4-targeted imaging agents.

## 2.3 Conclusions

Overall, we have developed an OBOC approach as a combinatorial method to produce a large-scale library of peptide imaging agent candidates. This can be useful for the screening against any target of interest for imaging purposes. Our library conveniently includes the chosen imaging moiety (fluorine-18, with fluorine-19 as a standard) through copper-free click chemistry in order to produce hits that can be easily translated into radiolabelled imaging agents. Although the discovery of imaging agents from this method still proves to be laborious and fraught with challenges, the screening steps directly produced a lead imaging agent with micromolar affinity. Modifications based on this sequence could be explored to further improve the affinity for CXCR4. Exciting new advancements in technologies for tracking synthetic histories of solid-phase syntheses with DNA tags or RFID microtransponders are highly complementary to this sort of application.<sup>31,32</sup> As improvements upon some of the challenges encountered in this library development will be explored in future generations of OBOC imaging agent libraries. Focused library synthesis would aid in the throughput of sequence deconvolution when part of the sequence is known, as well as likely produce higher affinity hits.<sup>5,14</sup> Other library conformations where the imaging moiety is dispersed through the peptide sequences could also be explored to promote discovery of imaging agents where the imaging moiety is integrated into the binding pocket.

## 2.4 Experimental

### 2.4.1 General Experimental

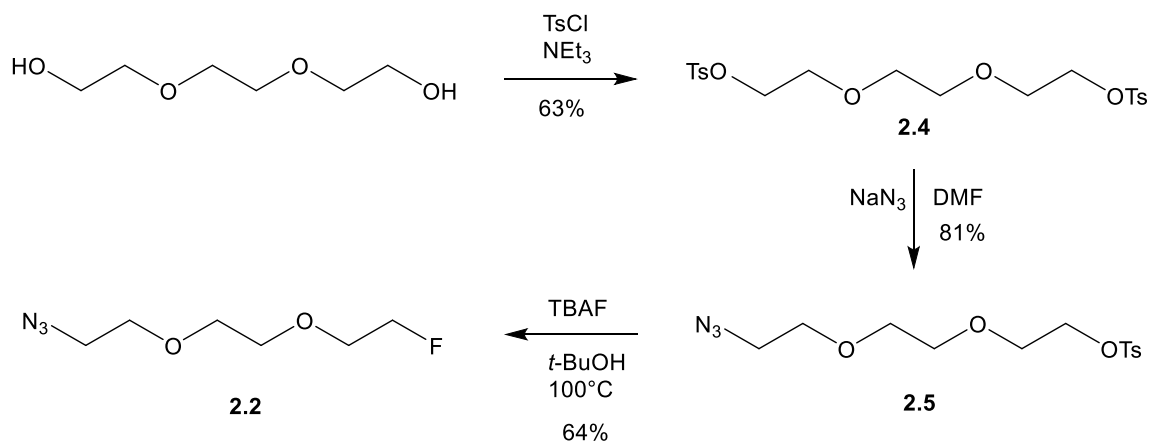
All reactions were carried out under a nitrogen atmosphere using oven-dried glassware. Dichloromethane (DCM) was distilled over CaH<sub>2</sub>. Other reagents and solvents were used as received from Sigma-Aldrich, Alfa Aesar, or Fisher Scientific. Amino acids and resins were received from Peptides International or Chem. Impex.. Flash chromatography was performed on a Biotage Isolera Prime automated flash purification system. Biotage SNAP KP-Sil 10 g, 25 g, or 50 g cartridges (45-60 micron) were used with flow rates of 12, 25,

and 50 mL/min respectively for gradient solvent systems. Fractions were monitored and collected by UV absorbance using the internal UV detector set at 254 nm and 280 nm. NMR spectra were recorded on either an Agilent Mercury VX 400 or a Bruker AvIII HD 400 MHz Spectrometer. Chemical shifts are recorded in parts per million. EI and CI HRMS was measured on a Thermo Scientific DFS (Double Focusing Sector) mass spectrometer. Peptides were purified by preparative reverse-phase HPLC-MS and analytical reverse-phase HPLC-MS was performed to assess purities. The system consists of a Waters 600 controller, Waters Prep degasser, Waters Quattro micro Mass, and Waters Mass Lynx software. The UV absorbance was detected using a Waters 2998 Photodiode array detector. A preparative column (Agilent Zorbax PrepHT SB-C18 Column 21.2 x 150 mm, 5  $\mu$ m) or analytical column (Agilent Zorbax SB-C18 column 4.6 x 150 mm, 5  $\mu$ m) was used. The solvent system runs gradients of 0.1 % trifluoroacetic acid (TFA) in ACN and 0.1 % TFA in water at a flow rate of 20 mL/min or 1.5 mL/min over 10 minutes with a 5 minute wash. After purification, the collected fractions were frozen at -78 °C and lyophilized.

## 2.4.2 Small Molecule Synthesis

### **5-[11,12-Didehydrodibenzo[*b,f*]azocin-5(6*H*)-yl]-4-oxobutanoic Acid (ADIBO-COOH) (2.1)**

ADIBO-COOH **2.1** was prepared as described by Chadwick *et al.*<sup>25</sup> <sup>1</sup>H NMR (400 MHz, CDCl<sub>3</sub>):  $\delta$  7.67 (d,  $J$  = 7.5 Hz, 1H), 7.50 – 7.20 (m, 7H), 5.16 (d,  $J$  = 13.9 Hz, 1H), 3.70 (d,  $J$  = 13.9 Hz, 1H), 2.72 (ddd,  $J$  = 16.6, 8.9, 5.2 Hz, 1H), 2.60 (ddd,  $J$  = 17.0, 8.9, 5.2 Hz, 1H), 2.36 (ddd,  $J$  = 16.8, 6.4, 5.1 Hz, 1H), 1.99 (ddd,  $J$  = 16.6, 6.6, 5.2 Hz, 1H). <sup>13</sup>C NMR (100 MHz, CDCl<sub>3</sub>):  $\delta$  176.1, 172.6, 151.2, 147.8, 132.4, 129.3, 128.7, 128.6, 128.5, 128.03, 127.4, 125.7, 123.2, 122.8, 115.2, 107.6, 55.8, 29.7, 29.6. HRMS (EI):  $m/z$  calculated for C<sub>19</sub>H<sub>15</sub>NO<sub>3</sub> : 305.1052; found: 305.1045.



**Scheme 2.2** Scheme for synthesis of **2.2**.

**2,2'-(ethane-1,2-diylbis(oxy))bis(ethane-2,1-diyl)bis(4-methylbenzenesulfonate) (2.4)**

Tosyl chloride (7.61 g, 39.9 mmol) was slowly added to a solution of triethylene glycol (2.00 g, 13.3 mmol) in triethylamine (50 mL). The reaction mixture was stirred overnight at room temperature, and the solvent was removed by rotary evaporation. The product was washed with water and extracted into EtOAc. The combined organic layers were dried over MgSO<sub>4</sub> and concentrated under reduced pressure. The product was isolated by automated Isolera flash column chromatography (SNAP KP-Sil cartridge, 12-100% EtOAc/hexanes) yielding the ditosyl **2.4** (2.77 g, 63%) as an orange solid. <sup>1</sup>H NMR (400 MHz, CDCl<sub>3</sub>): δ 7.77 (d, *J* = 8.0 Hz, 4 H), 7.33 (d, *J* = 8.0 Hz, 4 H), 4.12 (t, *J* = 4.8 Hz, 4 H), 3.63 (t, *J* = 4.8 Hz, 4 H), 3.50 (s, 4 H), 2.42 (s, 6 H). <sup>13</sup>C NMR (100 MHz, CDCl<sub>3</sub>): δ 145.0, 133.0, 129.9, 128.0, 70.7, 69.3, 68.8, 21.7. HRMS (EI): *m/z* calculated for C<sub>20</sub>H<sub>26</sub>O<sub>8</sub>S<sub>2</sub>: 458.1069; found: 458.1079.

**2-(2-(2-azidoethoxy)ethoxy)ethyl 4-methylbenzenesulfonate (2.5)**

A solution of ditosyl **2.4** (90.0 mg, 1.96 mmol) and sodium azide (113 mg, 1.72 mmol) in dry DMF (5 mL) was stirred at room temperature overnight. The reaction mixture was quenched with water and extracted into DCM. The organic fractions were washed with water, brine, and dried over MgSO<sub>4</sub>. The combined organic layers were concentrated under reduced pressure and the product was isolated by automated Isolera flash column chromatography (SNAP KP-Sil cartridge, 17-100% EtOAc/hexanes), yielding the azide

**2.5** (57.0 mg, 81%) as a yellow oil.  $^1\text{H}$  NMR (400 MHz,  $\text{CDCl}_3$ ):  $\delta$  7.89 (d,  $J = 8$  Hz, 2 H), 7.34 (d,  $J = 8$  Hz, 2 H), 4.16 (t,  $J = 5$  Hz, 2 H), 3.70 (t,  $J = 5$  Hz, 2 H), 3.64 (t,  $J = 5$  Hz, 2 H), 3.60 (s, 4 H), 3.36 (t,  $J = 5$  Hz, 2 H), 2.44 (s, 3 H).  $^{13}\text{C}$  NMR (100 MHz,  $\text{CDCl}_3$ ):  $\delta$  144.9, 133.1, 129.9, 128.1, 70.9, 70.7, 70.2, 69.4, 68.9, 50.8, 21.8. HRMS (CI):  $m/z$  calculated for  $\text{C}_{13}\text{H}_{20}\text{N}_3\text{O}_5\text{S}$   $[\text{M}+\text{H}]^+$  : 330.1118; found: 330.1123.

### **1-azido-2-(2-(2-fluoroethoxy)ethoxy)ethane (2.2)**

A commercially available solution of 1.0 M TBAF in THF (6.94 mL, 6.94 mmol) was added to a solution of azide **2.5** (1.14 g, 3.47 mmol) in *t*-BuOH (30 mL). The reaction mixture was stirred at 100 °C overnight. The reaction mixture was quenched with water and extracted into DCM. The combined organic layers were dried over  $\text{MgSO}_4$  and concentrated under reduced pressure. The product was purified by automated Isolera flash column chromatography (SNAP KP-Sil cartridge, 0-2% MeOH/DCM), yielding the product **2.2** (390 mg, 64%) as a pale yellow oil.  $^1\text{H}$  NMR (400 MHz,  $\text{CDCl}_3$ ):  $\delta$  4.60 (t,  $J = 2.8$  Hz, 1 H), 4.52 (t,  $J = 2.8$  Hz, 1 H), 3.77 (t,  $J = 2.8$  Hz, 1 H), 3.72 (t,  $J = 2.8$  Hz, 1 H), 3.70-3.66 (m, 6 H), 3.38 (t,  $J = 3.2$  Hz, 2 H).  $^{13}\text{C}$  NMR (100 MHz,  $\text{CDCl}_3$ ):  $\delta$  83.3 (d,  $^1J_{\text{CF}} = 169$  Hz), 71.0, 70.9, 70.7 (d,  $^2J_{\text{CF}} = 19.6$  Hz), 70.3, 50.8. HRMS (CI):  $m/z$  calculated for  $\text{C}_6\text{H}_{12}\text{FN}_3\text{O}_2$   $[\text{M}+\text{H}]^+$  : 178.0986; found: 178.0990.

### **F-PEG<sub>2</sub>-ADIBO-COOH (2.3)**

ADIBO-COOH **2.1** (0.158 g, 0.52 mmol) and **2.2** (0.115 g, 0.65 mmol) were dissolved in 5 mL of a 3:2 EtOH:H<sub>2</sub>O mixture. The solution was shaken for two hours, diluted with water, frozen, and lyophilized. The product was purified as a combination of its two inseparable regioisomers by automated Isolera flash column chromatography (SNAP KP-Sil cartridge, 2-15% MeOH/DCM) to yield **2.3** as a yellow oily solid (0.200 g, 80%).  $^1\text{H}$  NMR (400 MHz,  $\text{CDCl}_3$ )  $\delta$  7.91 – 7.07 (m, 8H), 6.12 (d,  $J = 16.7$  Hz, 1H), 4.73-4.64 (m, 1H), 4.60-4.51 (m, 2H), 4.50 – 4.43 (m, 1H), 4.43 (d,  $J = 16.6$  Hz, 1H), 4.02-3.91 (m, 2H), 3.79 – 3.69 (m, 2H), 3.69 – 3.55 (m, 4H) 2.58 – 2.26 (m, 2H), 2.0 (m, 1H), 1.99 – 1.62 (m, 1H). HRMS (EI):  $m/z$  calculated for  $\text{C}_{25}\text{H}_{27}\text{FN}_4\text{O}_5$  : 482.1965; found: 482.1972.

### 2.4.3 OBOC Library Synthesis

The library was synthesized using standard Fmoc solid-phase peptide synthesis (SPPS) conditions on a Biotage SyroWave automated peptide synthesizer using a split-and-mix technique in the dark. Briefly, 1 g of Tentagel S-NH<sub>2</sub> resin (90 μm, 0.29 meq/g) was swelled in DCM and manually coupled to Fmoc-ANP-OH linker (4 eq) using HCTU (4 eq) and *N,N*-diisopropylethylamine (DIPEA) (8 eq) in DMF for two hours. The resin was split into seventeen vessels. Fmoc removal was achieved using 40% piperidine in dimethylformamide (DMF) over two steps (5 min and 15 min). Each well was coupled to a different Fmoc-amino acid (4 eq) using HCTU (4 eq) and DIPEA (8 eq) in DMF for one hour. After each Fmoc-deprotection/coupling cycle, the resin was recombined into one pool and then divided into seventeen vessels again. This was repeated eight times to achieve peptides eight amino acids in length. To the combined library, F-PEG<sub>2</sub>-ADIBO-COOH **3** (1.6 eq) was coupled using HATU (1.6 eq) and DIPEA (3.2 eq) in DMF for 5 hours. Full deprotection was achieved with 95% TFA, 2.5% triisopropylsilane (TIPS) and 2.5% water for 5 hours. The library was rinsed thoroughly with DMF, DCM, MeOH, and stored in 70% EtOH/H<sub>2</sub>O.

### 2.4.4 Hit Peptide Synthesis

Peptides were synthesized using standard Fmoc SPPS conditions on the Biotage SyroWave automated peptide synthesizer. Fmoc-protected Rink amide MBHA or Tentagel S- NH<sub>2</sub> resin was used as a solid support after swelling in DCM. Fmoc removal was achieved using 40% piperidine in dimethylformamide (DMF) over two steps (30 sec and 12 min). Amino acids were coupled with the Fmoc-protected amino acid (4 eq), HCTU (4 eq) and DIPEA (8 eq) in DMF/*N*-methyl pyrrolidinone (NMP) over 1 hour. The acid **2.3** was manually coupled to the N-terminus using 1 equivalent of **2.3**, 1 equivalent of HATU and 2 equivalents of DIPEA in DMF.

Tentagel peptides were deprotected using a solution of 95% TFA, 2.5% TIPS and 2.5% water for 4 hours. Beads were rinsed thoroughly with DMF, DCM, MeOH, H<sub>2</sub>O and stored in 70% EtOH/H<sub>2</sub>O.

Full cleavage of the Rink-amide peptides from resin along with removal of side chain protecting groups was achieved with a solution of 95% TFA, 2.5% TIPS and 2.5% water over 5 h. The cleaved peptides were precipitated in cold *tert*-butyl methyl ether (TBME) and centrifuged at 3000 rpm for 15 min. The TBME was decanted, the peptide dissolved in water, frozen at -78 °C and lyophilized. The peptides were then purified by preparative reverse-phase HPLC-MS over gradients of acetonitrile (0.1% TFA) in water (0.1% TFA). The peptides were isolated in >98% purity by analytical RP-HPLC. Peptides are a combination of the two inseparable regioisomers.

**Table 2.1** Sample list of select peptide sequences resynthesized for *in vitro* validation. All are coupled to **2.3** on the N-terminal and are amidated on the C-terminal.

Amino Acid Sequence	[M+H] <sup>+</sup> <i>m/z</i> theoretical	[M+H] <sup>+</sup> <i>m/z</i> found
<b>-YKFKRLWP-</b>	1600.86	1600.83
<b>-HLTKYWET-</b>	1540.74	1540.55
<b>-HLTQYWET-</b>	1540.70	1540.50
<b>-AKEDNFRN-</b>	1456.68	1456.54
<b>-AQEDNFRN-</b>	1456.64	1456.47
<b>-NDEDEEYA-</b>	1447.54	1447.39
<b>-RLDSHDPK-</b>	1430.70	1430.56
<b>-RLDSHDPQ-</b>	1430.66	1430.51
<b>-NFKEFDHA-</b>	1452.69	1452.53
<b>-NFQEFPHA-</b>	1452.65	1452.45
<b>-FLFWGPAG-</b>	1357.65	1357.52

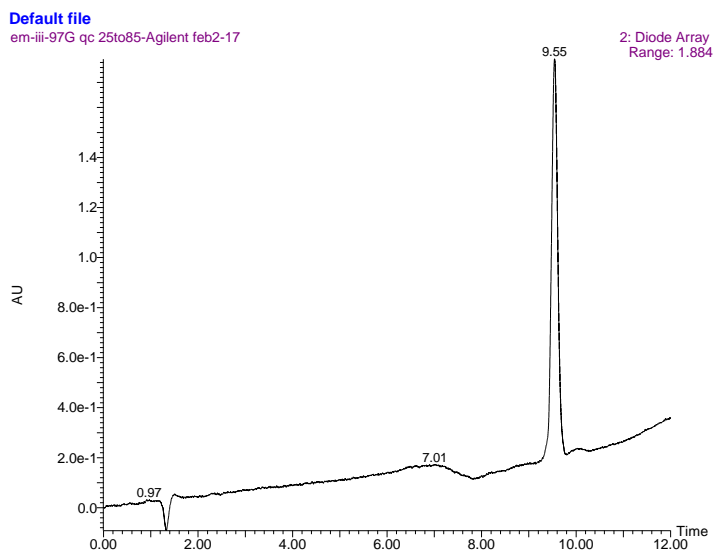


**Figure 2.3** Sample HPLC chromatogram (UV trace, 25-85% ACN/H<sub>2</sub>O with 0.1% TFA) of a purified peptide F-PEG<sub>2</sub>-ADIBO-YKFKRLWP-NH<sub>2</sub>.

#### 2.4.5 Cell Culture

U87.CD4 and U87.CD4.CXCR4 cells were obtained through the NIH AIDS Reagent Program, Division of AIDS, NIAID, NIH from Dr. Hong Kui Deng and Dr. Dan R. Littman. U87.CD4.CXCR4 cells were maintained in DMEM – high glucose (Sigma) containing 15% fetal bovine serum (FBS), 1  $\mu\text{g mL}^{-1}$  puromycin, 300  $\mu\text{g mL}^{-1}$  G418, and 1 $\times$  penicillin–streptomycin. U87.CD4 cells were maintained in DMEM – high glucose (Sigma) containing 10% FBS, 300  $\mu\text{g mL}^{-1}$  G418, and 1 $\times$  penicillin–streptomycin. All cell lines were cultured at 37 °C in humidified atmosphere with 5% CO<sub>2</sub> and passaged 2 to 3 times per week.

#### 2.4.6 Library Screening

U87.CD4.CXCR4 cells at 80% confluency were incubated with 5  $\mu\text{M}$  CellTracker™ Green CMFDA Dye (ThermoFisher) in serum-free DMEM media for 30 min at 37 °C. Dye was aspirated, and cells were lifted using an enzyme-free dissociation solution (Sigma). Cells were counted and resuspended in serum-free DMEM at 500,000 cells/mL. Library beads were suspended in phosphate-buffered saline (PBS) and dispersed in 6-well plates at ~20,000 beads/well (entire library is ~1.5 million beads). Cells were added to each well (1

mL, 500,000 cells) and total volumes were brought up to 3 mL with DMEM. Plates were shaken at 550 rpm for 1 hour at 37 °C. To each well, 0.33 mL of 37% paraformaldehyde was added for a final concentration of 4%. Fixing was quenched by the addition of 2 M glycine to a final concentration of 20%. The entire library of beads was recombined and rinsed with PBS repeatedly then suspended in PBS. Aliquots of this solution were added to the sample cup of a COPAS instrument (Union Biometrica) and diluted into the appropriate sheath reagent. Beads were sorted at ~20 events/s and excited by a 488 nm lamp to select for beads (via length (TOF) and optical density (Ext)) as well as to sort for fluorescence (green  $\lambda_{em} = 510 \pm 23$  nm) (Figure 2.4A-B & 2.5A-B). Beads were collected in bulk (~2500 events), rinsed, and then re-added to the sample cup and sorted with a higher set threshold of fluorescence for sorting (Figure 2.4C). In this sort, hit beads were deposited into individual wells of a 96 well plate (~200 events) (Figure 2.5C-D). Wells were imaged by confocal fluorescent microscopy to remove any remaining false positive beads (Figure 2.5D). Confocal fluorescence microscopy was performed on a Nikon A1R Confocal Laser Microscope with a 488 nm laser for excitation and the emission range set to 500-550 nm.

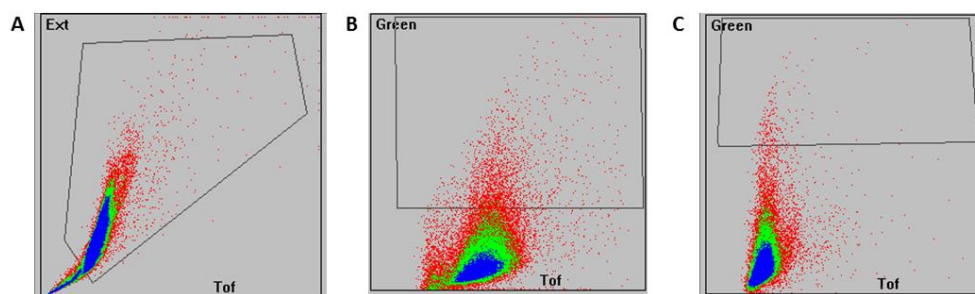


**Figure 2.4** Screenshots of COPAS software showing A) gating selection for bead-sized objects based on size (TOF) and optical density (Ext); B) sorting selection for initial screen based on bead size and above-average green fluorescence ( $\lambda_{em} = 510 \pm 23$  nm); C) sorting selection for second round with higher threshold of green fluorescence.



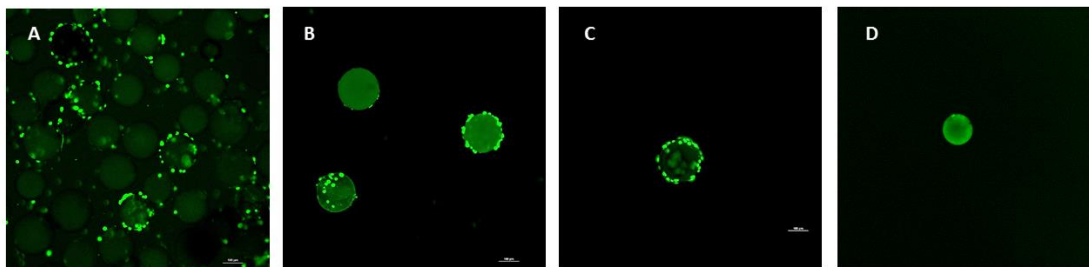


**Figure 2.5** Confocal fluorescence images of A) library pool after incubation with U87.CD4.CXCR4 cells tagged with CellTracker Green CMFDA; B) library beads after initial screen showing some hit beads with various degrees of cell coverage; C) isolated hit library bead in a well of a 96 well plate after second sorting round; D) isolated false positive bead displaying high autofluorescence.

#### 2.4.7 MALDI MS/MS

Hit beads from the library screen were suspended in 50  $\mu$ L of water in individual wells of 96-well plates and placed under UV light (365 nm) for 2 hours to achieve cleavage from the bead due to the ANP linker. The aqueous solution was mixed with matrix  $\alpha$ -cyano-4-hydroxycinnamic acid (CHCA) in acetonitrile and placed onto the MALDI target. MALDI TOF/TOF was performed on an AB Sciex TOF/TOF 5800 by the facility manager of the MALDI Mass Spectrometry Facility at the London Regional Proteomics Centre.

#### 2.4.8 Selectivity Analysis Assay

U87.CD4.CXCR4 or U87.CD4 cells at 80% confluency were incubated with 5  $\mu$ M CellTracker™ Green CMFDA Dye (ThermoFisher) in serum-free DMEM media for 30 min at 37 °C. Dye was aspirated, and cells were lifted using an enzyme-free dissociation solution (Sigma). Cells were counted and resuspended in serum-free DMEM at 150,000 cells/mL. Tentagel beads expressing re-synthesized potential hit sequences were suspended in phosphate-buffered saline (PBS) and dispersed in 12-well plates at ~10,000 beads/well. Cells were added to each well (1 mL, 150,000 cells) and total volumes were brought up to 2 mL with DMEM. Plates were shaken at 550 rpm for 1 hour at 37 °C. Wells were directly imaged using confocal fluorescent microscopy (Nikon).

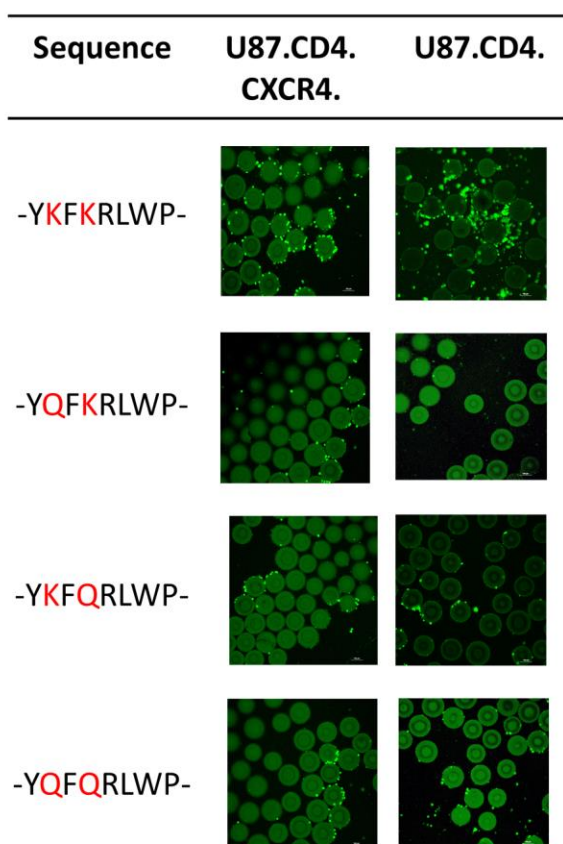


**Figure 2.6** Uncropped Images of Figure 2.2 to further display selectivity.

#### 2.4.9 Competitive Binding Assays

*In vitro* CXCR4 affinity of final hit peptides were determined through competitive binding assays using U87.CD4.CXCR4 cells with [<sup>125</sup>I]-SDF-1 $\alpha$  as the radioligand (Perkin Elmer). The compound of interest (30  $\mu$ L, at concentrations ranging from 10<sup>-6</sup> to 10<sup>-2</sup> M) and 20,000 cpm of [<sup>125</sup>I]-SDF-1 $\alpha$  (20 pM) were mixed with the binding buffer (20 mM HEPES, 0.5% BSA in PBS, pH 7) in 1.5 mL Eppendorf Protein LoBind vials. A suspension of U87.CD4.CXCR4 cells (50,000 cells in 50  $\mu$ L) was added to each vial to give a final volume of 300  $\mu$ L. The vials were shaken at 550 rpm for 20 minutes at 37 °C. Immediately after the incubation, the vials were centrifuged at 13,000 rpm for 5 minutes and the supernatant removed. The cell pellet was washed with 500  $\mu$ L of 50 mM Tris buffer (pH 7) and centrifuged again. The amount of [<sup>125</sup>I]-SDF-1 $\alpha$  bound to the cells was measured

using a gamma counter (PerkinElmer). IC<sub>50</sub> values were determined by non-linear regression analysis to fit a 4-parameter dose response curve using GraphPad Prism (Version 6.0c). All data points were obtained in triplicate.

## 2.5 References

- 1 K. S. Lam, S. E. Salmon, E. M. Hersh, V. J. Hruby, W. M. Kazmierski and R. J. Knapp, *Nature*, 1991, **354**, 82–84.
- 2 N. Yao, W. Xiao, X. Wang, J. Marik, S. H. Park, Y. Takada and K. S. Lam, *J. Med. Chem.*, 2009, **52**, 126–133.
- 3 V. V. Komnatnyy, T. E. Nielsen and K. Qvortrup, *Chem. Commun.*, 2018, **54**, 6759–6771.
- 4 O. H. Aina, R. Liu, J. L. Sutcliffe, J. Marik, C. X. Pan and K. S. Lam, *Mol. Pharm.*, 2007, **4**, 631–651.
- 5 W. Xiao, Y. Wang, E. Y. Lau, J. Luo, N. Yao, C. Shi, L. Meza, H. Tseng, Y. Maeda, P. Kumaresan, R. Liu, F. C. Lightstone, Y. Takada and K. S. Lam, *Mol. Cancer Ther.*, 2010, **9**, 2714–2723.
- 6 W. Wang, Z. Wei, D. Zhang, H. Ma, Z. Wang, X. Bu, M. Li, L. Geng, C. Lausted, L. Hood, Q. Fang, H. Wang and Z. Hu, *Anal. Chem.*, 2014, **86**, 11854–11859.
- 7 L. Y. Hu, K. A. Kelly and J. L. Sutcliffe, *Mol. Imaging Biol.*, 2017, **19**, 163–182.
- 8 M. K. J. Gagnon, S. H. Hausner, J. Marik, C. K. Abbey, J. F. Marshall and J. L. Sutcliffe, *Proc. Natl. Acad. Sci.*, 2009, **106**, 17904–17909.
- 9 W. Xiao, T. Li, F. C. Bononi, D. Lac, I. A. Kekessie, Y. Liu, E. Sanchez, A. Mazloom, A.-H. Ma, J. Lin, J. Tran, K. Yang, K. S. Lam and R. Liu, *EJNMMI Res.*, 2016, **6**, 18.
- 10 L. Peng, R. Liu, J. Marik, X. Wang, Y. Takada and K. S. Lam, *Nat. Chem. Biol.*, 2006, **2**, 381–389.
- 11 W. Beaino, J. R. Nedrow and C. J. Anderson, *Mol. Pharm.*, 2015, **12**, 1929–1938.
- 12 D. R. Cruickshank and L. G. Luyt, *Can. J. Chem.*, 2015, **93**, 234–243.
- 13 J. Singh, D. Lopes and D. Gomika Udugamasooriya, *Biopolymers*, 2016, **106**, 673–684.
- 14 Y. S. C. Tang, R. A. Davis, T. Ganguly and J. L. Sutcliffe, *Molecules*, 2019, **24**, 309.
- 15 N. J. Agard, J. A. Prescher and C. R. Bertozzi, *J. Am. Chem. Soc.*, 2005, **127**, 11196–11196.
- 16 J. P. Meyer, P. Adumeau, J. S. Lewis and B. M. Zeglis, *Bioconjug. Chem.*, 2016,

- 27, 2791–2807.
- 17 L. S. Campbell-Verduyn, L. Mirfeizi, A. K. Schoonen, R. A. Dierckx, P. H. Elsinga and B. L. Feringa, *Angew. Chem. Int. Ed.*, 2011, **50**, 11117–11120.
  - 18 S. T. Lim, E.-M. Kim, V. H. Jadhav, S. B. Lee, H.-J. Jeong, D. W. Kim, K. Sachin, H. L. Kim and M.-H. Sohn, *Bioconjug. Chem.*, 2012, **23**, 1680–1686.
  - 19 F. Balkwill, *Semin. Cancer Biol.*, 2004, **14**, 171–179.
  - 20 H. Tamamura, Y. Xu, T. Hattori, X. Zhang, R. Arakaki, K. Kanbara, A. Omagari, A. Otaka, T. Ibuka, N. Yamamoto, H. Nakashima and N. Fujii, *Biochem. Biophys. Res. Commun.*, 1998, **253**, 877–882.
  - 21 X. Yan, G. Niu, Z. Wang, X. Yang, D. O. Kiesewetter, O. Jacobson, B. Shen and X. Chen, *Mol. Imaging Biol.*, 2016, **18**, 135–142.
  - 22 X.-X. Zhang, Z. Sun, J. Guo, Z. Wang, C. Wu, G. Niu, Y. Ma, D. O. Kiesewetter and X. Chen, *Mol. Imaging Biol.*, 2013, **15**, 758–767.
  - 23 O. Jacobson, I. D. Weiss, D. O. Kiesewetter, J. M. Farber and X. Chen, *J. Nucl. Med.*, 2010, **51**, 1796–1804.
  - 24 W. L. Turnbull, L. Yu, E. Murrell, M. Milne, C. L. Charron and L. G. Luyt, *Org. Biomol. Chem.*, 2019, **17**, 598–608.
  - 25 R. C. Chadwick, S. Van Gyzen, S. Liogier and A. Adronov, *Synthesis*, 2014, **46**, 669–677.
  - 26 A. Björndal, H. Deng, M. Jansson, J. R. Fiore, C. Colognesi, A. Karlsson, J. Albert, G. Scarlatti, D. R. Littman and E. M. Fenyö, *J. Virol.*, 1997, **71**, 7478–87.
  - 27 C. F. Cho, B. Behnam Azad, L. G. Luyt and J. D. Lewis, *ACS Comb. Sci.*, 2013, **15**, 393–400.
  - 28 K. F. Medzihradzky and R. J. Chalkley, *Mass Spectrom. Rev.*, 2015, **34**, 43–63.
  - 29 A. Semmler, R. Weber, M. Przybylski and V. Wittmann, *J. Am. Soc. Mass Spectrom.*, 2010, **21**, 215–219.
  - 30 B. Meyer, D. G. Papisotiriou and M. Karas, *Amino Acids*, 2011, **41**, 291–310.
  - 31 A. B. MacConnell, P. J. McEnaney, V. J. Cavett and B. M. Paegel, *ACS Comb. Sci.*, 2015, **17**, 518–534.
  - 32 J. Vastl, T. Wang, T. B. Trinh and D. A. Spiegel, *ACS Comb. Sci.*, 2017, **19**, 255–261.

## Chapter 3

### 3 A Compact and Synthetically Accessible Fluorine-18 Labelled Cyclooctyne Prosthetic Group for Labelling of Biomolecules by Copper-free Click Chemistry

#### 3.1 Introduction

Positron emission tomography (PET) is an important molecular imaging technique used to non-invasively visualize and diagnose many different biological events and pathologies.<sup>1</sup> The use of fluorine-18 as a PET radionuclide is popular due to its relatively long half life (~110 minutes) among non-metallic isotopes, allowing ample time for radiosynthesis as well as other favourable nuclear and chemical properties.<sup>2</sup> Due to its small size, fluorine-18 has been incorporated into imaging agents of various complexities from small molecules to larger biomolecules.<sup>3-5</sup> However, an important consideration is the method of incorporating the fluoride such that rapid and facile radiolabelling is achieved. Direct labelling of a molecule with fluoride-18 can require harsh nucleophilic conditions, which the biologic “targeting” portion of an agent may not withstand. Instead, small-molecule fluorine-18 prosthetic groups are labelled first and used to introduce the radionuclide to a biomolecule under milder conditions. Careful selection of these prosthetic groups is necessary to ensure that the addition does not elicit a change in biological function.

The copper-catalyzed alkyne-azide 1,3-dipolar cycloaddition (CuAAC) reaction as a form of “click chemistry” was first introduced by Sharpless in 2001.<sup>6</sup> This concept has since been widely explored in applications to label biomolecules with various imaging components under bioorthogonal conditions. The click reaction satisfies the requirement of milder reaction conditions for appending a prosthetic group to a biomolecule; it also boasts the benefits of fast reaction kinetics and lack of by-products. Because of these properties, this reaction lends itself particularly well to synthetic radiolabelling strategies for the production of nuclear imaging agents.<sup>7</sup> This is especially true for shorter-lived PET isotopes such as fluorine-18. For the use of CuAAC in *in vivo* applications, the complete removal of copper reagents remaining after reactions is necessary in order to avoid cytotoxicity issues. These extra purification steps unfortunately hinder the efficiency of the

radiosynthesis. The strain-promoted alkyne-azide cycloaddition (SPAAC) reaction is a convenient copper-free alternative to click chemistry reactions which avoids cytotoxic copper reagents.<sup>8</sup>

Both CuAAC and SPAAC have been extensively used to label biomolecules such as proteins, oligonucleotides, peptides and other targeting entities with fluorine-18.<sup>9-13</sup> In SPAAC examples, the most commonly used cyclooctynes are azadibenzocyclooctynes (ADIBOs), due to their relatively fast reaction kinetics ( $0.4-0.9 \text{ M}^{-1}\text{s}^{-1}$  depending on modifications) and long-term stability compared to other reported cyclooctynes.<sup>14-15</sup> ADIBO is commonly synthesized with an acid or amine handle, which allows for conjugation to biomolecules through standard coupling techniques (Figure 3.1A). Fortunately, there have been a wide variety of fluorine-18 azide-containing prosthetic groups developed for copper-catalyzed click reactions which are also employable with cyclooctyne-modified biomolecules, allowing for quick transition into PET imaging agents.<sup>16</sup>

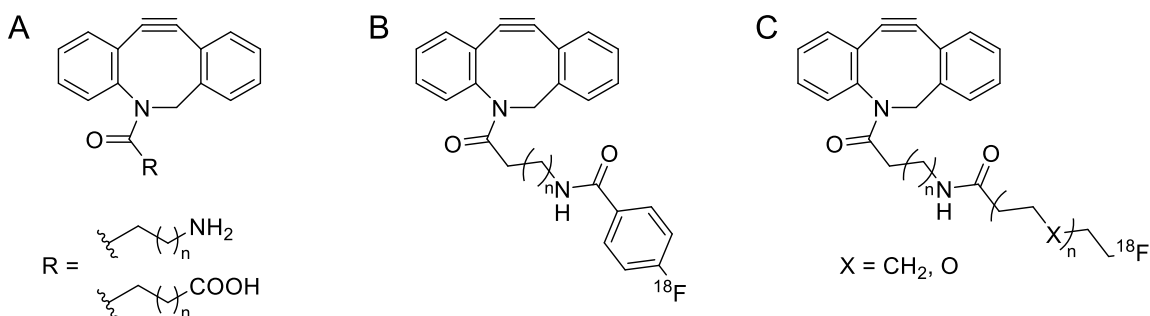


**Figure 3.1** Structures of A) non-labelled ADIBOs where R contains an acid or amine for conjugation to a biomolecule, B) ADIBOs that have been indirectly labelled with fluorine-18 and C) ADIBOs that have been further derivatized into fluorine-18 prosthetic groups.

To approach radiolabelling via the SPAAC reaction from the opposite direction, easily-accessed azide-containing biomolecules and targeting moieties can be employed. The complementary piece to this azido-derivatized biomolecule necessitates an  $^{18}\text{F}$ -labelled cyclooctyne.

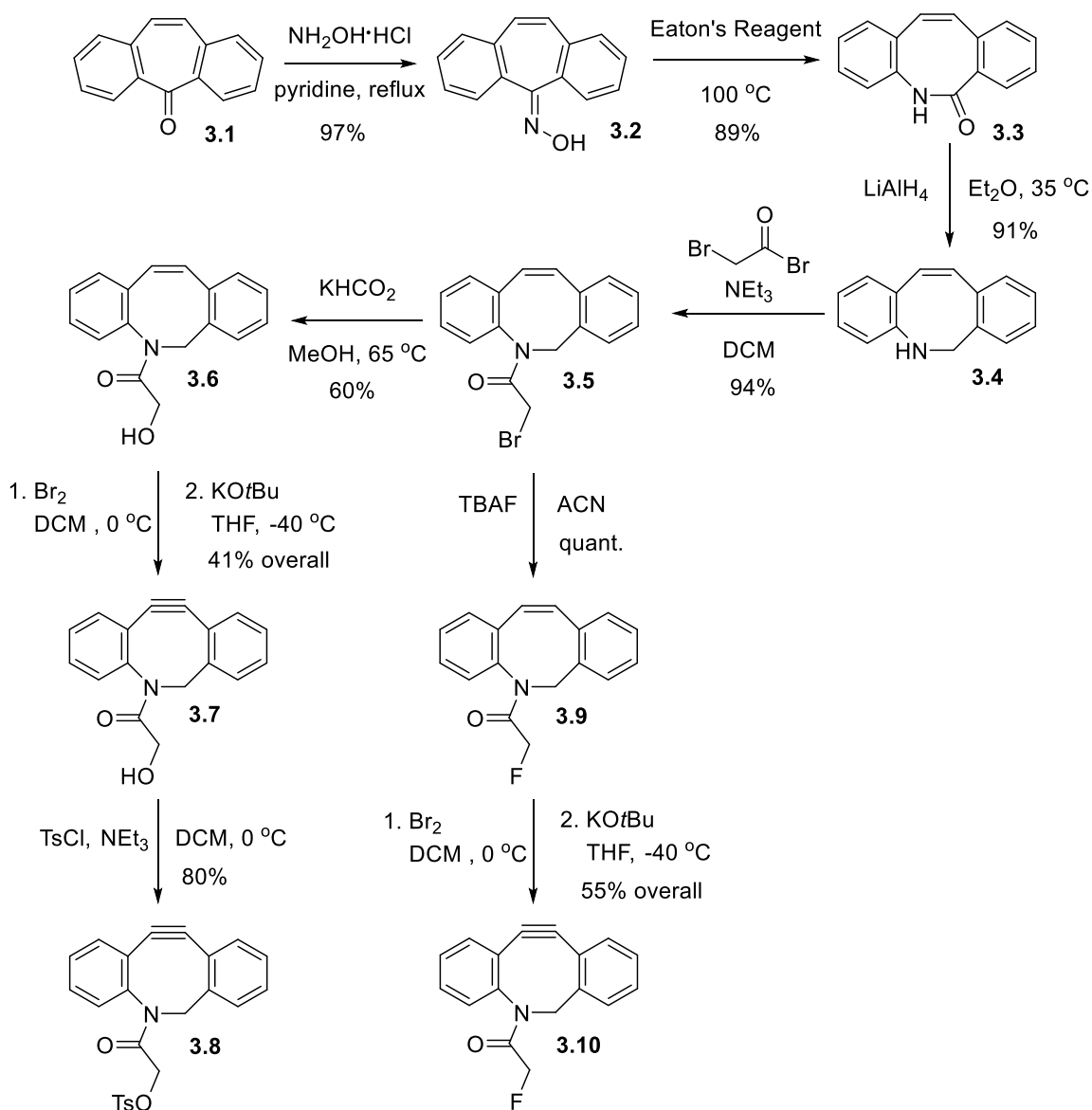
Indirect labelling of ADIBOs was first shown by using the prosthetic group 4-succinimidyl-[ $^{18}\text{F}$ ]fluorobenzoate to incorporate fluorine-18 into an amine-functionalized ADIBO (Figure 3.1B).<sup>17-18</sup> ADIBOs have also been shown to be sufficiently stable for direct fluorine-18 labelling conditions. Previous approaches in the literature make use of ADIBO-NH<sub>2</sub> by coupling a carboxylic acid-functionalized linker to the amine tail. This alkyl or PEG linker connects the ADIBO to a suitable leaving group for  $^{18}\text{F}$ -labelling of the resulting molecule (Figure 3.1C).<sup>19-20</sup> Recently, an oxodibenzocyclooctyne was labelled with fluorine-18 showing reactivity with micromolar concentrations of azide-modified bioconjugates.<sup>21</sup> While these are exciting and useful developments for the utilization of copper-free click techniques in fluorine-18 radiolabelling of peptides, these constructs can be fairly large and high in molecular-weight for a prosthetic group. Because the copper-free click reaction is not regioselective, this long tail also results in significantly different 1,4 and 1,5 regioisomers, which could affect receptor binding or pharmacokinetic properties of the imaging agent. Furthermore, the expense of ADIBO-NH<sub>2</sub> and ADIBO-COOH can be prohibitive when investigating the discovery of new imaging agents. We propose a new fluorine-containing ADIBO that seeks to: 1. simplify synthesis from inexpensive, readily-available starting materials; 2. minimize structural difference in regioisomers produced by the SPAAC reaction; 3. reduce the size and molecular weight of the prosthetic group in comparison to those previously reported.

## 3.2 Results and Discussion

### 3.2.1 Synthesis of ADIBO-F

We report a new fluorine-containing ADIBO that is synthetically accessible in nine linear steps via modifications to the Popik synthesis.<sup>22-23</sup> In brief, the inexpensive starting material dibenzosuberone **3.1** was converted to oxime **3.2**. A subsequent Beckmann rearrangement produces lactam **3.3**, which is then reduced by lithium aluminum hydride to its secondary amine **3.4**. The amine is acylated with bromoacetyl bromide to produce **3.5** with a handle for functionalization from the azadibenzocyclooctene core. Compound **3.5** is subsequently transformed into the alcohol **3.6**, which is stable to the reaction conditions used for the formation of the cyclooctyne. Bromination across the cyclooctene and subsequent elimination with potassium *tert*-butoxide produces the cyclooctyne **3.7**.

Tosylation of the alcohol to produce a suitable leaving group results in the precursor of the prosthetic group **3.8**. Conversely, the fluorine-19 standard of the prosthetic group can be formed by halide exchange of the bromide **3.5** to fluoride using tetrabutylammonium fluoride to produce **3.9**. This can be followed by a similar bromination/elimination of the cyclooctene to form the cyclooctyne **3.10** (Scheme 3.1).

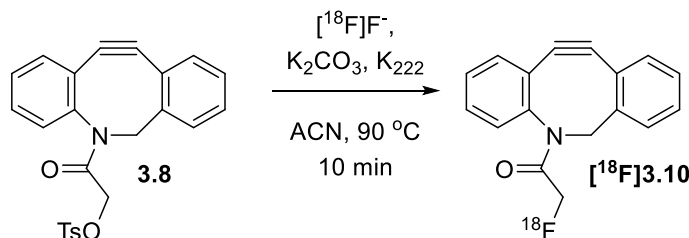


**Scheme 3.1** Branching synthesis of both ADIBO-OTs **3.8** and  $[^{19}\text{F}]$ ADIBO-F **3.10** standard via modifications to the Popik synthesis<sup>22-23</sup> of ADIBOs.



### 3.2.2 Radiolabelling of a [<sup>18</sup>F]ADIBO-F Prosthetic Group

The tosylate precursor **3.8** of this novel ADIBO has been labelled with dry [<sup>18</sup>F]fluoride under basic conditions in the presence of Kryptofix 222. The prosthetic group [<sup>18</sup>F]**3.10** was purified by semi-preparative HPLC and isolated in greater than 98% radiochemical purity to give 21-35% decay-corrected radiochemical yields in under 30 minutes of total reaction and purification time (Scheme 3.2).

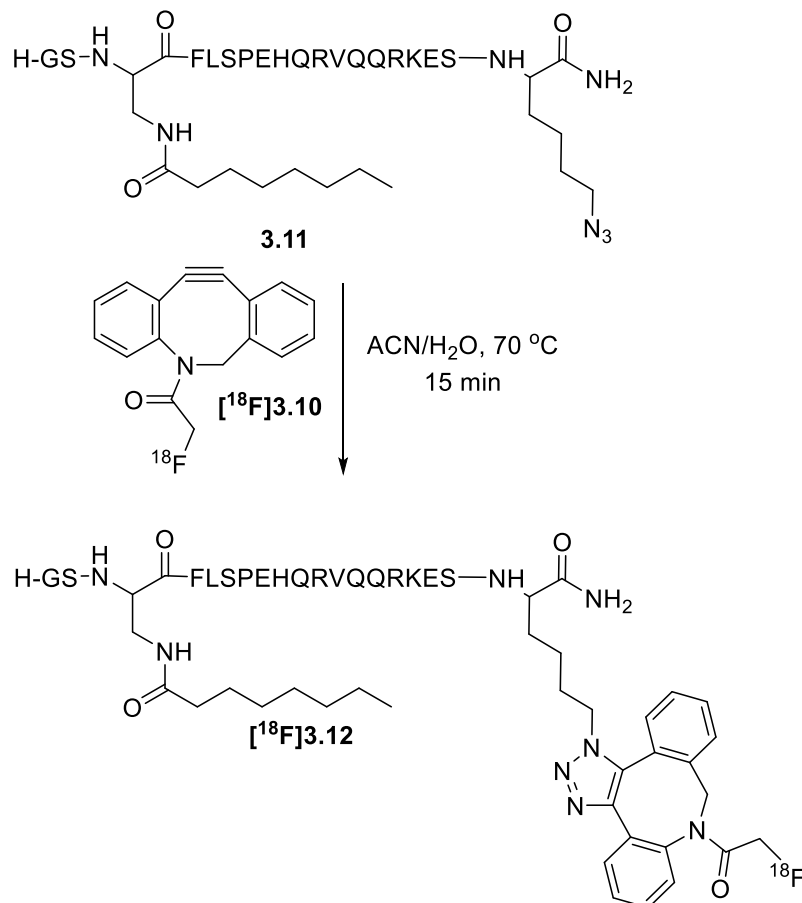


**Scheme 3.2** Radiosynthesis of [<sup>18</sup>F]ADIBO-F [<sup>18</sup>F]**3.10**.

### 3.2.3 Copper-Free Click Radiolabelling of Model Peptides using [<sup>18</sup>F]ADIBO-F

The potential for [<sup>18</sup>F]ADIBO-F [<sup>18</sup>F]**3.10** to be employed as a prosthetic group has been tested with two peptides that are known to be effective for targeting G protein-coupled receptors (GPCRs) overexpressed in a variety of cancers. The first example of using our novel prosthetic group for radiolabelling is demonstrated by incorporating it into [Dpr<sup>3</sup>(octanoyl),Lys<sup>19</sup>]ghrelin(1-19). It has been shown that peptides with various imaging moieties connected at the Lys<sup>19</sup> of this peptide sequence target the GHSR-1a receptor with nanomolar affinities.<sup>24-26</sup> By modifying Lys<sup>19</sup> to a lysine-azide (**3.11**), imaging moieties can be linked to the peptide by click reactions resulting in candidate imaging agents. Through triazole formation at the azide, our new cyclooctyne prosthetic group was linked to this peptide in 15 minutes at 70 °C, which is milder than typical nucleophilic fluoride addition conditions. The SPAAC reaction allows this labelling to proceed in neutral conditions in absence of any other reagents, and at a temperature that allows for increased reaction kinetics while ensuring peptide stability. Full radiochemical conversion was observed at this temperature with no remaining prosthetic group or production of radioactive by-products. The product, [<sup>18</sup>F][Dpr<sup>3</sup>(octanoyl),Lys<sup>19</sup>(triazole-ADIBO-F)]ghrelin(1-19) [<sup>18</sup>F]**3.12**, was isolated by semi-preparative HPLC resulting in good radiochemical yields

of 64-66% of the isolated product in greater than 98% radiochemical purities (Scheme 3.3). The SPAAC reaction was performed with quantities less than 200 MBq of the prosthetic group, resulting in molar activities of 0.6-0.9 GBq/ $\mu$ mol for the isolated product.



**Scheme 3.3** Strain-promoted alkyne-azide cycloaddition of [<sup>18</sup>F]ADIBO-F prosthetic group [<sup>18</sup>F]3.10 with an azide-modified ghrelin peptide **3.11**. Only one regioisomer of [<sup>18</sup>F]3.12 is shown for simplicity.

A non-radioactive fluorine-19 containing analogue of **3.12** was synthesized to serve as a reference standard. Co-injection of the nonradioactive standard **3.12** with the labelled peptide [<sup>18</sup>F]3.12, in addition to an overlay of the UV chromatogram for the standard and the radio-chromatogram of the labelled peptide confirms the success of the radiolabelling SPAAC reaction (Figure 3.2). Interestingly, the two regioisomers produced had no distinguishable difference in retention times, even with various HPLC gradients, reflecting the minimal structural difference between these regioisomers.

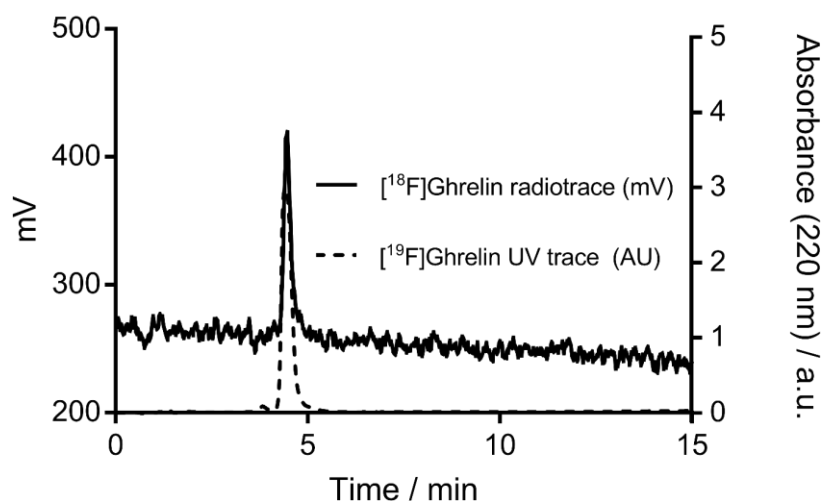


**Figure 3.2** Overlaid analytical C18 RP-HPLC chromatograms at 25 to 80% (ACN/H<sub>2</sub>O, 0.1% TFA) over 15 minutes of purified peptide [ $^{18}\text{F}$ ]**3.12** (solid trace, radiochromatogram) and its non-radioactive [ $^{19}\text{F}$ ]**3.12** analogue (dashed trace, UV chromatogram,  $\lambda = 220$  nm).

Using the nonradioactive **3.12**, an  $\text{IC}_{50}$  of 9.7 nM was obtained from a competitive binding assay for the receptor GHSR-1a. This value is comparable to that of similar known ghrelin-targeting imaging probes (9.5-25.8 nM)<sup>24-25</sup> (Figure 3.9) and shows that this peptide maintains a strong affinity for the receptor of interest with the addition of our new prosthetic group, making it potentially suitable as a cancer-targeting PET imaging probe. The stability of the fluorine towards hydrolysis was assessed using a 1 mg/mL solution of **3.12** in water at 37 °C over 24 h. No degradation of the peptide or fluoride lability was observed as indicated by HPLC-MS analysis.

In a similar manner, [D-Phe<sup>6</sup>, $\beta$ -Ala<sup>11</sup>,Phe<sup>13</sup>,Nle<sup>14</sup>]bombesin(6-14) is known to target all four of the gastrin-releasing peptide receptor (GRPR) subtypes with sub-nanomolar affinities.<sup>27</sup> An *N*-terminal modification of bombesin-targeted peptides does not disrupt affinity,<sup>28-31</sup> therefore [D-Phe<sup>6</sup>, $\beta$ -Ala<sup>11</sup>,Phe<sup>13</sup>,Nle<sup>14</sup>]bombesin(6-14) with an azido-PEG<sub>8</sub> linker on the *N*-terminus was synthesized and linked to [ $^{18}\text{F}$ ]ADIBO-F in the same process as described above resulting in full radiochemical conversion and excellent isolated

radiochemical yields for this step of 81-88%. The labelled peptide was purified by semi-preparative RP-HPLC in greater than 98% radiochemical purities and molar activities of 0.6-1.1 GBq/ $\mu$ mol. The non-radioactive standard of this peptide was used to validate the identity of the labelled peptide by co-injection and for in vitro studies (Chapter 3.4). This modified peptide-based imaging agent maintained a high affinity to the GRPR receptor with an IC<sub>50</sub> value of 0.50 nM, which is comparable to that of the unmodified bombesin peptide (0.70 nM) (Figure 3.10).

**Table 3.1** Characterization of the <sup>18</sup>F-labelled ghrelin and bombesin peptides.

<b>Peptide</b>	<sup>[18F]</sup> [Dpr <sup>3</sup> (octanoyl),Lys <sup>19</sup> (triazole-ADIBO-F)] ghrelin(1-19)	<sup>[18F]</sup> [D-Phe <sup>6</sup> , $\beta$ -Ala <sup>11</sup> ,Phe <sup>13</sup> ,Nle <sup>14</sup> ]bombesin(6-14)-PEG <sub>8</sub> (triazole-ADIBO-F)
<b>Target Receptor</b>	GHSR-1a	GRPR
<b>IC<sub>50</sub><sup>[a]</sup> (nM)</b>	9.7	0.5
<b>Azido-Peptide Concentration (mM)</b>	3.7	5.6
<b>Yields<sup>[b]</sup> (%)</b>	64-66	81-88
<b>Purities<sup>[c]</sup> (%)</b>	>98	>98
<b>Molar Activities<sup>[d]</sup> (GBq/<math>\mu</math>mol)</b>	0.6-0.9	0.6-1.1

[a] Determined using the <sup>19</sup>F standard analogue. [b] Decay-corrected radiochemical yields for isolated products. [c] Radiochemical purity by analytical RP-HPLC. [d] Determined by analytical HPLC area under the curve (AUC) at 220 nm of an aliquot of the isolated fraction. (n=3 for all values)

### 3.3 Conclusions

We have reported a novel ADIBO-F and its tosylate precursor which can be synthesized on the side chain of the ADIBO core structure with minimal additional sterics or molecular

weight. The tosylate precursor is accessible in a scalable synthetic procedure over eight steps in 15% overall yield from inexpensive starting materials via modifications to the Popik synthesis. The radiolabelling of the [ $^{18}\text{F}$ ]ADIBO-F precursor was carried out efficiently in yields of 21-35% and isolated for use as a prosthetic group in approximately an hour from fluoride-18 trapping. The availability of a minimally-sized ADIBO-based fluorine-18 prosthetic group in the radiolabelling toolbox allows for copper-free click labelling of a wide range of biomolecules and targeting moieties for PET imaging agents.

As proof-of-principle this prosthetic group's utility was shown by incorporating it into two different cancer-targeting peptides. These reactions were carried out in high yields with simple and quick purifications. The entire two-step labelling process can be performed manually within two hours including purifications resulting in good molar activities. The excellent radiochemical yields of this click reaction in mild, aqueous reaction conditions lends itself favourably to the labelling of sensitive biomolecules.

This novel cyclooctyne prosthetic group demonstrates a new, rapid labelling option for the incorporation of fluorine-18 into azide-containing biomolecules to make imaging agents.

## 3.4 Experimental

### 3.4.1 General Experimental

All reactions were carried out under a nitrogen atmosphere using oven-dried glassware. Dichloromethane (DCM) was distilled over  $\text{CaH}_2$ . Other reagents and solvents were used as received from Sigma-Aldrich, Alfa Aesar, or Fisher Scientific. Amino acids and resin were received from Peptides International or Chem. Impex. QMA carbonate SPE cartridges were purchased from Waters. [ $^{125}\text{I}$ ]-Ghrelin and [ $^{125}\text{I}$ ]Tyr<sup>4</sup>-bombesin were purchased from Perkin Elmer. Flash chromatography was performed on a Biotage Isolera Prime automated flash purification system. Biotage SNAP KP-Sil 10 g, 25 g, or 50 g cartridges (45-60 micron) were used with flow rates of 12, 25, and 50 mL/min respectively for gradient solvent systems as specified. Fractions were monitored and collected by UV absorbance using the internal UV detector set at 254 nm and 280 nm. NMR spectra were recorded on a Bruker 400 MHz Spectrometer. Chemical shifts are referenced to the residual solvent peaks and recorded in parts per million. ESI HRMS was measured on a Bruker

microOTOF 11. EI and CI HRMS was measured on a Thermo Scientific DFS (Double Focusing Sector) mass spectrometer. Peptides were purified by preparative reverse-phase HPLC-MS and analytical reverse-phase HPLC-MS was performed to assess purities. The system consists of a Waters 600 controller, Waters Prep degasser, and Waters Mass Lynx software. The UV absorbance was detected using a Waters 2998 Photodiode array detector. A preparative column (Agilent Zorbax PrepHT SB-C18 Column 21.2 x 150 mm, 5  $\mu$ m) or analytical column (Agilent Zorbax SB-C18 column 4.6 x 150 mm, 5  $\mu$ m) was used. The system runs gradients of 0.1% trifluoroacetic acid (TFA) in ACN and 0.1% TFA in water at a flow rate of 20 mL/min or 1.5 mL/min over 10 minutes with a 5 minute wash. After purification, the collected fractions were frozen at -78 °C and lyophilized.

Cyclotron-produced [ $^{18}$ F]fluoride was obtained from Dr. Mike Kovacs at the Cyclotron & PET Radiochemistry Facility at St. Joseph's Hospital in London, Ontario, Canada. Analytical radio-RP-HPLC (Agilent RP-C18 column 4.6 x 150 mm, 5  $\mu$ m) and semipreparative RP-HPLC (Agilent RP-C18 column 19 x 150 mm, 5 $\mu$ m) were performed on a Waters 1525 Binary HPLC Pump containing a Waters 2487 dual  $\lambda$  absorbance detector (292 and 220 nm), Waters InLine degasser, a gamma detector and Breeze software. This system runs gradients of 0.1% trifluoroacetic acid (TFA) in ACN and 0.1% TFA in water at a flow rate of 1.5 mL/min or 4 mL/min.

### 3.4.2 Small Molecule Synthesis

#### **5H-Dibenzo[*a,d*]cyclohepten-5-one oxime (3.2)**

Following a literature procedure,<sup>23</sup> dibenzosuberone **3.1** (7.14 g, 34.6 mmol) and hydroxylamine hydrochloride (3.60 g, 51.9 mmol) were dissolved in pyridine (30 mL) and stirred under reflux for 24 h. The reaction mixture was concentrated under reduced pressure and the residue was poured into ice cold 5% HCl (150 mL) and stirred vigorously for 30 min at 0 °C. The white precipitate was collected by filtration, washed with water, and dried *in vacuo*, yielding oxime **3.2** (7.46 g, 97%) as an off-white powder.  $^1\text{H}$  NMR (400 MHz,  $\text{CDCl}_3$ ):  $\delta$  9.32 (br s, 1 H), 7.69-7.67 (m, 1 H), 7.62-7.58 (m, 1 H), 7.46-7.34 (m, 6 H), 6.94 (d,  $J$  = 12 Hz, 1 H), 6.90 (d,  $J$  = 12 Hz, 1 H).  $^{13}\text{C}$  NMR (100 MHz,  $\text{CDCl}_3$ ):  $\delta$  156.6, 135.5, 134.6, 133.8, 130.8, 130.7, 130.5, 129.5, 129.2, 129.1, 129.0, 129.0, 128.9, 127.8, 127.7. MS (EI):  $m/z$  calculated for  $\text{C}_{15}\text{H}_{11}\text{NO}$  : 221.0841; found: 221.0821.

**Dibenzo[*b,f*]azocin-6(5*H*)-one (3.3)**

According to a procedure by Chadwick *et al.*<sup>23</sup> with slight modifications, Eaton's reagent (P<sub>2</sub>O<sub>5</sub>/MeSO<sub>3</sub>H, 20 mL) was added to a flask containing oxime **3.2** (3.00 g, 14.1 mmol). The reaction mixture was stirred at 100 °C for 2 h. The reaction was quenched with water (65 mL) and extracted into hot EtOAc multiple times. The combined organic layers were concentrated under reduced pressure and cooled. The precipitate was filtered (G4 fritted filter) and washed with cold EtOAc. The lactam **3.3** (2.63 g, 89%) was obtained as a light grey powder. <sup>1</sup>H NMR (400 MHz, CDCl<sub>3</sub>): δ 7.73 (br s, 1 H), 7.47 (dd, *J* = 7.6, 1.2 Hz, 1 H), 7.32-7.23 (m, 2 H), 7.22-7.11(m, 4H) 7.05 (dt, *J* = 7.6, 0.6 Hz, 1 H), 6.96 (d, *J* = 11.8 Hz, 1 H), 6.85 (d, *J* = 11.8 Hz, 1 H). <sup>13</sup>C NMR (100 MHz, CDCl<sub>3</sub>): δ 173.7, 135.4, 135.3, 134.8, 134.2, 133.2, 129.8, 129.7, 129.3, 128.5, 128.4, 128.2, 127.8, 127.2, 126.4. HRMS (EI): *m/z* calculated for C<sub>15</sub>H<sub>11</sub>NO : 221.0841; found: 221.0849.

**5,6-Dihydrodibenzo[*b,f*]azocine (3.4)**

From a slight modification to a procedure by Chadwick *et al.*,<sup>23</sup> a dry flask was charged with lactam **3.3** (5.00 g, 22.6 mmol) and LiAlH<sub>4</sub> (8.58 g, 226 mmol) and flushed with N<sub>2</sub>. Dry Et<sub>2</sub>O (50 mL) was added slowly and the mixture was subsequently stirred under reflux for 12 h. The reaction mixture was cooled at 0 °C, diluted with DCM (100 mL), and carefully quenched by the dropwise addition of water. Additional water was added (50 mL), and the white inorganic precipitate was removed by filtration. The organic layer was extracted from water with additional DCM, dried over MgSO<sub>4</sub>, and concentrated under reduced pressure, yielding amine **3.4** (4.25 g, 91%) as a bright yellow solid. <sup>1</sup>H NMR (400 MHz, CDCl<sub>3</sub>): δ 7.30-7.18 (m, 4 H), 7.00 (dd, *J* = 7.8, 1.6 Hz, 1 H), 6.91 (m, 1 H), 6.64 (m, 1 H), 6.56 (d, *J* = 13.3 Hz, 1 H), 6.47 (dd, *J* = 8.1, 1.2 Hz, 1 H), 6.38 (d, *J* = 13.3 Hz, 1 H), 4.58 (s, 2 H). <sup>13</sup>C NMR (100 MHz, CDCl<sub>3</sub>): δ 147.2, 139.3, 138.2, 134.8, 132.8, 130.2, 129.0, 128.0, 127.7, 127.4, 121.8, 118.0, 117.8, 49.6. HRMS (EI): *m/z* calculated for C<sub>15</sub>H<sub>13</sub>N : 207.1048; found: 207.1056.

**(*Z*)-2-bromo-1-(dibenzo[*b,f*]azocin-5(6*H*)-yl)ethenone (3.5)**

To a solution of amine **3.4** (500 mg, 2.41 mmol) and triethylamine (488 mg, 4.82 mmol) in dry DCM (10 mL), bromoacetyl bromide (973 mg, 4.82 mmol) was added dropwise. The solution was stirred for 1 h at room temperature. The reaction mixture was diluted with

DCM, and washed with 1 M HCl (3x), 2 M NaOH (3x), water and brine. The organic fraction was dried over Na<sub>2</sub>SO<sub>4</sub>, and concentrated under reduced pressure. The product **3.5** was obtained as a yellow oil (744 mg, 94%). <sup>1</sup>H NMR (400 MHz, CDCl<sub>3</sub>): δ 7.32-7.26 (m, 5H), 7.21-7.11 (m, 3H), 6.84 (d, *J* = 12.9 Hz, 1 H), 6.66 (d, *J* = 12.6 Hz, 1 H), 5.42 (d, *J* = 14.9 Hz, 1 H), 4.32 (d, *J* = 14.9 Hz, 1 H), 3.58-3.52 (m, 2 H). <sup>13</sup>C NMR (100 MHz, CDCl<sub>3</sub>): δ 166.2, 140.0, 136.6, 136.5, 133.8, 133.1, 131.6, 131.2, 130.7, 128.7, 128.7, 128.0, 128.0, 127.6, 127.5, 55.3, 27.7. HRMS (EI): *m/z* calculated for C<sub>17</sub>H<sub>14</sub>BrNO : 327.0259; found: 327.0251.

### **(Z)-1-(dibenzo[*b,f*]azocin-5(6*H*)-yl)-2-hydroxyethanone (3.6)**

A mixture of **3.5** (795 mg, 2.42 mmol) and potassium formate (1.22 g, 14.5 mmol) was refluxed in dry methanol for 12 hours. The mixture was diluted with water, extracted into DCM, was washed with brine. The organic fraction was dried over Na<sub>2</sub>SO<sub>4</sub>, and concentrated under reduced pressure. The product was isolated by automated Isolera flash column chromatography (SNAP KP-Sil cartridge, 12-100% EtOAc/Hexanes), to yield alcohol **3.6** (357 mg, 60%) as a pale yellow amorphous solid. <sup>1</sup>H NMR (400 MHz, CDCl<sub>3</sub>): δ 7.32-7.10 (m, 8 H), 6.84 (d, *J* = 12.6 Hz, 1 H), 6.62 (d, *J* = 12.6 Hz, 1 H), 5.59 (d, *J* = 14.5 Hz, 1 H), 4.37 (d, *J* = 14.9 Hz, 1 H), 3.84 (d, *J* = 14.1 Hz, 1 H), 3.43 (d, *J* = 15.5 Hz, 1 H), 3.31 (br t, *J* = 4.3 Hz, 1 H). <sup>13</sup>C NMR (100 MHz, CDCl<sub>3</sub>): δ 171.7, 137.5, 137.0, 136.1, 133.5, 133.3, 131.5, 130.6, 130.1, 129.0, 128.8, 128.1, 127.6, 127.4, 127.4, 61.1, 54.5. HRMS (CI): *m/z* calculated for C<sub>17</sub>H<sub>16</sub>NO<sub>2</sub> [M+H]<sup>+</sup> : 266.1176; found: 266.1171.

### **Prosthetic group precursor branch**

#### **1-(11,12-didehydrodibenzo[*b,f*]azocin-5(6*H*)-yl)-2-hydroxyethanone (3.7)**

A solution of alcohol **3.6** (200 mg, 0.75 mmol) in dry DCM (20 mL) was cooled to 0 °C, and bromine (116 μL, 2.26 mmol) was added dropwise. The reaction was stirred for one hour at 0 °C and then quenched with sat. aq. Na<sub>2</sub>SO<sub>3</sub>. The mixture was extracted into DCM, washed with sat. aq. Na<sub>2</sub>SO<sub>3</sub> and brine. The organic fraction was dried over Na<sub>2</sub>SO<sub>4</sub>, and concentrated under reduced pressure. The product was used without further purification.

The crude product was dissolved in dry THF (50 mL) and cooled to -40 °C. A solution of 1 M KO<sup>*t*</sup>Bu in THF (2.46 mL, 2.46 mmol) was added dropwise and the mixture was stirred



at -40 °C for 1.5 h. Another aliquot of KO<sup>t</sup>Bu in THF (0.71 mL, 0.71 mmol) was added and the mixture stirred for a further 30 minutes. The mixture was brought to room temperature and poured into 100 mL of water. The product was extracted with DCM, and the combined organic layers were washed with 1M HCl, water and brine. The organic fraction was dried over Na<sub>2</sub>SO<sub>4</sub>, and concentrated under reduced pressure. The product was isolated by automated Isolera flash column chromatography (SNAP-KP-Sil cartridge, 12-100% EtOAc/Hexanes), to yield cyclooctyne **3.7** (82 mg, 41%) as an off-white powder. <sup>1</sup>H NMR (400 MHz, CDCl<sub>3</sub>): δ 7.71 (d, *J* = 7.5, 1 H), 7.45-7.28 (m, 7 H), 5.21 (d, *J* = 14.1 Hz, 1 H), 4.20 (d, *J* = 16.0 Hz, 1 H), 3.79 (d, *J* = 14.1 Hz, 1 H), 3.40 (d, *J* = 16.0 Hz, 1 H), 2.63 (br s, 1 H). <sup>13</sup>C NMR (100 MHz, CDCl<sub>3</sub>): δ 172.6 148.8, 147.3, 132.2, 129.2, 128.7, 128.7, 128.6, 128.3, 127.6, 126.0, 123.2, 123.1, 115.0, 107.3, 60.8, 56.2. HRMS (EI): *m/z* calculated for C<sub>17</sub>H<sub>13</sub>NO<sub>2</sub> : 263.0946; found: 263.0936.

**2-(11,12-didehydridibenzo[*b,f*]azocin-5(6*H*)-yl)-2-oxoethyl 4-methylbenzenesulfonate (3.8)**

A solution of cyclooctyne **3.7** (30 mg, 0.11 mmol), tosyl chloride (32 mg, 0.17 mmol), and triethylamine (48 μL, 0.33 mmol) in DCM (5 mL) was stirred for 24 hours. The mixture was diluted with DCM, washed with 1 M HCl, water, and brine. The organic fraction was dried over Na<sub>2</sub>SO<sub>4</sub>, and concentrated under reduced pressure to yield tosylate **3.8** (40 mg, 80%) as an orange solid. The product was stored under a nitrogen atmosphere at -20 °C prior to use in radiolabelling. <sup>1</sup>H NMR (400 MHz, CDCl<sub>3</sub>): δ 7.66-7.25 (m, 10 H), 7.21 (d, *J* = 7.9 Hz, 2 H), 5.16 (d, *J* = 13.9 Hz, 1 H), 4.62 (d, *J* = 13.9 Hz, 1 H), 4.07 (d, *J* = 13.9 Hz, 1 H), 3.67 (d, *J* = 13.9 Hz, 1 H), 2.39 (s, 3 H). <sup>13</sup>C NMR (100 MHz, CDCl<sub>3</sub>): δ 165.0, 149.4, 147.0, 145.0, 132.7, 132.6, 129.8, 129.2, 128.9, 128.5, 128.4, 128.2, 128.1, 127.7, 125.8, 123.3, 122.9, 115.3, 107.5, 65.7, 56.0, 21.8. HRMS (EI): *m/z* calculated for C<sub>24</sub>H<sub>19</sub>NO<sub>4</sub>S : 417.1035; found: 417.1031.

**Standard branch**

**(*Z*)-1-(dibenzo[*b,f*]azocin-5(6*H*)-yl)-2-fluoroethanone (3.9)**

To a solution of **3.5** (736 mg, 2.25 mmol) in acetonitrile (10 mL), a 1 M solution of TBAF in THF (4.50 mL, 4.50 mmol) was added dropwise. The reaction was stirred overnight and

then solvent was removed under reduced pressure. The organic fraction was dissolved in DCM, washed repeatedly with water, dried over Na<sub>2</sub>SO<sub>4</sub> and concentrated under reduced pressure. The product was isolated by automated Isolera flash column chromatography (SNAP-KP-Sil cartridge, 12-100% EtOAc/Hexanes), and **3.9** was obtained as a yellow solid (600 mg, quant.). <sup>1</sup>H NMR (400 MHz, CDCl<sub>3</sub>): δ 7.32-7.10 (m, 8 H), 6.86 (d, *J* = 12.6 Hz, 1 H), 5.56 (d, *J* = 14.9 Hz, 1 H), 4.62 (dd, *J* = 47.4, 13.8 Hz, 1 H), 4.32 (d, *J* = 15.3, 1 H), 4.31 (dd, *J* = 46.8, 13.9 Hz, 1 H). <sup>13</sup>C NMR (100 MHz, CDCl<sub>3</sub>): δ 166.4 (d, <sup>2</sup>*J*<sub>CF</sub> = 20 Hz), 137.9, 136.8, 136.2, 133.5, 131.4, 130.9, 130.4, 128.9, 128.8, 127.9, 127.6, 127.4, 127.3, 79.1 (d, <sup>1</sup>*J*<sub>CF</sub> = 177 Hz), 54.2. HRMS (EI): *m/z* calculated for C<sub>17</sub>H<sub>14</sub>FNO : 267.1059; found: 267.1056.

### **1-(11,12-didehydrodibenzo[*b,f*]azocin-5(6*H*)-yl)-2-fluoroethanone (3.10)**

A solution of **3.9** (600 mg, 2.25 mmol) in dry DCM (40 mL) was cooled to 0 °C, and bromine (346 μL, 6.75 mmol) was added dropwise. The reaction was stirred for one hour at 0 °C and then quenched with sat. aq. Na<sub>2</sub>SO<sub>3</sub>. The mixture was extracted into DCM, washed with sat. aq. Na<sub>2</sub>SO<sub>3</sub> and brine. The organic fraction was dried over Na<sub>2</sub>SO<sub>4</sub>, and concentrated under reduced pressure. The product was used without further purification.

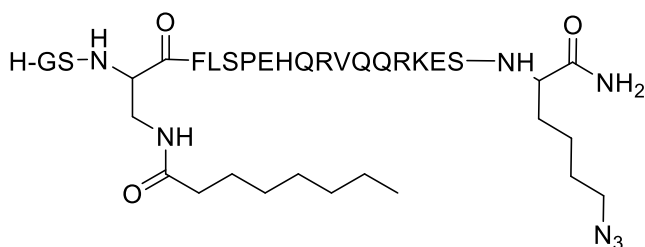
The crude product was dissolved in dry THF (50 mL) and cooled to -40 °C. A solution of 1 M KO<sup>*t*</sup>Bu in THF (7.00 mL, 7.00 mmol) was added dropwise and the mixture was stirred at -40 °C for 1.5 h. Another aliquot of KO<sup>*t*</sup>Bu in THF (2.00 mL, 2.00 mmol) was added and the mixture stirred for a further 30 minutes. The mixture was brought to room temperature and poured into 100 mL of water. The product was extracted with DCM, and the combined organic layers were washed with water and brine. The organic fraction was dried over Na<sub>2</sub>SO<sub>4</sub>, and concentrated under reduced pressure. The product was isolated by automated Isolera flash column chromatography (SNAP-KP-Sil cartridge, 12-100% EtOAc/Hexanes), to yield cyclooctyne **3.10** (380 mg, 55%) as a yellow solid. <sup>1</sup>H NMR (400 MHz, CDCl<sub>3</sub>): δ 7.72 (d, *J* = 7.5, 1 H), 7.44-7.26 (m, 7 H), 5.23 (d, *J* = 13.9 Hz, 1 H), 4.85 (dd, *J* = 47.3, 13.5 Hz, 1 H), 4.34 (dd, *J* = 46.9, 13.5 Hz, 1 H), 3.71 (d, *J* = 13.9 Hz, 1 H). <sup>13</sup>C NMR (100 MHz, CDCl<sub>3</sub>): δ 167.1 (d, <sup>2</sup>*J*<sub>CF</sub> = 20 Hz), 149.3, 147.1, 132.6, 129.0, 128.7, 128.6, 128.2, 128.2, 127.6, 125.6, 123.2, 123.0, 115.4, 107.5, 78.9 (d, <sup>1</sup>*J*<sub>CF</sub> = 177 Hz), 55.8. HRMS (EI): *m/z* calculated for C<sub>17</sub>H<sub>12</sub>FNO : 265.0903; found: 265.0893.

### 3.4.3 Peptide Synthesis

Dpr<sup>3</sup>(alloc),Lys<sup>19</sup>(N<sub>3</sub>)-ghrelin(1-19) and (D-Phe<sup>6</sup>,β-Ala<sup>11</sup>,Phe<sup>13</sup>,Nle<sup>14</sup>)-Bombesin(6-14) peptides were synthesized using standard Fmoc SPPS conditions on the Biotage SyroWave automated peptide synthesizer. Fmoc-protected Rink amide MBHA resin was used as a solid support after swelling in DCM. Fmoc removal was achieved using 40% piperidine in dimethylformamide (DMF) over two steps (30 sec and 12 min). Amino acids were coupled with 4 equivalents of the Fmoc-protected amino acid, 4 equivalents of HCTU and 8 equivalents of *N,N*-diisopropylethylamine (DIPEA) in DMF/*N*-methyl pyrrolidinone (NMP) over 1 hour. Alloc removal was achieved with 24 equivalents of phenylsilane and 0.1 equivalents of tetrakis(triphenylphosphine) palladium (0) in dry DCM. Octanoic acid was manually coupled to the diaminopropionic acid side chain using 3 equivalents of octanoic acid, 3 equivalents of HCTU and 6 equivalents of DIPEA in DMF. N<sub>3</sub>-(PEG)<sub>7</sub>-COOH (NovaBioChem) was manually coupled to the N-terminus of (D-Phe<sup>6</sup>,β-Ala<sup>11</sup>,Phe<sup>13</sup>,Nle<sup>14</sup>)-bombesin(6-14) using the above standard coupling conditions.

Full cleavage of the azido-peptides from resin along with removal of side chain protecting groups was achieved with a solution of TFA (95%), triisopropylsilane (TIPS) (2.5%), and water (2.5%) over 5 h. The cleaved peptide was precipitated in cold *tert*-butyl methyl ether (TBME) and centrifuged at 3000 rpm for 15 min. The TBME was decanted, the peptide dissolved in water, frozen at -78 °C and lyophilized. The azido-peptides were then purified by preparative reverse-phase HPLC-MS over a gradient of 30-80% acetonitrile (0.1% TFA) in water (0.1% TFA). The peptides were isolated in >98% purity by analytical RP-HPLC.

#### Dpr<sup>3</sup>(octanoyl),Lys<sup>19</sup>(N<sub>3</sub>)-ghrelin(1-19) (3.11)



HRMS (ESI):  $m/z$  calculated for C<sub>102</sub>H<sub>168</sub>N<sub>36</sub>O<sub>30</sub> [M + H]<sup>+</sup>: 2378.2805; found: 2378.2839.

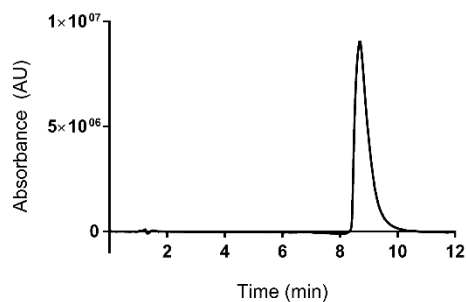
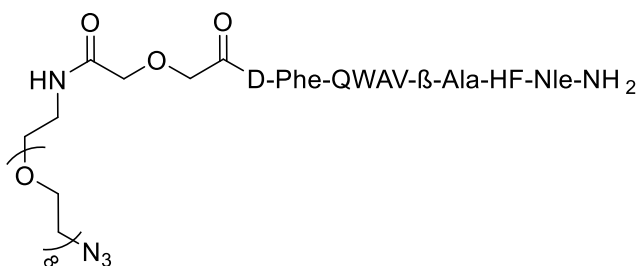


**Figure 3.3** Analytical UV chromatogram from RP-HPLC of purified **3.11** (25-80% ACN/H<sub>2</sub>O, 0.1% TFA, 10 minutes, RT = 8.69 min).

**(D-Phe<sup>6</sup>,β-Ala<sup>11</sup>,Phe<sup>13</sup>,Nle<sup>14</sup>)-Bombesin(6-14)-PEG<sub>8</sub>(N<sub>3</sub>)**



HRMS (ESI):  $m/z$  calculated for C<sub>79</sub>H<sub>117</sub>N<sub>18</sub>O<sub>21</sub> [M + H]<sup>+</sup>: 1653.8641; found: 1653.8605.

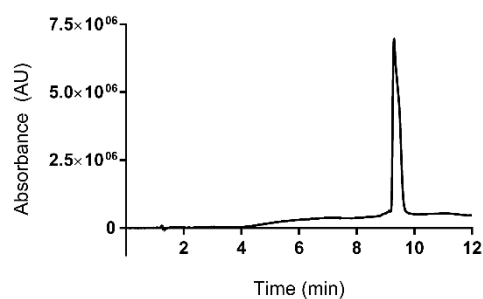
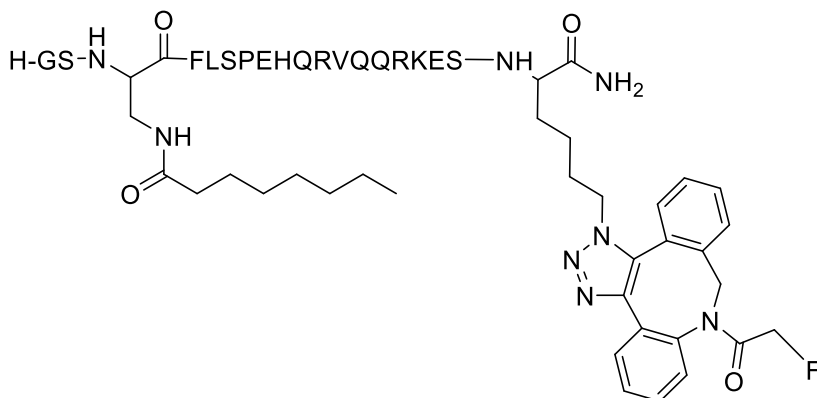


**Figure 3.4** Analytical UV chromatogram from RP-HPLC of purified (D-Phe<sup>6</sup>,β-Ala<sup>11</sup>,Phe<sup>13</sup>,Nle<sup>14</sup>)-Bombesin(6-14)-PEG<sub>8</sub>(N<sub>3</sub>) (30-85% ACN/H<sub>2</sub>O, 0.1% TFA, 10 minutes, RT = 9.30 min).

**Dpr<sup>3</sup>(octanoyl),Lys<sup>19</sup>(triazole-ADIBO-F)-ghrelin(1-19) ([<sup>19</sup>F]3.12)**



Azido-ghrelin peptide **3.11** (10 mg, 3.39  $\mu\text{mol}$ ) was dissolved in 1 mL of a 3:2 EtOH/H<sub>2</sub>O solution. ADIBO-F **3.10** (1 mg, 3.77  $\mu\text{mol}$ ) was added and the solution was stirred for 5 hours, diluted with water, frozen and lyophilized. The peptide was purified by preparative RP-HPLC, with no difference in retention time between the two regioisomers (25-80% ACN/H<sub>2</sub>O, 0.1% TFA). The non-radioactive fluorine-19 containing ghrelin standard [<sup>19</sup>F]**3.12** was obtained (4 mg, 37%, >98% purity by analytical HPLC) as a 5·TFA salt. One regioisomer of **3.12** is shown. HRMS (ESI):  $m/z$  calculated for C<sub>119</sub>H<sub>181</sub>FN<sub>37</sub>O<sub>31</sub> [M + H]<sup>+</sup>: 2643.3708; found: 2643.3582.

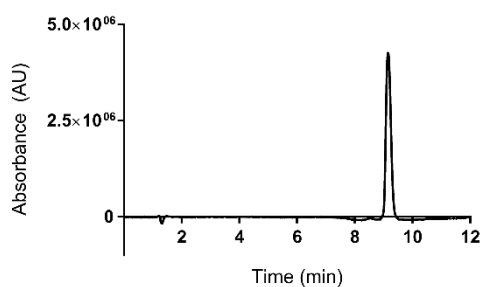
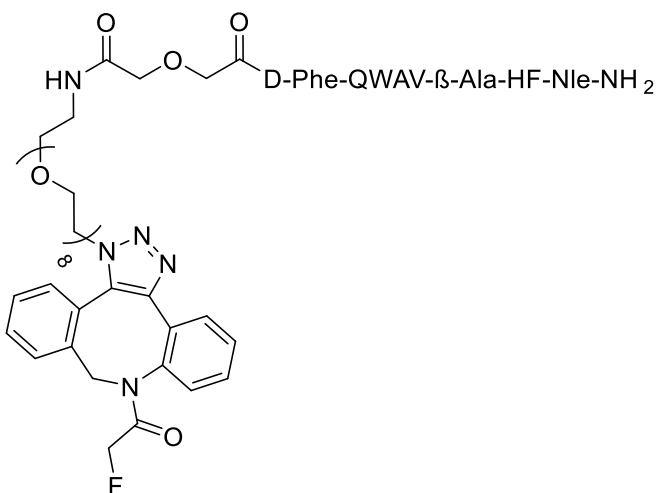


**Figure 3.5** Analytical UV chromatogram from RP-HPLC of purified [<sup>19</sup>F]**3.12** (25-80% ACN/H<sub>2</sub>O, 0.1% TFA, 10 minutes, RT = 9.15 min).

**(D-Phe<sup>6</sup>,β-Ala<sup>11</sup>,Phe<sup>13</sup>,Nle<sup>14</sup>)-Bombesin(6-14)-PEG<sub>8</sub>(triazole-ADIBO-F)**



Azido-bombesin peptide (6 mg, 3.39  $\mu\text{mol}$ ) was dissolved in 1 mL of a 3:2 EtOH/H<sub>2</sub>O solution. ADIBO-F **3.10** (1 mg, 3.77  $\mu\text{mol}$ ) was added and the solution was stirred for 5 hours, diluted with water, frozen and lyophilized. The peptide was purified by preparative RP-HPLC, with no difference in retention time between the two regioisomers (25-80% ACN/H<sub>2</sub>O, 0.1% TFA). The non-radioactive fluorine-19 containing bombesin standard was obtained (2 mg, 30%, >98% purity by analytical HPLC) as a TFA salt. One regioisomer is shown. HRMS (ESI):  $m/z$  calculated for C<sub>96</sub>H<sub>129</sub>FN<sub>19</sub>O<sub>22</sub> [M + H]<sup>+</sup>: 1918.9544; found: 1918.9551.

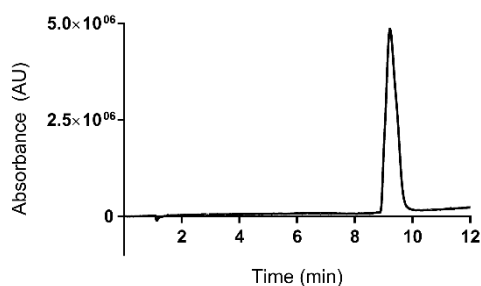


**Figure 3.6** Analytical UV chromatogram from RP-HPLC of purified (D-Phe<sup>6</sup>,β-Ala<sup>11</sup>,Phe<sup>13</sup>,Nle<sup>14</sup>)-Bombesin(6-14)-PEG<sub>8</sub>(triazole-ADIBO-F) (35-80% ACN/H<sub>2</sub>O, 0.1% TFA, 10 minutes, RT = 9.22 min).

### 3.4.4 Radiochemistry

All radiochemical yields are determined for the isolated product and are decay-corrected. All radiochemical purities are determined by radio-HPLC analysis of the isolated product.

Fluorine-18 was trapped on a Waters QMA carbonate SepPak. The activity was eluted into a vial with a solution of 2 mg potassium carbonate and 8 mg of kryptofix 222 in 200  $\mu$ L of MilliQ water and 800  $\mu$ L of ACN. The solution was evaporated to dryness on a Biotage Speed Rotary Evaporator and further dried azeotropically with 1 mL of ACN, repeated twice. The dried fluoride-18 was then transferred in two 150  $\mu$ L washes of ACN to a reaction vial containing 1 mg of the tosylate precursor **8**. This was allowed to react at 80  $^{\circ}$ C for 10 minutes. The crude reaction mixture was then diluted with 300  $\mu$ L of MilliQ water and loaded onto a semi-preparative column (50% ACN/H<sub>2</sub>O 0.1% TFA). The ADIBO-F prosthetic group [<sup>18</sup>F]**3.10** was isolated in 21-35% decay-corrected radiochemical yields in greater than 98% purity. The identity of [<sup>18</sup>F]**3.10** was confirmed by co-injection with the non-radioactive standard **3.10** showing a consistent retention time of 6.5 minutes.

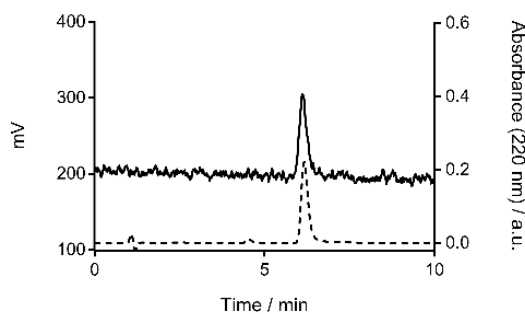


**Figure 3.7** Overlaid analytical RP-HPLC UV chromatogram at 220 nm of [<sup>19</sup>F]**3.10** (dashed) and radio-chromatogram of [<sup>18</sup>F]**3.10** (solid) (50% ACN/H<sub>2</sub>O 0.1% TFA).

[<sup>18</sup>F]ADIBO-F [<sup>18</sup>F]**3.10** collected semi-preparatively was dried on a Biotage Speed Rotary Evaporator. To this vial, 2 mg of either Dpr<sup>3</sup>(octanoyl)Lys<sup>19</sup>(N<sub>3</sub>)-ghrelin(1-19) (**3.11**) or (D-Phe<sup>6</sup>, $\beta$ -Ala<sup>11</sup>,Phe<sup>13</sup>,Nle<sup>14</sup>)-bombesin(6-14)-PEG<sub>8</sub>(N<sub>3</sub>) in 200  $\mu$ L of a 1:1 solution of MilliQ water and ACN was added. This was heated at 70  $^{\circ}$ C for 15 minutes. The crude reaction mixture was diluted with 300  $\mu$ L of MilliQ water and loaded onto a

semipreparative column (25 to 80% ACN/H<sub>2</sub>O, 0.1% TFA) In either case, retention time between regioisomers was indistinguishable. The labelled peptides were isolated in 64-66% ([<sup>18</sup>F]**3.12**) or 81-88% decay-corrected radiochemical yields, respectively, with greater than 98% radiochemical purity. Their identities were confirmed by analytical HPLC co-injection with their nonradioactive analogues with consistent retention times at 4.5 or 6.6 minutes, respectively.

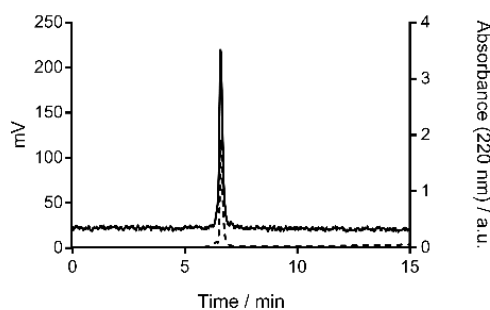


**Figure 3.8** Overlaid analytical RP-HPLC UV chromatogram at 220 nm of standard (D-Phe<sup>6</sup>,β-Ala<sup>11</sup>,Phe<sup>13</sup>,Nle<sup>14</sup>)-Bombesin(6-14)-PEG<sub>8</sub>(triazole-ADIBO-F) (dashed) and radiochromatogram of [<sup>18</sup>F](D-Phe<sup>6</sup>,β-Ala<sup>11</sup>,Phe<sup>13</sup>,Nle<sup>14</sup>)-Bombesin(6-14)-PEG<sub>8</sub>(triazole-ADIBO-F) (solid) (25 to 80% ACN/H<sub>2</sub>O, 0.1% TFA).

Molar activities for the isolated labelled peptides were determined based on the area under the curve (AUC) for the UV absorption at 220 nm. A calibration curve for each peptide was constructed from varying concentrations of the nonradioactive analogue ( $R^2 > 0.99$ ). For the ghrelin peptide, 10 μL of 0.0125-0.5 mg/mL solutions of [<sup>19</sup>F]**3.12** were injected onto an analytical column running a gradient of 25 to 80% (ACN/H<sub>2</sub>O, 0.1% TFA) over 15 minutes. For the bombesin peptide, 10 μL of 0.0125-0.1 mg/mL solutions were injected onto an analytical column running a gradient of 25 to 80% (ACN/H<sub>2</sub>O, 0.1% TFA) over 15 minutes. Molar activities for the isolated labelled peptides were then determined from the total activity collected and volume of the fraction collected semipreparatively, and the AUC for a 10 μL aliquot of the collected fraction run on the same gradient. This gave rise to molar activities of 0.6-0.9 GBq/μmol for [<sup>18</sup>F]**3.12**, and 0.6-1.1 GBq/μmol for the labelled bombesin peptide.



### 3.4.5 *In Vitro* Competitive Binding Assays

#### **GHSR-1a**

*In vitro* GHSR-1a affinity for [<sup>19</sup>F]**3.12** was determined through a competitive binding assay using HEK293 cells transiently transfected to express GHSR-1a and [<sup>125</sup>I]Ghrelin as the GHSR-1a-specific radioligand. The compound of interest (30 μL, at concentrations ranging from 10<sup>-11</sup> to 10<sup>-5</sup> M) and 15,000 cpm of [<sup>125</sup>I]Ghrelin were mixed with the binding buffer (25 mM HEPES, 0.4% BSA, 5 mM MgCl<sub>2</sub>, 1 mM CaCl<sub>2</sub>, 1 mM EDTA in H<sub>2</sub>O, pH 7.4) in 1.5 mL Eppendorf vials. A suspension of 50,000 HEK293 cells in 50 μL binding buffer was added to each vial to give a final volume of 300 μL.

#### **GRPR**

*In vitro* GRPR affinity for the standard (D-Phe<sup>6</sup>,β-Ala<sup>11</sup>,Phe<sup>13</sup>,Nle<sup>14</sup>)-bombesin(6-14) and (D-Phe<sup>6</sup>,β-Ala<sup>11</sup>,Phe<sup>13</sup>,Nle<sup>14</sup>)-bombesin(6-14)PEG<sub>8</sub>(triazole-ADIBO-F) was determined through a competitive binding assay using PC-3 cells and [<sup>125</sup>I]Tyr<sup>4</sup>-Bombesin as the GRPR-specific radioligand. PC-3 cells were grown in Ham's F-12K medium supplemented with 10% fetal bovine serum. The compound of interest (30 μL, at concentrations ranging from 10<sup>-12</sup> to 10<sup>-5</sup> M) and 20,000 cpm of [<sup>125</sup>I]Tyr<sup>4</sup>-Bombesin were mixed with the binding buffer (25 mM HEPES, 0.4% BSA, 5 mM MgCl<sub>2</sub>, 1 mM CaCl<sub>2</sub>, 1 mM EDTA in H<sub>2</sub>O, pH 7.4) in 1.5 mL Eppendorf vials. A suspension of 500,000 PC-3 cells in 50 μL binding buffer was added to each vial to give a final volume of 300 μL.

In each binding assay the vials were shaken at 550 rpm for 20 minutes at 37 °C. Immediately after the incubation, the vials were centrifuged at 13,000 xg, and the supernatant removed. The cell pellet was washed with 500 μL of 50 mM Tris buffer (pH 7.4), centrifuged again, and the supernatant was removed. The amount of [<sup>125</sup>I]-radioligand bound to the cells was measured using a gamma counter (Perkin-Elmer). IC<sub>50</sub> values were determined by nonlinear regression analysis to fit a 4-parameter dose response curve using GraphPad Prism (Version 6.0c). All data points were obtained in triplicate. IC<sub>50</sub> values were as follows: [<sup>19</sup>F]**3.12**, 9.7 nM; (D-Phe<sup>6</sup>,β-Ala<sup>11</sup>,Phe<sup>13</sup>,Nle<sup>14</sup>)-bombesin(6-14)PEG<sub>8</sub>(triazole-ADIBO-F), 0.50 nM; and (D-Phe<sup>6</sup>,β-Ala<sup>11</sup>,Phe<sup>13</sup>,Nle<sup>14</sup>)-bombesin(6-14), 0.70 nM.

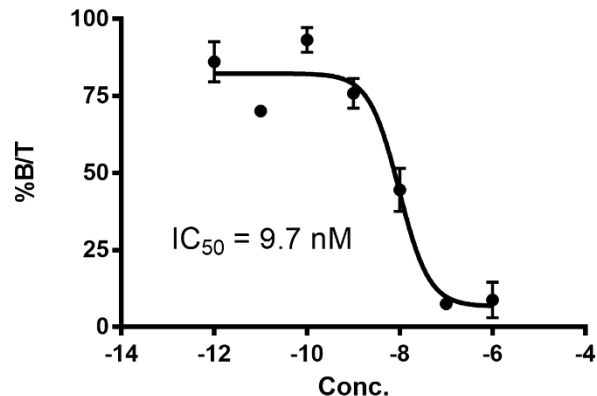


**Figure 3.9** Binding curve for the competitive binding assay of  $[^{19}\text{F}]\mathbf{3.12}$  in HEK293-GHSR-1a cells. The  $\text{IC}_{50}$  value determined was 9.7 nM.

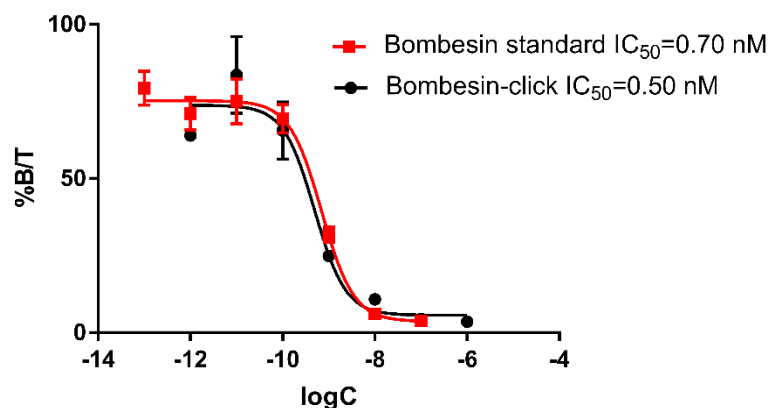


**Figure 3.10** Binding curves for the competitive binding assay of standard (D-Phe<sup>6</sup>, $\beta$ -Ala<sup>11</sup>,Phe<sup>13</sup>,Nle<sup>14</sup>)-bombesin(6-14) (red), and of (D-Phe<sup>6</sup>, $\beta$ -Ala<sup>11</sup>,Phe<sup>13</sup>,Nle<sup>14</sup>)-bombesin(6-14)PEG<sub>8</sub>(triazole-ADIBO-F) (black) with PC3 cells. The  $\text{IC}_{50}$  values determined were 0.70 and 0.50 nM, respectively.

### 3.5 References

- 1 M. L. James, S. S. Gambhir, *Physiol. Rev.*, 2012, **92**, 897-965.
- 2 D. Le Bars, *J. Fluorine Chem.*, 2006, **127**, 1488-1493.
- 3 T. Ido, C. N. Wan, V. Casella, J. S. Fowler, A. P. Wolf, M. Reivich, D. E. Kuhl, *J. Label. Compd. Radiopharm.*, 1978, **14**, 175-183.

- 4 J. R. Grierson, A. F. Shields, *Nucl. Med. Biol.*, 2000, **27**, 143-156.
- 5 R. Haubner, H.-J. Wester, W. A. Weber, C. Mang, S. I. Ziegler, S. L. Goodman, R. Senekowitsch-Schmidtke, H. Kessler, M. Schwaiger, *Cancer Res.*, 2001, **61**, 1781-1785.
- 6 H. C. Kolb, M. G. Finn, K. B. Sharpless, *Angew. Chem. Int. Ed.*, 2001, **40**, 2004-2021.
- 7 J.-P. Meyer, P. Adumeau, J. S. Lewis, B. M. Zeglis, *Bioconjug. Chem.*, 2016, **27**, 2791-2807.
- 8 N. J. Agard, J. A. Prescher, C. R. Bertozzi, *J. Am. Chem. Soc.*, 2004, **126**, 15046-15047.
- 9 T. Ramenda, R. Bergmann, F. Wuest, *Lett. Drug Des. Discovery*, 2007, **4**, 279-285.
- 10 L. S. Campbell-Verduyn, L. Mirfeizi, A. K. Schoonen, R. A. Dierckx, P. H. Elsinga, B. L. Feringa, *Angew. Chem. Int. Ed.*, 2011, **50**, 11117-11120.
- 11 T. Ramenda, T. Kniess, R. Bergmann, J. Steinbach, F. Wuest, *Chem. Commun.*, 2009, **0**, 7521-7523.
- 12 K. Sachin, V. H. Jadhav, E. M. Kim, H. L. Kim, S. B. Lee, H. J. Jeong, S. T. Lim, M. H. Sohn, D. W. Kim, *Bioconjug. Chem.*, 2012, **23**, 1680-1686.
- 13 L. Wang, O. Jacobson, D. Avdic, B. H. Rotstein, I. D. Weiss, L. Collier, X. Chen, N. Vasdev, S. H. Liang, *Angew. Chem. Int. Ed.*, 2015, **54**, 12777-12781.
- 14 M. F. Debets, S. S. van Berkel, S. Schoffelen, F. P. J. T. Rutjes, J. C. M. van Hest, F. L. van Delft, *Chem. Commun.*, 2010, **46**, 97-99.
- 15 M. F. Debets, J. S. Prins, D. Merckx, S. S. van Berkel, F. L. van Delft, J. C. M. van Hest, F. P. J. T. Rutjes, *Org. Biomol. Chem.*, 2014, **12**, 5031-5037.
- 16 K. Kettenbach, H. Schieferstein, T. L. Ross, *BioMed. Res. Int.*, 2014, **2014**, 16.
- 17 R. D. Carpenter, S. H. Hausner, J. L. Sutcliffe, *ACS Med. Chem. Lett.*, 2011, **2**, 885-889.
- 18 V. Bouvet, M. Wuest, F. Wuest, *Org. Biomol. Chem.*, 2011, **9**, 7393-7399.
- 19 K. Kettenbach, T. L. Ross, *Med. Chem. Commun.*, 2016, **7**, 654-657.
- 20 S. Arumugam, J. Chin, R. Schirmacher, V. V. Popik, A. P. Kostikov, *Bioorg. Med. Chem. Lett.*, 2011, **21**, 6987-6991.
- 21 M. Boudjemeline, C. D. McNitt, T. A. Singleton, V. V. Popik, A. P. Kostikov, *Org. Biomol. Chem.*, 2018, **16**, 363-366.

- 22 A. Kuzmin, A. Poloukhtine, M. A. Wolfert, V. V. Popik, *Bioconjug. Chem.*, 2010, **21**, 2076-2085.
- 23 R. C. Chadwick, S. Van Gyzen, S. Liogier, A. Adronov, *Synthesis*, 2014, **46**, 669-677.
- 24 G. A. Douglas, R. McGirr, C. L. Charlton, D. B. Kagan, L. M. Hoffman, L. G. Luyt, S. Dhanvantari, *Peptides*, 2014, **54**, 81-88.
- 25 R. McGirr, M. S. McFarland, J. McTavish, L. G. Luyt, S. Dhanvantari, *Regul. Pept.*, 2011, **172**, 69-76.
- 26 C. L. Charlton, R. McGirr, S. Dhanvantari, M. Kovacs, L. Luyt, *J. Label. Compd. Radiopharm.*, 2013, **56**, S192.
- 27 T. K. Pradhan, T. Katsuno, J. E. Taylor, S. H. Kim, R. R. Ryan, S. A. Mantey, P. J. Donohue, H. C. Weber, E. Sainz, J. F. Battey, D. H. Coy, R. T. Jensen, *Eur. J. Pharmacol.*, 1998, **343**, 275-287.
- 28 R. La Bella, E. Garcia-Garayoa, M. Bahler, P. Blauenstein, R. Schibli, P. Conrath, D. Tourwe, P. A. Schubiger, *Bioconjug. Chem.*, 2002, **13**, 599-604.
- 29 K. E. Baidoo, K. S. Lin, Y. Zhan, P. Finley, U. Scheffel, H. N. Wagner, Jr., *Bioconjug. Chem.*, 1998, **9**, 218-225.
- 30 C. Van de Wiele, F. Dumont, R. A. Dierckx, S. H. Peers, J. R. Thornback, G. Slegers, H. Thierens, *J. Nucl. Med.*, 2001, **42**, 1722-1727.
- 31 C. J. Smith, G. L. Sieckman, N. K. Owen, D. L. Hayes, D. G. Mazuru, R. Kannan, W. A. Volkert, T. J. Hoffman, *Cancer Res.*, 2003, **63**, 4082-4088.

## Chapter 4

# 4 Synthesis and Screening of a Combinatorial Library of Fluorine-Integrated Peptides for PET Imaging Agent Discovery

## 4.1 Introduction

Advances in the fields involving molecular imaging are increasingly allowing for non-invasive imaging of biological processes and markers related to a variety of disease states. Imaging of specific targets can aid in diagnosis and staging of disease, as well as predicting and monitoring response to targeted treatment. This is an especially advantageous tool with the advent of personalized medicine wherein knowledge of the presence of specific biomarkers can determine course of treatment. For imaging modalities such as positron emission tomography (PET), the scope and progression of its clinical relevance depends on the development of new radiopharmaceutical agents towards an expanding variety of targets.

Peptides are especially useful as the targeting ligand component of PET radiopharmaceuticals because they are easy to synthesize and modify, have biological half-lives that match those of the radioisotopes used, and often have high specificity and selectivity towards their target.<sup>1</sup> Peptide radiopharmaceuticals can be constructed through rational design or discovered through screening campaigns of libraries of compounds. In the former, the radiopharmaceutical is designed by modifying a known ligand of the target or designing a peptide based on the microenvironment of the target. In contrast, screening campaigns can be undertaken which lead to the discovery of new targeting ligands, which is impactful when the target is unknown, there are no known ligands for a target, or those that exist do not have an appropriate pharmacokinetic profile for imaging. Common methods include high-throughput screening (HTS) of compound libraries, *in silico* screening of libraries, or screening of combinatorial libraries such as one-bead one-compound (OBOC) or phage display.

The synthesis of OBOC libraries through a split-and-mix approach creates libraries of millions of unique peptides on-resin, where each resin bead hosts multiple copies of a

single random peptide sequence.<sup>2</sup> Screening these beads against targets of interest has resulted in the successful identification of peptides targeting cancer biomarkers and other disease states.<sup>3-7</sup> Unfortunately, peptides discovered from these libraries have only rarely been converted into imaging agents, as appending an imaging moiety often leads to a decrease in the target affinity observed during the library screen.<sup>8-15</sup> An OBOC library is a useful combinatorial approach in that they are synthesized via solid-phase peptide synthesis (SPPS), and unnatural peptide modifications are trivial to include. Surprisingly, only a few descriptions exist where an imaging component was included in the synthesis of an OBOC library; in all cases, the imaging moiety was appended to a terminal of the peptides or peptoids.<sup>16-18</sup> Screening of an imaging agent library would allow for the discovery of new radiopharmaceutical imaging agents where the imaging moiety is already accounted for in target binding.

Bioconjugation through click chemistry is a popular technique for radiolabelling of PET imaging agents because of its fast reaction kinetics, physiologically friendly reaction conditions and significantly reduced byproducts.<sup>19</sup> A particularly interesting click reaction is the strain-promoted alkyne-azide cycloaddition (SPAAC) which is a substitute for traditional copper-catalyzed click chemistry reactions using strained cyclooctynes, avoiding the use of cytotoxic copper and its consequential removal thereafter.<sup>20-22</sup>

As stated previously, there is a need for new receptor-targeted PET agents, and a recent exciting target is the CXCR4 chemokine receptor that has been implicated in over 23 types of cancer.<sup>23</sup> CXCR4 has only two known endogenous ligands, SDF-1 $\alpha$  (also known as CXCL12) and ubiquitin.<sup>24</sup> Together CXCR4 and SDF-1 $\alpha$  are known to have roles in chemotactic and angiogenic pathways, which corresponds to the expression of CXCR4 in metastatic cancers. While CXCR4 is normally expressed in bone marrow, the spleen, thymus, lymph nodes, pituitary gland, and adrenal glands at low rates, its expression is significantly higher in malignant tissue compared to healthy adjacent tissues. These aspects make it an interesting target for imaging of CXCR4-expressing cancers.<sup>25</sup> Current peptide-based radiopharmaceutical imaging agents for CXCR4 were all developed from polyphemusin II, an antimicrobial peptide found in horseshoe crab extracts (*Tachypleus tridentatus*). Structure-activity studies and truncation of this peptide resulted in T140, a 14

amino acid peptide with a single disulfide bond with nanomolar affinity for CXCR4.<sup>26,27</sup> Radiolabelling of T140 with fluorine-18 has been performed on the N-terminus or the Lys<sup>7</sup> side chain with various prosthetic groups. In many cases, non-CXCR4 specific binding to red blood cells or significant liver and kidney uptake was observed which limits their utility as targeted imaging agents.<sup>28-30</sup> A novel cyclic pentapeptide, FC131, was derived from the most important binding residues of T140.<sup>31</sup> It has been modified to contain a DOTA chelator, which has been radiolabelled with <sup>68</sup>Ga (Pentixafor), and is now being explored as a tool to image a variety of CXCR4-expressing cancers in humans.<sup>32-34</sup> In the development of a fluorine-18 version of FC131, the ligand was radiolabelled via a click reaction on a side chain, but has not yet been explored for *in vivo* biodistribution or imaging.<sup>35</sup> Unsurprisingly, due to the rational design approach in which all the peptides were all derived from the same starting peptide, they have similar biodistribution properties *in vivo*. The use of combinatorial libraries could lead to the discovery of imaging agents targeting CXCR4 with a different pharmacokinetic profile (Chapter 2).

Herein, we describe an OBOC library in which fluorine has been randomly inserted within the peptide side chains. The use of converging and diverging pools during synthesis allows for the imaging component to be included exactly once in each peptide sequence. The imaging component is distributed evenly among the eight positions in the octamer peptides; the remaining seven amino acids are randomized using fifteen different natural amino acids. Screening of the library against the target CXCR4 will thus result in the discovery of peptides where the imaging component is included in ligand-target interactions. Notably, the fluorine has been incorporated into the peptide structure through a SPAAC reaction using the non-radioactive standard of a recently reported fluorine-18 prosthetic group.<sup>36</sup> This design allows for hits from the library to be simply and directly translated into their fluorine-18 counterpart for PET imaging.

## 4.2 Results and Discussion

### 4.2.1 Library Design

Although high-throughput techniques such as combinatorial OBOC libraries are effective at identifying potential ligands for receptor targeting, these technologies are rarely adapted

into the discovery of complete imaging agents.<sup>16-18</sup> By incorporating an imaging component directly into such a library, screening for target affinity will involve the entire imaging agent and no major post-screening modifications should be necessary. Our library design sought to integrate the imaging entity within the peptide structure, rather than simply appending the imaging component onto one of the peptide termini away from potential binding interactions. We chose to design a library of potential PET imaging agents, using a non-radioactive surrogate containing fluorine-19. Fluorine-19 takes the place of fluorine-18, which is an important radioisotope commonly used in PET imaging due to its half-life (~ 110 min), high abundance of positron decay and availability from cyclotrons. In addition, fluorine-18 can be incorporated into biomolecules via carbon-fluorine bonds, which has decreased bulk and increased *in vivo* stability compared to some other radiolabels. We chose to use copper-free click chemistry for simple translation of our hit peptides into imaging agents for PET imaging using SPAAC radiolabelling. We developed a relatively small fluorine-containing azadibenzocyclooctyne (ADIBO-F) that can be radiolabelled with fluorine-18 and incorporated into an azide-containing amino acid side chain to produce a cyclooctatriazole-fluorine-containing residue.<sup>36</sup> Fmoc-protected azide-containing amino acids such lysine azide are widely available commercially and therefore amenable to including in the SPPS of an OBOC library (Figure 4.1).

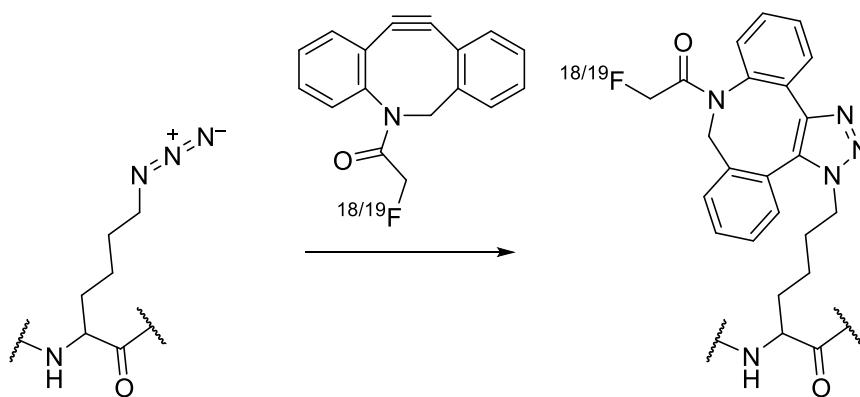


**Figure 4.1** Incorporation of an <sup>18/19</sup>F-ADIBO-F into a lysine-azide residue in a peptide.

Although amino acids in an OBOC library are traditionally incorporated equally at each coupling step, including a lysine azide in such a way could result in peptides in the library containing multiple or, more likely, zero azide functional groups, and subsequently



multiple or zero locations of the fluorine imaging component. Unfortunately, hits such as these would limit the utility of the library, as hits may have to be modified to include an imaging component after all. We decided to design an octamer library that included setting the location of the lysine azide at each of the eight residue positions. Instead of creating and screening eight separate libraries, we chose to design a two-pool technique that would allow for the synthesis of these eight “mini-libraries” at once (Figure 4.2). In brief, at each coupling step, one eighth of the initial library mass is diverted from the original pool to the lysine azide pool to ensure even distribution of the imaging component through the eight residue locations. Initially, one eighth of the library pool is separated and coupled to lysine azide. After coupling with lysine azide the beads are placed into a separate “lysine azide” pool (Figure 4.2, top cascade, pool 2). The remaining seven eighths of the library in the original pool (Figure 4.2, bottom cascade, pool 1) undergo a traditional split-and-mix step with  $n$  natural amino acids in  $n$  wells. All beads are combined in their respective separate pools for Fmoc deprotection and mixing between coupling steps. For the second coupling step, another eighth of the initial library size is separated from pool 1 and coupled to lysine azide. All remaining beads in both pools 1 and 2 undergo traditional split-and-mix steps in their respective pools. The newly azide-containing peptides are then added to the rest of the dipeptides in pool 2. This process continues for eight coupling, mixing and deprotection steps where resin switches pools after azide incorporation to ensure only a single azide is present in each library bead sequence. After eight coupling cycles, the resin is all in pool 2. At this point, each peptide in the library contains a single azide and can be conjugated to our non-radioactive ADIBO-F prosthetic group surrogate to incorporate an imaging moiety into the entire library. By using 15 amino acids for the split-and-mix steps, the theoretical library diversity is around 1.37 billion unique amino acid sequences ( $= 8 \times 15^7$ ). In 1.5 million beads, there is only around 0.1 % of the potential sequences expressed, and thus no redundancy is likely. Therefore, the result of this synthesis cascade is a library of approximately 1.5 million potential peptide-based imaging agents that should each express a different peptide sequence and contain a single imaging moiety.

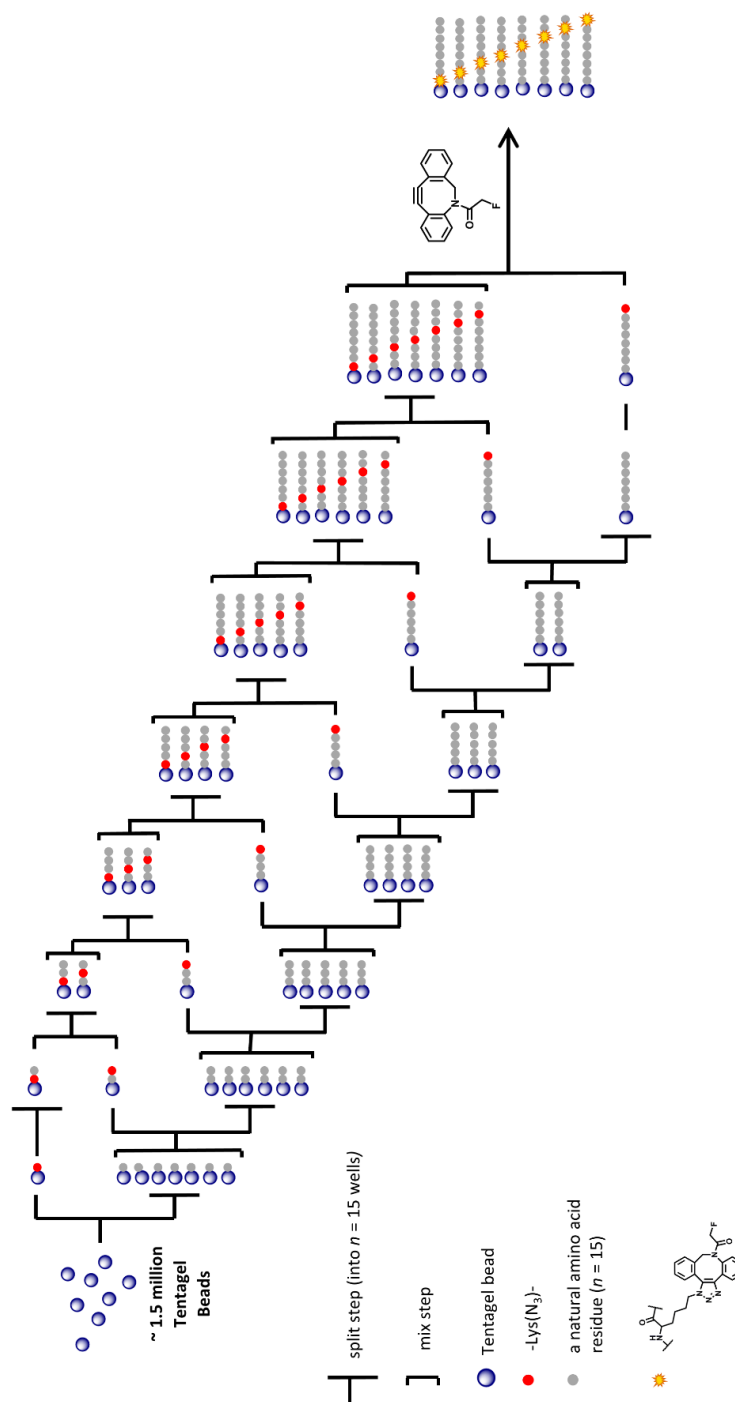


**Figure 4.2** Synthesis cascade showing two-pool split-and-mix SPPS steps to incorporate a lysine-azide into a library of octapeptides in single random position. This allows a fluorine-containing cyclooctyne (ADIBO-F) to be globally clicked to the library to produce a library of on-bead imaging agents.

### 4.2.2 Library Synthesis

The library was synthesized on one gram of amine-functionalized Tentagel resin (~1.5 million beads), due to its loading, amenability to aqueous solvents, and uniform size of beads. All peptides were linked to the resin beads using a photocleavable linker ((3-amino-3-(2-nitro-phenyl)propionic acid) (ANP)) and library synthesis and screening was performed in the dark. This linker allows the peptides to stay attached to the bead during side chain deprotection, while also allowing for cleavage from the hit beads under UV light for peptide sequence determination. The library was then synthesized using SPPS using the synthesis cascade as described above (Figure 4.2). Fifteen natural Fmoc-amino acids were used excluding those that would complicate sequencing by tandem mass spectrometry (MS/MS): tryptophan, cysteine, and methionine due to their tendency to oxidize; as well as leucine and glutamine because they are isobaric with isoleucine and lysine. All library beads were combined at the end, swelled in an acetonitrile/water mixture and 1.5 equivalents of ADIBO-F was added to afford the library of globally clicked products with a lysine(cyclooctatriazole-F) residue. Side chain protecting groups were removed with a cocktail of 95% trifluoroacetic acid (TFA), 2.5% triisopropylsilane (TIPS) and 2.5% water and the resin was washed thoroughly. To confirm complete library synthesis on-resin, eight beads were analyzed by MALDI MS/MS. Since there is an amide bond in the ADIBO prosthetic group, a  $m/z$  ratio of the peptide parent mass minus 61 Da was observed in all MS/MS spectra. This corresponds to the  $m/z$  of the entire peptide missing the 2-fluoroacetyl radical fragment of the cyclooctatriazole-F and confirming that the peptides indeed each contained a clicked triazole component (Figure 4.3).

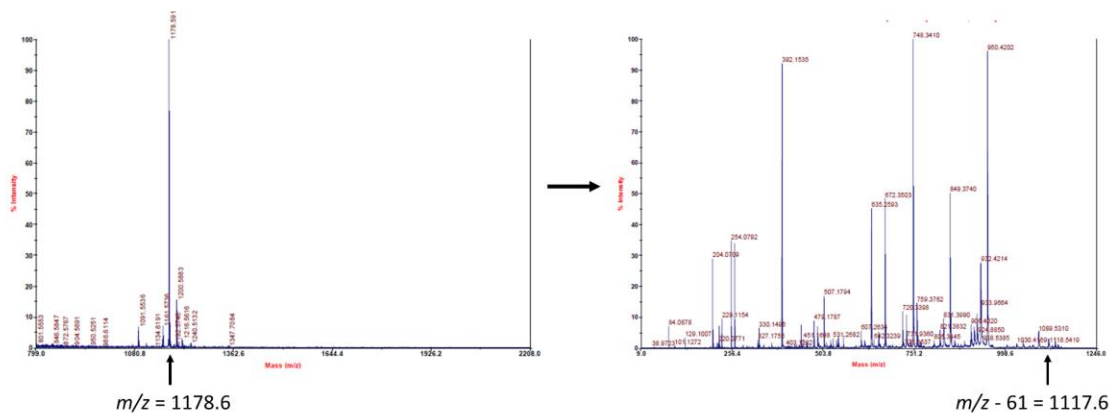


**Figure 4.3** Sample MS and MS/MS spectra demonstrating presence of an ion fragment resulting from loss of 61 Da from the parent peptide  $m/z$  to confirm inclusion of imaging component cyclooctatriazole-F.

#### 4.2.3 On-Bead Two-Colour Screen

The imaging agent library was screened by employing a two-colour method wherein the bead-hosted peptides can be screened for both affinity and selectivity to the target in a single step.<sup>37</sup> As CXCR4 was the target of choice due to its implication in over 23 cancer types, the cell lines utilized were U87.CD4.CXCR4 as a positive cell line that is transfected to overexpress the receptor of interest, and U87.CD4 as a control cell line that lacks this transfection.<sup>38</sup> To aid in visualization by fluorescence microscopy, U87.CD4.CXCR4 or U87.CD4 cells were preincubated with a CellTracker dye (ThermoFisher), Green CMFDA or Red CMTPX, respectively. In stages, the library was incubated in multiple 6-well plates at concentrations of  $\sim 10,000$  beads/well and 200,000 cells/well of each cell line in a total of 3 mL of serum-free DMEM media. The plates were shaken gently for 1 hour at 37 °C, at which point receptor-peptide interactions between the cells and beads were fixed with 4% paraformaldehyde. To stop cross-linking, glycine was added to each well, and the entire library was then combined and rinsed with water and resuspended in phosphate-buffered saline (PBS). The library was visualized by confocal fluorescence microscopy and 25 beads that displayed binding with only green fluorescent cells (dye  $\lambda_{\text{ex/em}} = 492/517$  nm) and not red fluorescent cells (dye  $\lambda_{\text{ex/em}} = 577/602$  nm) were manually isolated as CXCR4-selective hits for further investigation (Figure 4.4). Although hundreds of suitable hit beads were observed, only 25 beads which appeared to have high affinity to the target were chosen

from this screening to ease the bottleneck step of manual *de novo* sequencing to follow. The beads were rinsed with ethanol to remove bound cells, and then placed into individual wells of a 96 well plate. These hit beads were swollen in methanol and placed under a 160 W 365 nm UV lamp for 1.5 hours to afford photolysis of peptides from the beads. Photocleavage of the *o*-nitrophenyl ANP linker results in a carboxamide at the C-terminal.<sup>39</sup> The supernatant was then subjected to MALDI MS/MS for peptide sequence deconvolution.

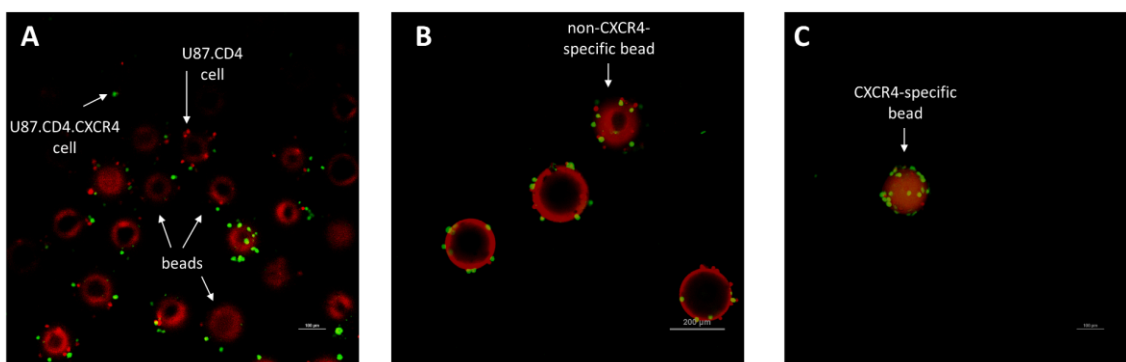


**Figure 4.4** Representative confocal fluorescence microscopy images of library Tentagel beads during two-colour screening depicting A) bulk beads B) isolated beads showing affinity for CXCR4 C) individual bead showing specificity to CXCR4.

#### 4.2.4 MALDI MS/MS *De Novo* Sequencing of Hits

MALDI MS/MS was chosen as a method of hit deconvolution due its high sensitivity and because of the cost-effectiveness for sequencing multiple peptide hits. MALDI was performed using  $\alpha$ -cyano-4-hydroxycinnamic acid (CHCA) as the matrix, the highest intensity peaks were chosen as the parent MS and fragmented to produce MS/MS spectra for each peptide. Peptides predictably fragment through the polyamide backbone in a collision cell, which allows for comparison of mass differences between ion peaks to masses of amino acid residues to determine peptide sequences (Figure 4.5).<sup>40</sup> Of the 25 peptides, six showed no MS ion in the mass range of interest for our library constructs (~1000-1500 Da) (Figure 4.8). Of the remaining, eight sequences (**4.1-4.8**) were fully deconvoluted by manual *de novo* sequencing (Table 4.1).

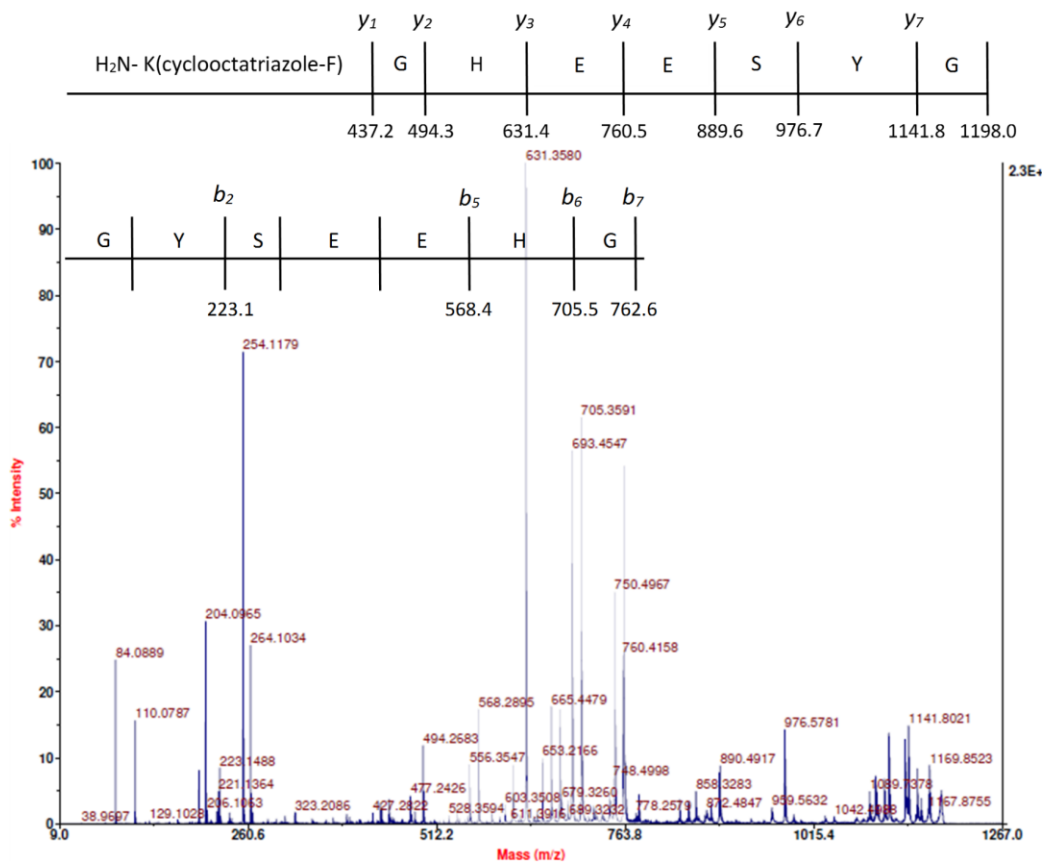


**Figure 4.5** MALDI MS/MS deconvolution of hit peptide imaging agent **4.3** showing a full y series of ions and some b series ions.

**Table 4.1** Sequences and IC<sub>50</sub> values of hit peptide structures as determined by *de novo* MS/MS sequencing. Where **X** = lysine(cyclooctatriazole-F). Peptides have a free N-terminus and an amidated C-terminus.

NUMBER	SEQUENCE	IC <sub>50</sub> (μM)
<b>4.1</b>	H- E R R H S Y H X -NH <sub>2</sub>	28
<b>4.2</b>	H- F A R Y P A S X -NH <sub>2</sub>	86
<b>4.3</b>	H- G Y S E E H G X -NH <sub>2</sub>	109
<b>4.4</b>	H- A I F H E R V X -NH <sub>2</sub>	≈ 700

<b>4.5</b>	H-	N	P	R	N	I	E	R	<b>X</b>	-NH <sub>2</sub>	≈ 700
<b>4.6</b>	H-	N	F	A	H	V	I	<b>X</b>	D	-NH <sub>2</sub>	>1000
<b>4.7</b>	H-	T	N	D	<b>X</b>	N	H	I	G	-NH <sub>2</sub>	>1000
<b>4.8</b>	H-	K	N	H	P	V	P	G	<b>X</b>	-NH <sub>2</sub>	>1000

A sequencing success rate of 42% is not unreasonable for this technique. Incomplete and non-uniform fragmentation within the peptide backbone limits success and is a known drawback to this sequencing approach. Complete fragmentation has been described as “a modern form of surrealism.”<sup>41–43</sup> Although databases exist to perform *de novo* sequencing of natural peptides, peptides including unnatural amino acids such as the lysine(cyclooctatriazole-F) moiety in our library require additional input and result in lengthy and unreliable automated sequencing. It is apparent that a disproportional number of solvable hit sequences contain the lysine(cyclooctatriazole-F) residue close to or at the C-terminus of the peptide. This bias likely exists for two reasons. First, sequences with the bulky cyclooctyne may not be favourable for binding to this particular target, resulting in hits where this residue is placed close to the bead and is less likely to project into a binding pocket of the CXCR4 receptor. Secondly, peptide sequences where the high mass residue is at an end of the peptide appears to result in more complete fragmentation during MS/MS, which can be partially attributed to better detection capability of ions in the middle of the mass range analyzed (Figure 4.6). Peptide sequences (**4.1-4.8**) as determined from MALDI MS/MS sequencing were re-synthesized on Rink amide resin and purified as their C-terminal amides and once again subjected to MALDI MS/MS at higher (micromolar) concentrations. MS/MS spectra were compared to those from the library hit bead for confirmation of accurate structure determination.

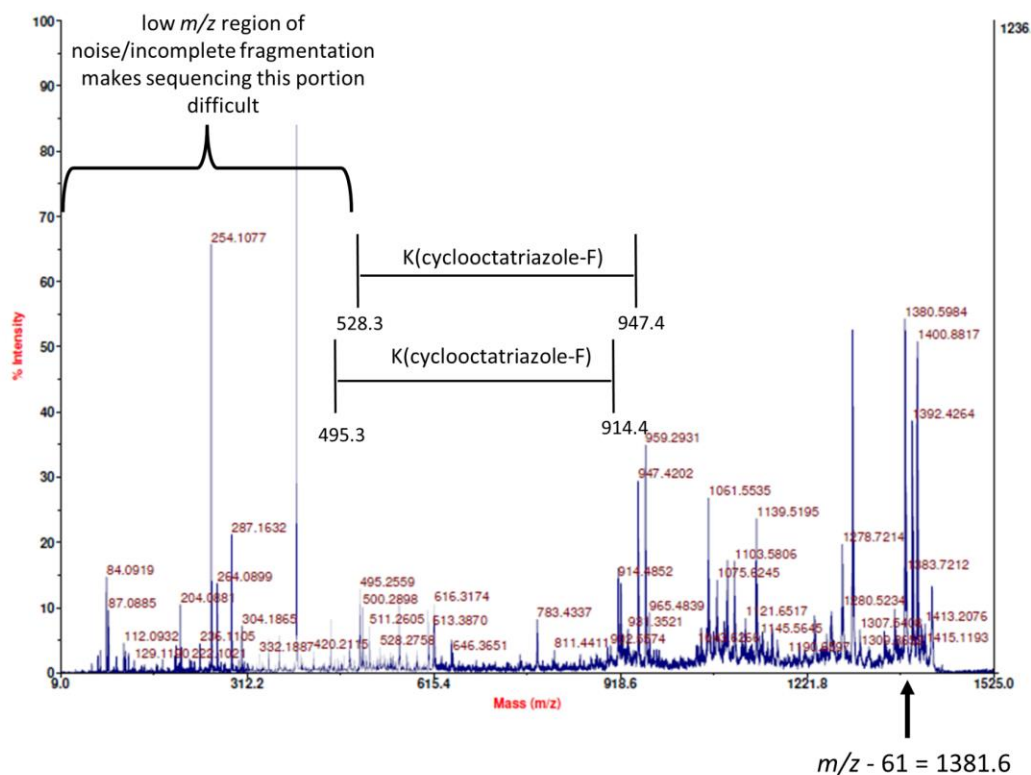


**Figure 4.6** MALDI MS/MS showing insufficient fragmentation to deconvolute entire peptide sequence when the Lys(cyclooctatriazole) residue is centered in the peptide sequence.

#### 4.2.5 CXCR4 Affinity Determination of Hit Peptides

Re-synthesized, purified peptides were then further tested for affinity by means of in-solution *in vitro* binding assays. Eight peptide sequences (**4.1-4.8**) were tested using a competitive radioligand binding assay with U87.CD4.CXCR4 cells and [<sup>125</sup>I]-SDF-1 $\alpha$  as the radioligand. Binding affinities towards the receptor were determined as IC<sub>50</sub> values that ranged from 28  $\mu$ M to the mM range (Table 4.1). Three peptides were observed to have micromolar affinity for the target, while others required millimolar concentrations before any displacement of the <sup>125</sup>I-ligand was observed. This was an encouraging result as screening of non-focused libraries typically results in hits with micromolar affinities to the target, which are then subjected to further lead optimization. Importantly, our three hits were found to have micromolar affinity to CXCR4 from our combinatorial library of 1.5 million random peptide sequences that include a fluorine moiety. Therefore, further lead



optimization could be based on straightforward modifications to the peptide sequence and optimizing *in vivo* stability, instead of focusing on incorporating an imaging component without concomitant loss of receptor affinity. Furthermore, we believe that peptide hits with on-bead CXCR4 affinity yet displaying no or poor affinity to the target based upon the competitive binding assay, could instead be binding allosterically to the receptor and would require other methods to reconfirm and evaluate their affinity. Nonetheless, peptide hits **4.1-4.3** serve as a starting point to continue structure-activity relationship studies to further optimize new fluorine-containing peptides as CXCR4-binders for PET imaging. Importantly, peptide **4.3** is particularly interesting; although it does not have the highest affinity of those studied, it maintains micromolar affinity with only one basic residue and two acidic residues. Most previously identified CXCR4-binding peptides and small molecules are highly positively charged due to the negatively charged surface of the CXCR4 binding pocket,<sup>44,45</sup> so this peptide structure presents potential for a new CXCR4 ligand with a unique binding mode and different overall physicochemical properties.

### 4.3 Conclusions

A unique combinatorial library of fluorine-containing peptides was synthesized using an OBOC two-pool approach to insert a single imaging component randomly into each peptide sequence in the library. This library was used to discover potential PET imaging agents for CXCR4. Three new peptide imaging agents with micromolar affinity and selectivity to CXCR4 were discovered as initial hits in a single step two-colour library screen and can undergo lead optimization to improve their CXCR4 affinity. Subsequently, they can be easily translated into cancer imaging probes by replacing the <sup>19</sup>F-moiety in each hit by labelling the azido-peptides with our established <sup>18</sup>F-labelled prosthetic group. This labelling can be performed in high radiochemical yields and purities due to the nature of the click reaction. The bottleneck step in hit identification from this library is due to the laborious and inconsistent process of manual *de novo* sequencing by MS/MS. Fortunately, recent advances in OBOC technologies are beginning to ease these challenges,<sup>46,47</sup> and our application could be combined with these new technologies for high-throughput implementation. This novel type of OBOC library can be used to screen against various targets to discover new <sup>18</sup>F-based PET imaging agents. In addition, any appropriate alkyne-

based imaging moiety could be clicked into such libraries at the lysine-azide residue to afford OBOC libraries for a wide variety of imaging applications.

## 4.4 Experimental

### 4.4.1 General Experimental

All reagents and solvents were used as received from Sigma-Aldrich, Alfa Aesar, or Fisher Scientific. Amino acids and resins were received from Peptides International or Chem. Impex.. ADIBO-F was prepared as previously described.<sup>36</sup> Peptides were purified by preparative reverse-phase HPLC-MS and analytical reverse-phase HPLC-MS was performed to assess purities. The system consists of a Waters 600 controller, Waters Prep degasser, Waters Quattro micro Mass, and Waters Mass Lynx software. The UV absorbance was detected using a Waters 2998 Photodiode array detector. A preparative column (Agilent Zorbax PrepHT SB-C18 Column 21.2 x 150 mm, 5  $\mu$ m) or analytical column (Agilent Zorbax SB-C18 column 4.6 x 150 mm, 5  $\mu$ m) was used. The solvent system runs gradients of 0.1 % trifluoroacetic acid (TFA) in ACN and 0.1 % TFA in water at a flow rate of 20 mL/min or 1.5 mL/min over 10 minutes with a 5 minute wash. After purification, the collected fractions were frozen at -78 °C and lyophilized. ESI HRMS was measured on a Bruker microTOF 11.

### 4.4.2 OBOC Library Synthesis

The library was synthesized using a split-and-mix approach with standard Fmoc solid phase peptide synthesis (SPPS) conditions on a Biotage SyroWave automated peptide synthesizer combined with manual peptide coupling steps. Due to the photolabile linker, synthesis was performed in the dark. Briefly, 1 g of Tentagel S-NH<sub>2</sub> resin (90  $\mu$ m, 0.26 meq/g) was swelled in DCM and manually coupled to Fmoc-ANP-OH linker (4 eq) using HCTU (4 eq) and *N,N*-diisopropylethylamine (DIPEA) (8 eq) in DMF for two hours. Automated Fmoc removal was achieved using 40% piperidine in dimethylformamide (DMF) over two steps (30 sec and 12 min). The following synthesis cascade approach follows Figure 4.2. Initially, one eighth of the library was separated (0.0325 mmol) and the remaining resin was split evenly into fifteen synthesizer vessels. To the 0.0325 mmol of resin, Fmoc-Lys(N<sub>3</sub>)-OH was manually coupled (0.13 mmol, 4 eq) with HCTU (4 eq) and

DIPEA (8 eq) for 2 hours. To the fifteen wells, resin in each well was coupled to a different Fmoc-amino acid (4 eq) (all natural L-amino acids excluding tryptophan, cysteine, methionine, leucine and glutamine) using HCTU (4 eq) and DIPEA (8 eq) in DMF for 1.5 hours, followed by automated Fmoc removal and recombination of the resin. Another 0.0325 mmol of resin was separated from this pool, coupled to Fmoc-Lys(N<sub>3</sub>)-OH as above, and the rest was split evenly into fifteen synthesizer vessels again. After each coupling cycle/Fmoc removal cycle, the resin was recombined into one pool, 0.0325 mmol removed and manually coupled to Fmoc-Lys(N<sub>3</sub>)-OH and the remainder divided into fifteen vessels again (until there was no remaining pool). This was repeated eight times to afford peptides of 1-8 amino acids in length where the Lys(N<sub>3</sub>) is the N-terminal amino acid in each separated 0.0325 mmol portion. To finish the synthesis of the peptides as octamers in length, the initial 0.0325 mmol portion coupled to Lys(N<sub>3</sub>) was split evenly into fifteen synthesizer vessels, and resin in each was coupled to a different Fmoc-amino acid (4 eq) using HCTU (4 eq) and DIPEA (8 eq) in DMF for 1.5 hours. This was followed by automated Fmoc removal and recombination of the resin, at which point the next 0.0325 mmol azide-containing portion of appropriate peptide length was added to this pool. This coupling/Fmoc removal cycle was repeated until all peptides were eight amino acids in length. All library resin was the combined, and ADIBO-F (1.5 eq) was added in a 60:40 ACN/H<sub>2</sub>O mixture (10 mL) and shaken for 2 hours. The resin was rinsed with DCM (x6). Full side-chain deprotection was afforded with 95% TFA, 2.5% triisopropylsilane and 2.5% water for 5 hours (20 mL). The library was rinsed thoroughly with DCM, 5% DIPEA/DMF, DMF, DCM, MeOH, H<sub>2</sub>O, EtOH, and stored in 70% EtOH/H<sub>2</sub>O.

#### 4.4.3 Cell Culture

U87.CD4 and U87.CD4.CXCR4 cells were obtained through the NIH AIDS Reagent Program, Division of AIDS, NIAID, NIH from Dr. Hong Kui Deng and Dr. Dan R. Littman. U87.CD4.CXCR4 cells were maintained in DMEM – high glucose (Sigma) containing 15% fetal bovine serum (FBS), 1  $\mu\text{g mL}^{-1}$  puromycin, 300  $\mu\text{g mL}^{-1}$  G418, and 1 $\times$  penicillin–streptomycin. U87.CD4 cells were maintained in DMEM – high glucose (Sigma) containing 10% FBS, 300  $\mu\text{g mL}^{-1}$  G418, and 1 $\times$  penicillin–streptomycin. All cell

lines were cultured at 37 °C in humidified atmosphere with 5% CO<sub>2</sub> and passaged 2 to 3 times per week.

#### 4.4.4 On-Bead Two-Colour Fluorescent Screening

U87.CD4.CXCR4 cells or U87.CD4 cells at 80% confluency were incubated with 5 µM CellTracker™ Green CMFDA Dye (ThermoFisher) or 5 µM CellTracker™ Red CMTPX Dye (ThermoFisher) in serum-free DMEM media for 30 min at 37 °C. Dye was aspirated, and cells were lifted using an enzyme-free dissociation solution (Sigma). Cells were counted and resuspended in serum-free DMEM at 200,000 cells/mL. Library beads were suspended in Dulbecco's modified eagle medium (DMEM) and dispersed in non-treated 6-well plates at ~20 mg/10,000 beads/well (entire library is ~1.5 million beads). Cells from each cell suspension were added to each well (1 mL, 200,000 cells each) and total volumes were brought up to 3 mL with DMEM. Plates were shaken at 550 rpm for 1 hour at 37 °C. To each well, 0.33 mL of 37% paraformaldehyde was added for a final concentration of 4%. Fixing was quenched after ten minutes by the addition of 2 M glycine to a final concentration of 20%. The entire library of beads was recombined and rinsed with water and phosphate buffered saline (PBS) repeatedly then suspended in PBS. The library beads were dispersed in culture dishes for visualization by fluorescence microscopy. Confocal fluorescence microscopy was performed on a Nikon A1R Confocal Laser Microscope with either a 488 nm laser for green fluorescence excitation and the emission range set to 500-550 nm and a 561 nm laser for red fluorescence with the emission collected at 600-660 nm. Beads showing high levels of interactions with only green fluorescent U87.CD4.CXCR4 cells were manually isolated using a micropipette and placed in individual wells of a 96-well plate. Beads were then carefully washed multiple times with 95% ethanol to remove bound cells and visualized to confirm removal of cells.

#### 4.4.5 Photocleavage and MALDI MS/MS

To confirm library synthesis, eight beads were placed in individual wells of a 96 well plate, swollen in methanol, and placed under a 160 W 365 nm lamp for 1.5 hours to afford photolysis from the resin. The single bead peptide solutions were approximately nanomolar in concentration based on <10% cleavage from the 0.26 mmol/g loading of an individual

bead. MALDI MS/MS was obtained for the highest intensity MS peak and *de novo* sequencing was performed to identify peptide sequences.

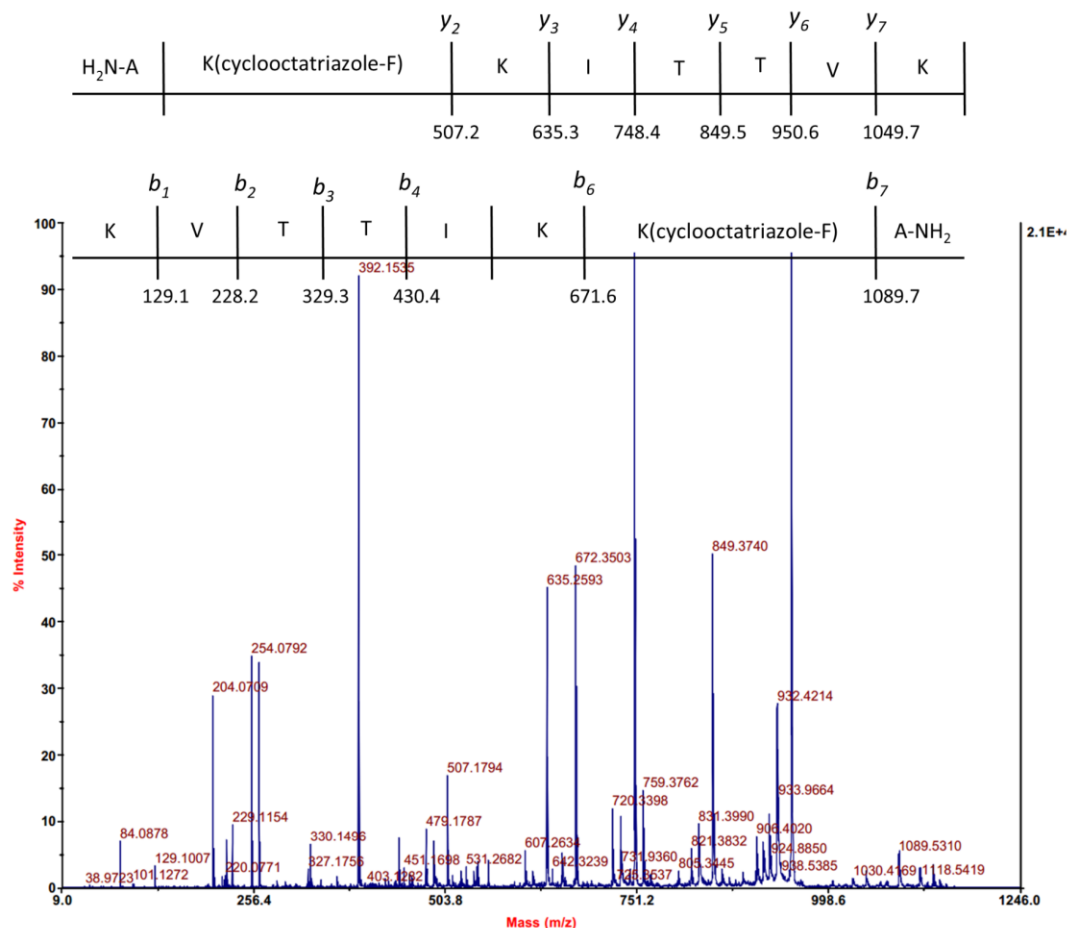


**Figure 4.7** Sample *de novo* sequencing of a random library peptide of 1177 Da showing almost complete coverage of *b* and *y* ion series.

Twenty-five individual hit beads from the library screen were suspended in 40  $\mu$ L of methanol in individual wells of 96-well plates and placed under UV light (160 W, 365 nm) for 1.5 hours to achieve <10% cleavage from the bead due to the ANP linker. Conversely, 1 mg/mL solutions of purified peptides **4.1-4.3** in acetonitrile were prepared. The solutions were then mixed with equal parts matrix  $\alpha$ -cyano-4-hydroxycinnamic acid (CHCA) in acetonitrile and placed onto the MALDI target. MALDI TOF/TOF was performed on an AB Sciex TOF/TOF 5800 by the facility manager of the MALDI Mass Spectrometry

Facility at the London Regional Proteomics Centre. Mass spectra were obtained and analyzed for each sample (Figure 4.8). The highest intensity peak in each MS spectra was subjected to MS/MS analysis and peptide sequences were deconvoluted manually by examining mass differences between fragment ions in these spectra (Chapter 6 Appendix).

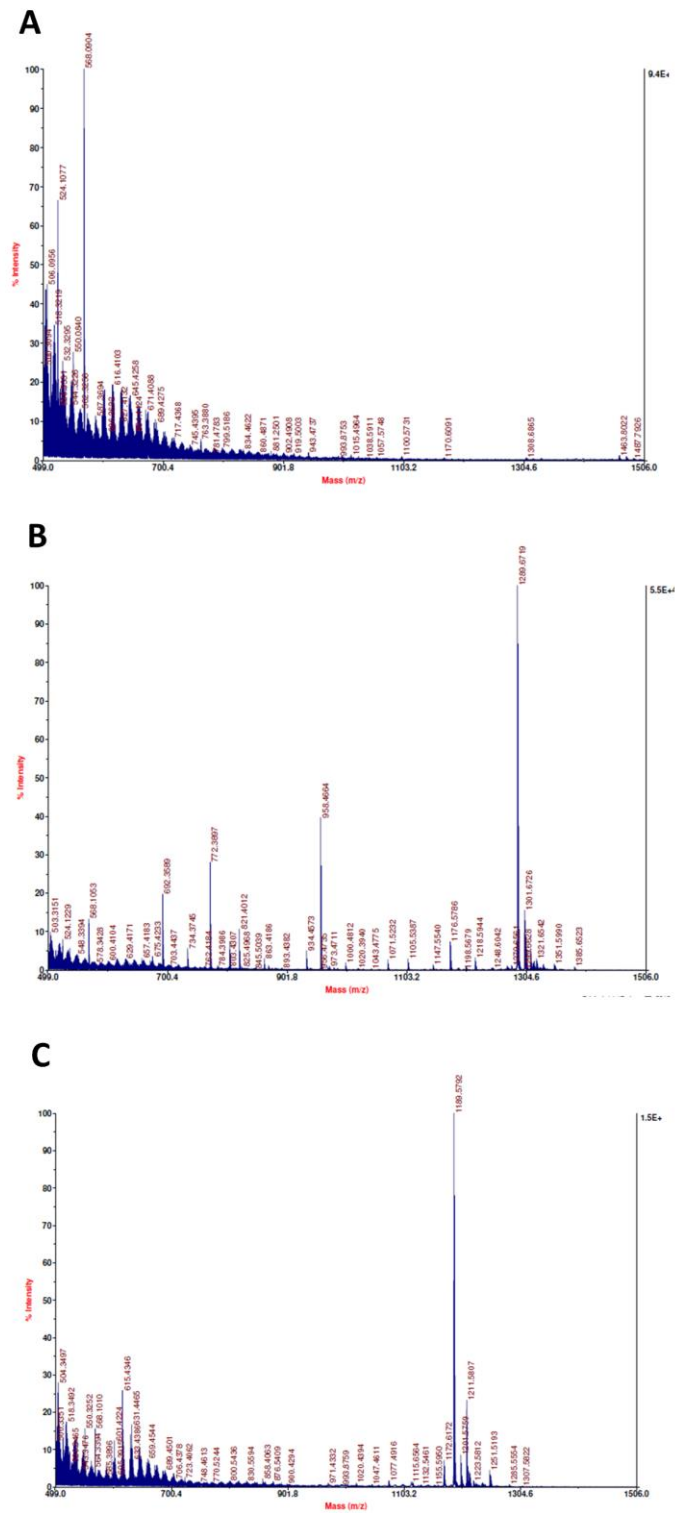
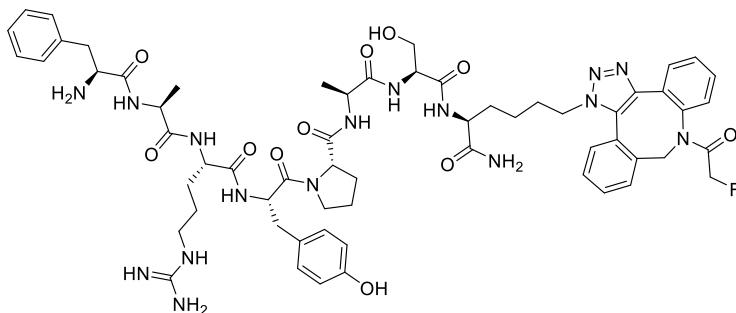


**Figure 4.8** MALDI mass spectra for hit peptides demonstrating A) MS with no ions present in the mass range of interest for our library, B) MS with multiple ion peaks, and C) MS with a single parent ion present (and its sodium adduct).



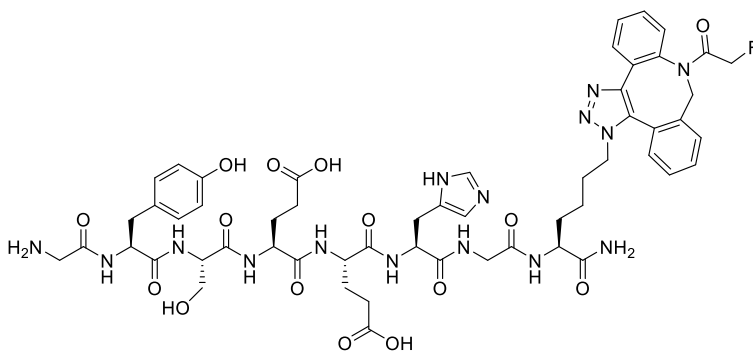


## 4.2



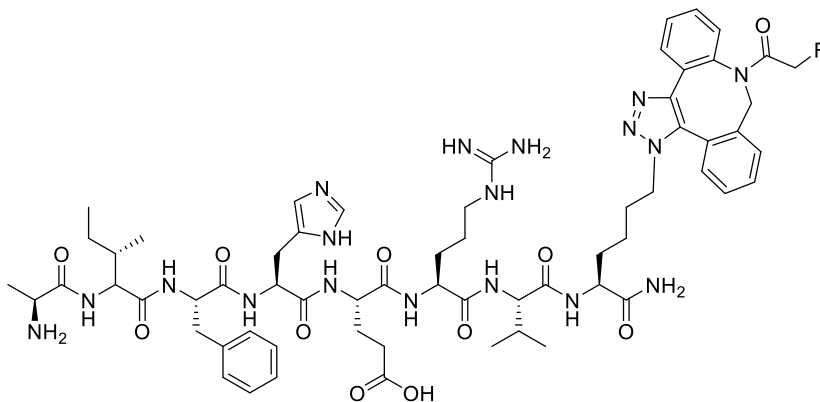
HRMS (ESI):  $m/z$  calculated for  $C_{61}H_{77}FN_{16}O_{11}$   $[M + H]^+$ : 1229.6020; found: 1229.5989

## 4.3



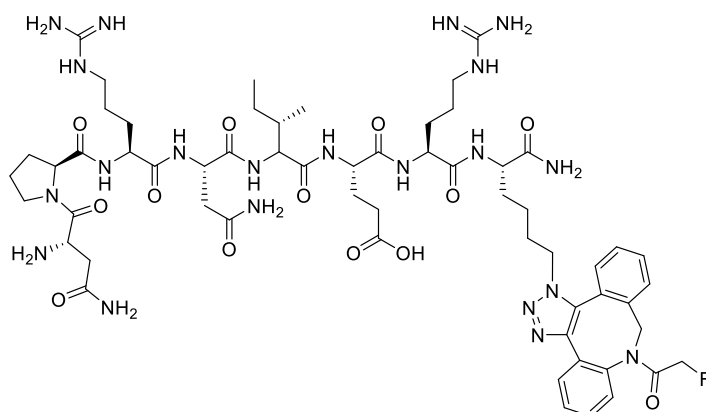
HRMS (ESI):  $m/z$  calculated for  $C_{55}H_{66}FN_{15}O_{15}$   $[M + H]^+$ : 1196.4925; found: 1196.4909

## 4.4



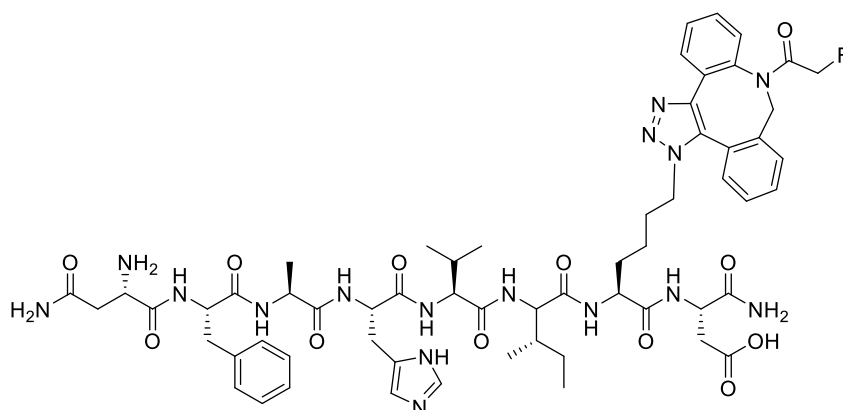
HRMS (ESI):  $m/z$  calculated for  $C_{63}H_{85}FN_{18}O_{11}$   $[M + H]^+$ : 1289.6708; found: 1289.665

## 4.5



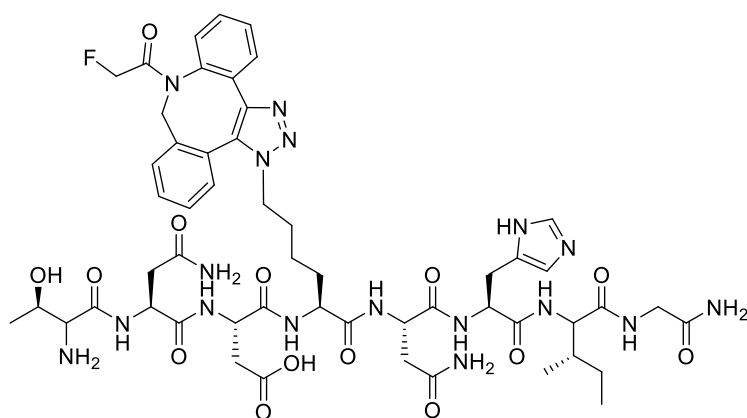
HRMS (ESI):  $m/z$  calculated for  $C_{59}H_{86}FN_{21}O_{13}$   $[M + H]^+$ : 1316.6776; found: 1316.6728

## 4.6



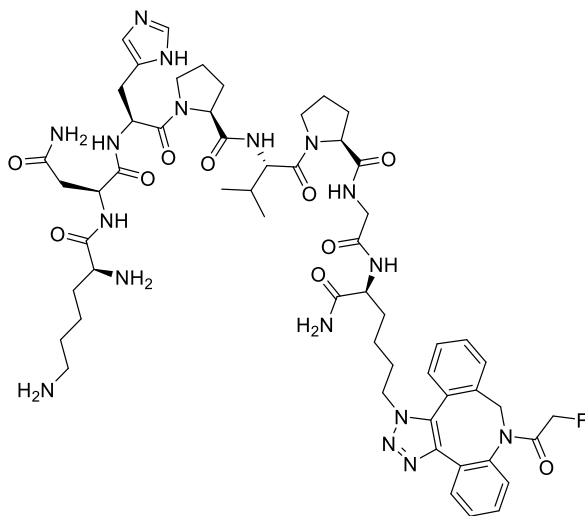
HRMS (ESI):  $m/z$  calculated for  $C_{60}H_{77}FN_{16}O_{12}$   $[M + H]^+$ : 1233.5983; found: 1233.5933

## 4.7



HRMS (ESI):  $m/z$  calculated for  $C_{53}H_{70}FN_{17}O_{14}$   $[M + H]^+$ : 1188.5350; found: 1188.5350

## 4.8



HRMS (ESI):  $m/z$  calculated for  $C_{56}H_{76}FN_{17}O_{10}$   $[M + H]^+$ : 1166.6023; found: 1166.5992

### 4.4.7 Radioligand Competitive Binding Assays

*In vitro* CXCR4 affinity of hit peptides **4.1-4.8** were determined through competitive binding assays using U87.CD4.CXCR4 cells with  $[^{125}I]$ -SDF-1 $\alpha$  as the radioligand (Perkin Elmer). The compound of interest (30  $\mu$ L, at concentrations ranging from  $10^{-8}$  to  $10^{-2}$  M) or buffer (30  $\mu$ L as background control) and 20,000 cpm of  $[^{125}I]$ -SDF-1 $\alpha$  (20 pM) were mixed with the binding buffer (20 mM HEPES, 0.5% BSA in PBS, pH 7) in 1.5 mL Eppendorf Protein LoBind vials. A suspension of U87.CD4.CXCR4 cells (50,000 cells in 50  $\mu$ L) was added to each vial to give a final volume of 300  $\mu$ L. The vials were shaken at 550 rpm for 20 minutes at 37 °C. Immediately after the incubation, the vials were centrifuged at 13,000 rpm for 5 minutes and the supernatant removed. The cell pellet was washed with 500  $\mu$ L of 50 mM Tris buffer (pH 7) and centrifuged again. The amount of  $[^{125}I]$ -SDF-1 $\alpha$  bound to the cells was measured using a gamma counter (PerkinElmer). Background uptake of the  $[^{125}I]$ -SDF-1 $\alpha$  onto vials was subtracted from all assay vials.  $IC_{50}$  values were determined by non-linear regression analysis to fit a 4-parameter dose response curve using GraphPad Prism (Version 6.0c). All data points were obtained in triplicate.

## 4.5 References

- 1 R. Davis, S. Hausner and J. Sutcliffe, in *Radiopharmaceutical Chemistry*, ed. Lewis J., Windhorst A., Zeglis, B., Springer, pp. 137–162.
- 2 K. S. Lam, S. E. Salmon, E. M. Hersh, V. J. Hruby, W. M. Kazmierski and R. J. Knapp, *Nature*, 1991, **354**, 82–84.
- 3 O. H. Aina, R. Liu, J. L. Sutcliffe, J. Marik, C. X. Pan and K. S. Lam, *Mol. Pharm.*, 2007, **4**, 631–651.
- 4 V. V. Komnatnyy, T. E. Nielsen and K. Qvortrup, *Chem. Commun.*, 2018, **54**, 6759–6771.
- 5 Y. Gao, S. Amar, S. Pahwa, G. Fields and T. Kodadek, *ACS Comb. Sci.*, 2015, **17**, 49–59.
- 6 N. Yao, W. Xiao, X. Wang, J. Marik, S. H. Park, Y. Takada and K. S. Lam, *J. Med. Chem.*, 2009, **52**, 126–133.
- 7 L. Geng, C. Lausted, L. Hood, Q. Fang, H. Wang and Z. Hu, *Anal. Chem.*, 2014, **86**, 11854–11859.
- 8 L. Peng, R. Liu, J. Marik, X. Wang, Y. Takada and K. S. Lam, *Nat. Chem. Biol.*, 2006, **2**, 381–389.
- 9 L. Y. Hu, K. A. Kelly and J. L. Sutcliffe, *Mol. Imaging Biol.*, 2017, **19**, 163–182.
- 10 D. Walker, Y. Li, Á. Roxin, P. Schaffer, M. J. Adam and D. M. Perrin, *Bioorg. Med. Chem. Lett.*, 2016, **26**, 5126–5131.
- 11 O. H. Aina, J. Marik, R. Gandour-Edwards and K. S. Lam, *Mol. Imaging*, 2005, **4**, 439–447.
- 12 M. Jiang, R. Ferdani, M. Shokeen and C. J. Anderson, *Nucl. Med. Biol.*, 2013, **40**, 245–251.
- 13 M. K. J. Gagnon, S. H. Hausner, J. Marik, C. K. Abbey, J. F. Marshall and J. L. Sutcliffe, *Proc. Natl. Acad. Sci.*, 2009, **106**, 17904–17909.
- 14 W. Xiao, T. Li, F. C. Bononi, D. Lac, I. A. Kekessie, Y. Liu, E. Sanchez, A. Mazloom, A.-H. Ma, J. Lin, J. Tran, K. Yang, K. S. Lam and R. Liu, *EJNMMI Res.*, 2016, **6**, 18.
- 15 W. Beaino, J. R. Nedrow and C. J. Anderson, *Mol. Pharm.*, 2015, **12**, 1929–1938.
- 16 D. R. Cruickshank and L. G. Luyt, *Can. J. Chem.*, 2014, **93**, 234–243.

- 17 Y. S. C. Tang, R. A. Davis, T. Ganguly and J. L. Sutcliffe, *Molecules*, 2019, **24**, 309.
- 18 J. Singh, D. Lopes and D. Gomika Udugamasooriya, *Biopolymers*, 2016, **106**, 673–684.
- 19 H. C. Kolb, M. G. Finn and K. B. Sharpless, *Angew. Chem. Int. Ed.*, 2001, **40**, 2004–2021.
- 20 G. Wittig and A. Krebs, *Chem. Ber.*, 1961, **94**, 3260–3275.
- 21 N. J. Agard, J. A. Prescher and C. R. Bertozzi, *J. Am. Chem. Soc.*, 2005, **127**, 11196–11196.
- 22 M. F. Debets, S. S. Van Berkel, S. Schoffelen, F. P. J. T. Rutjes, J. C. M. Van Hest and F. L. Van Delft, *Chem. Commun.*, 2010, **46**, 97–99.
- 23 F. Balkwill, *Semin. Cancer Biol.*, 2004, **14**, 171–179.
- 24 V. Saini, A. Marchese and M. Majetschak, *J. Biol. Chem.*, 2010, **285**, 15566–15576.
- 25 N. Liu, Q. Wan, Z. Cheng and Y. Chen, *Curr. Top. Med. Chem.*, 2019, **19**, 17–32.
- 26 M. Masuda, H. Nakashima, T. Ueda, H. Naba, R. Ikoma, A. Otaka, Y. Terakawa, H. Tamamura, T. Ibuka, T. Murakami, Y. Koyanagi, M. Waki, A. Matsumoto, N. Yamamoto, S. Funakoshi and N. Fujii, *Biochem. Biophys. Res. Commun.*, 1992, **189**, 845–850.
- 27 H. Tamamura, Y. Xu, T. Hattori, X. Zhang, R. Arakaki, K. Kanbara, A. Omagari, A. Otaka, T. Ibuka, N. Yamamoto, H. Nakashima and N. Fujii, *Biochem. Biophys. Res. Commun.*, 1998, **253**, 877–882.
- 28 O. Jacobson, I. D. Weiss, D. O. Kiesewetter, J. M. Farber and X. Chen, *J. Nucl. Med.*, 2010, **51**, 1796–1804.
- 29 X. Yan, G. Niu, Z. Wang, X. Yang, D. O. Kiesewetter, O. Jacobson, B. Shen and X. Chen, *Mol. Imaging Biol.*, 2016, **18**, 135–142.
- 30 X.-X. Zhang, Z. Sun, J. Guo, Z. Wang, C. Wu, G. Niu, Y. Ma, D. O. Kiesewetter and X. Chen, *Mol. Imaging Biol.*, 2013, **15**, 758–767.
- 31 N. Fujii, S. Oishi, K. Hiramatsu, T. Araki, S. Ueda, H. Tamamura, A. Otaka, S. Kusano, S. Terakubo, H. Nakashima, J. A. Broach, J. O. Trent, Z. Wang and S. C. Peiper, *Angew. Chem. Int. Ed.*, 2003, **42**, 3251–3253.
- 32 O. Demmer, E. Gourni, U. Schumacher, H. Kessler and H.-J. Wester, *ChemMedChem*, 2011, **6**, 1789–1791.

- 33 T. Vag, C. Gerngross, P. Herhaus, M. Eiber, K. Philipp-Abbrederis, F.-P. Graner, J. Ettl, U. Keller, H.-J. Wester and M. Schwaiger, *J. Nucl. Med.*, 2016, **57**, 741–746.
- 34 K. Philipp-Abbrederis, K. Herrmann, S. Knop, M. Schottelius, M. Eiber, K. Lückerath, E. Pietschmann, S. Habringer, C. Gerngroß, K. Franke, M. Rudelius, A. Schirbel, C. Lapa, K. Schwamborn, S. Steidle, E. Hartmann, A. Rosenwald, S. Kropf, A. J. Beer, C. Peschel, H. Einsele, A. K. Buck, M. Schwaiger, K. Götze, H.-J. Wester and U. Keller, *EMBO Mol. Med.*, 2015, **7**, 477–487.
- 35 G. P. C. George, F. Pisaneschi, E. Stevens, Q. D. Nguyen, O. Åberg, A. C. Spivey and E. O. Aboagye, *J. Label. Compd. Radiopharm.*, 2013, **56**, 679–685.
- 36 E. Murrell, M. S. Kovacs and L. G. Luyt, *ChemMedChem*, 2018, **13**, 1625–1628.
- 37 D. G. Udugamasooriya and T. Kodadek, *Curr. Protoc. Chem. Biol.*, 2012, **4**, 35–48.
- 38 A. Björndal, H. Deng, M. Jansson, J. R. Fiore, C. Colognesi, A. Karlsson, J. Albert, G. Scarlatti, D. R. Littman and E. M. Fenyö, *J. Virol.*, 1997, **71**, 7478–87.
- 39 B. B. Brown, D. S. Wagner and H. M. Geysen, *Mol. Divers.*, 1995, **1**, 4–12.
- 40 B. Palzs and S. Suhal, *Mass Spectrom. Rev.*, 2005, **24**, 508–548.
- 41 K. F. Medzihradzsky and R. J. Chalkley, *Mass Spectrom. Rev.*, 2015, **34**, 43–63.
- 42 A. Semmler, R. Weber, M. Przybylski and V. Wittmann, *J. Am. Soc. Mass Spectrom.*, 2010, **21**, 215–219.
- 43 B. Meyer, D. G. Papasotiriou and M. Karas, *Amino Acids*, 2011, **41**, 291–310.
- 44 L. Picard, D. A. Wilkinson, Á. McKnight, P. W. Gray, J. A. Hoxie, P. R. Clapham and R. A. Weiss, *Virology*, 1997, **231**, 105–111.
- 45 M. M. Rosenkilde, L.-O. Gerlach, J. S. Jakobsen, R. T. Skerlj, G. J. Bridger and T. W. Schwartz, *J. Biol. Chem.*, 2004, **279**, 3033–41.
- 46 J. Vastl, T. Wang, T. B. Trinh and D. A. Spiegel, *ACS Comb. Sci.*, 2017, **19**, 255–261.
- 47 A. B. MacConnell, P. J. McEnaney, V. J. Cavett and B. M. Paegel, *ACS Comb. Sci.*, 2015, **17**, 518–534.

## Chapter 5

### 5 Conclusions

#### 5.1 Summary and Outlook

Molecular imaging is a rapidly expanding field due to the advent of new technologies that can be used for medical imaging. The ability to image cellular and metabolic targets as markers of disease with nuclear imaging techniques like PET and SPECT allows clinicians and scientists to learn more about these disease states, establish earlier diagnoses, and stratify patients based on biomarker presence, allowing for personalized medicine. The chemokine receptor CXCR4 is an interesting GPCR target that is present in over 23 types of cancers, while being absent in healthy tissue.<sup>1,2</sup> Due to its involvement in chemotactic and angiogenic pathways, it is a potential marker for metastatic cancers. While some CXCR4 imaging agents have been developed, the only one to show clinical utility is [<sup>68</sup>Ga]Pentixafor, and no ideal fluorine-18 tracers have been yet established.<sup>3</sup> This illustrates the need for the development of a toolbox of radiopharmaceutical imaging agents for CXCR4 and other markers that can be used to non-invasively determine patient-specific biomarkers. These new imaging agents can be developed based on a rational medicinal chemistry design from a known ligand-receptor interaction, which can be a lengthy process. When no such interaction is known, or the possible structures do not have an appropriate pharmacokinetic profile for imaging, new candidates must be discovered. This highlights a need for improved discovery methods with regards to receptor-targeted imaging agents.

Unfortunately, the well-established high-throughput screening approaches that can be used to observe new drug-target interactions are not commonly translated into the discovery of new imaging agents. Ligands discovered from these screening campaigns still need modification into an imaging agent, which limits the utility of the approach. One-bead one-compound (OBOC) libraries are a combinatorial method for synthesizing peptide libraries,<sup>4</sup> and have the advantage of being able to synthetically incorporate non-amino acid structures. This approach serves as an ideal scaffold for the design of libraries of imaging agents.

In this research we explored the development of libraries of millions of imaging agents that included a fluorine atom as a surrogate for the placement of fluorine-18. This allows screening of the libraries to be performed on entire imaging agents, limiting the need for post-screening modifications. We developed the chemistry for two such libraries, and chose to employ strain-promoted alkyne-azide cycloaddition click (SPAAC) reactions<sup>5</sup> to incorporate the fluorine in each. This reaction is particularly amenable to radiolabelling with fluorine-18 and the components can be introduced into peptides in a variety of ways.

In Chapter 2, an OBOC library is described where the imaging moiety was placed on the N-terminus of the peptides. Since this placement of the imaging surrogate results in it projecting away from the bead, we proposed this would encourage discovery of imaging agents where the imaging entity was involved in receptor binding. We employed an existing SPAAC cyclooctyne as well as a reported azido fluorine PEG-based prosthetic group. Automated screening of this library against a CXCR4-expressing cell line resulted multiple hits, of which a hit with micromolar affinity to the receptor was discovered. Unfortunately, multiple obstacles were encountered during this process which limited the possibility of utilizing the library to its full ability for high-throughput imaging agent discovery. Firstly, multiple rounds of screening were necessary to establish high-affinity hits to the target, and screening was not inherently receptor-specific. Hit peptide sequences needed to be resynthesized to probe target specificity as well as affirm receptor affinity due to bead autofluorescence complicating automated screening. Secondly, *de novo* sequence deconvolution was hindered due to the high fragmentation percentage in the chosen cyclooctyne portion of the peptide, limiting observation of complete ion series in MS/MS. Isobaric amino acids included in the library also caused the need for synthesis of multiple possible iterations of hit sequences for *in vitro* affinity assays. We addressed these aspects in our second-generation imaging agent library described in Chapter 4.

The purpose of the work described in Chapter 3 was to establish a novel fluorine-containing cyclooctyne that could be incorporated rapidly into azide-containing peptides by SPAAC for <sup>18</sup>F-radiolabelling. Although other such cyclooctynes exist,<sup>6-9</sup> we needed the cyclooctyne to be small enough to not impede receptor-peptide binding or have variable binding based on regioisomers, have minimal functionalities that would result in



fragmentation in MALDI MS/MS, and be synthetically accessible on a large scale for incorporation into our libraries. This resulted in the design and synthesis of our azadibenzocyclooctyne ADIBO-F.<sup>10</sup> We were able to access this in eight steps, radiolabel it with fluorine-18 in good radiochemical yields, and showed its utility as a prosthetic group for radiolabelling biomolecules with fluorine-18 by subsequently clicking it into established cancer-targeting peptides. We demonstrated that its presence in relatively small peptides did not impede binding. This is a useful addition to the radiochemist's toolbox of prosthetic groups for using mild conditions to afford <sup>18</sup>F-labelled biomolecules and other targeting agents.

Chapter 4 relays the design and synthesis of an OBOC library where the imaging moiety was able to be randomly dispersed within the peptide sequences. The cyclooctyne prosthetic group established in Chapter 3 allowed us this opportunity. We also approached the experimental design with obstacles from Chapter 2 in mind, and sought to overcome these challenges in this chapter. To this end, some sequencing complications were mitigated by completely removing isobaric amino acids from the library, and by employing a new cyclooctyne/azide pair with fewer possible MS/MS fragmentation locations. In addition, an on-bead two-colour screen<sup>11</sup> was employed to search for hit peptide beads with both affinity and selectivity to the target in one step. This eliminated the need for multiple in-solution assays for hit confirmation.

Aside from improving the library design, we were also able to demonstrate that multiple hits with micromolar affinity to the chosen receptor, CXCR4, could be discovered from this imaging agent library. The on-bead two-colour screening was simple and efficient, and has potential to be automated.<sup>12</sup>

The libraries described herein serve as an excellent starting point for the development and expansion of libraries to find new imaging agents for any given target. Libraries of our design with other imaging components could be produced for any imaging entity of interest; this gives the potential to produce libraries of SPECT or PET tracers using other isotope mimics, MRI contrast agents using paramagnetic metal ions, or optical imaging agents using fluorescent moieties. Other fluorine-18 prosthetic groups could also be

explored that are smaller in size and have established radiolabelling methods. An imaging agent OBOC library with a 4-fluorobenzoyl-containing amino acid as the imaging surrogate was described recently.<sup>13</sup> The fluorine-containing amino acid was fixed at the C-terminus on the beads, and the remaining peptide sequences contained a known binding motif to the target of interest and was randomized at other locations. This library shows the promise in designing focused peptide-based imaging agent libraries as a method of lead optimization where peptide-target interactions have been previously explored. Pairing our newly designed imaging agent library approach with other classic OBOC approaches would improve upon any hits obtained from such libraries. For example, making OBOC libraries that incorporate non-canonical or D-amino acids into the synthesis could also result in peptide imaging agents that have better *in vivo* stability. Most research surrounding OBOC is currently focused on improving the automation of the screening and hit validation process to make the approach truly high-throughput. Therefore, combination of our application-based imaging agent OBOC approach with new bead-based screening technologies would only improve the throughput and efficacy of our discovery process. Importantly, OBOC technologies are being developed to establish more efficient screening steps,<sup>14,15</sup> improve upon sequencing bottlenecks,<sup>16,17</sup> and perform affinity assays from single bead quantities of peptide.<sup>18,19</sup> Others have shown the utility of the OBOC approach in synthesizing libraries of various small molecules or peptoid structures, which would also be interesting scaffolds to incorporate an imaging component.<sup>20,21</sup>

In summary, we have proved the usefulness of OBOC libraries in the discovery of new imaging agents for CXCR4. Hits with micromolar affinities to CXCR4 were discovered directly from library screens and are good candidates for lead optimization to improve upon affinity. New imaging agents for CXCR4 could be important in the early detection of metastatic cancers, and also in imaging of disease load for late-stage patients. With the advent of targeted radiotherapy, agents that are capable of imaging widespread metastatic cancers show potential for transformation into theranostic agents. Incorporating SPAAC into our library designs gives us the ability to immediately translate direct hits from the library into the radiolabelled counterparts. As part of this, we also developed a new synthetically accessible fluorine-18 prosthetic group for SPAAC radiolabelling, which can be useful for quick, clean <sup>18</sup>F-labelling of any azide-modified structure.

## 5.2 References

- 1 F. Balkwill, *Semin. Cancer Biol.*, 2004, **14**, 171–179.
- 2 H. Zhao, L. Guo, H. Zhao, J. Zhao, H. Weng and B. Zhao, *Oncotarget*, 2015, **6**, 5022–5040.
- 3 N. Liu, Q. Wan, Z. Cheng and Y. Chen, *Curr. Top. Med. Chem.*, 2019, **19**, 17–32.
- 4 K. S. Lam, S. E. Salmon, E. M. Hersh, V. J. Hruby, W. M. Kazmierski and R. J. Knapp, *Nature*, 1991, **354**, 82–84.
- 5 N. J. Agard, J. A. Prescher and C. R. Bertozzi, *J. Am. Chem. Soc.*, 2005, **127**, 11196–11196.
- 6 K. Kettenbach and T. L. Ross, *MedChemComm*, 2016, **7**, 654–657.
- 7 V. Bouvet, M. Wuest and F. Wuest, *Org. Biomol. Chem.*, 2011, **9**, 7393–7399.
- 8 S. Arumugam, J. Chin, R. Schirrmacher, V. V. Popik and A. P. Kostikov, *Bioorganic Med. Chem. Lett.*, 2011, **21**, 6987–6991.
- 9 R. D. Carpenter, S. H. Hausner and J. L. Sutcliffe, *ACS Med. Chem. Lett.*, 2011, **2**, 885–889.
- 10 E. Murrell, M. S. Kovacs and L. G. Luyt, *ChemMedChem*, 2018, **13**, 1625–1628.
- 11 D. G. Udugamasooriya and T. Kodadek, *Curr. Protoc. Chem. Biol.*, 2012, **4**, 35–48.
- 12 C. F. Cho, B. Behnam Azad, L. G. Luyt and J. D. Lewis, *ACS Comb. Sci.*, 2013, **15**, 393–400.
- 13 Y. S. C. Tang, R. A. Davis, T. Ganguly and J. L. Sutcliffe, *Molecules*, 2019, **24**, 309.
- 14 C. F. Cho, G. A. Amadei, D. Breadner, L. G. Luyt and J. D. Lewis, *Nano Lett.*, 2012, **12**, 5957–5965.
- 15 O. Erharuyi, S. Simanski, P. J. McEnaney and T. Kodadek, *Bioorganic Med. Chem. Lett.*, 2018, **28**, 2773–2778.
- 16 A. B. MacConnell, P. J. McEnaney, V. J. Cavett and B. M. Paegel, *ACS Comb. Sci.*, 2015, **17**, 518–534.
- 17 J. Vastl, T. Wang, T. B. Trinh and D. A. Spiegel, *ACS Comb. Sci.*, 2017, **19**, 255–261.

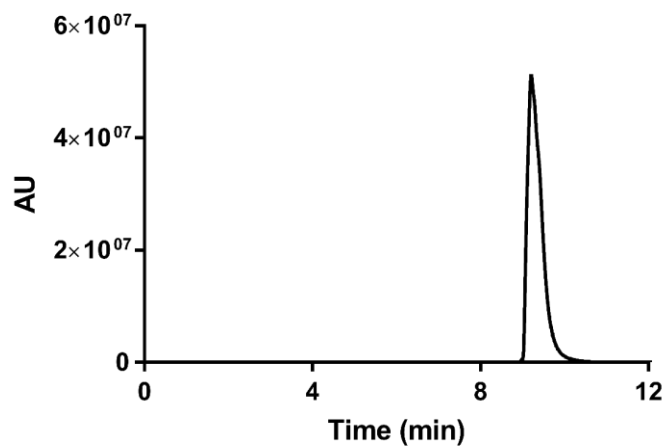
- 18 W. Wang, D. Zhang, Z. Wei, Z. Wang, X. Bu, S. Yang, Q. Fang and Z. Hu, *Talanta*, 2015, **134**, 705–711.
- 19 W. Wang, Z. Wei, D. Zhang, H. Ma, Z. Wang, X. Bu, M. Li, L. Geng, C. Lausted, L. Hood, Q. Fang, H. Wang and Z. Hu, *Anal. Chem.*, 2014, **86**, 11854–11859.
- 20 Y. Gao and T. Kodadek, *J. Vis. Exp.*, 2014, 1–12.
- 21 T. Kodadek and P. J. McEnaney, *Chem. Commun.*, 2016, **52**, 6038–6059.

## Chapter 6

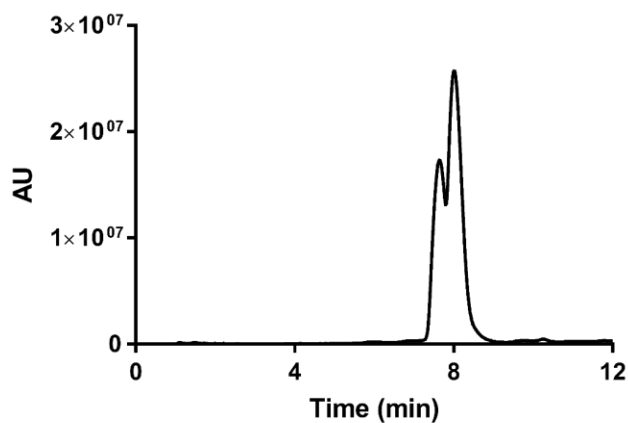
### 6 Appendix – Additional Data for Chapter 4

#### 6.1 HPLC Traces for Hit Peptides

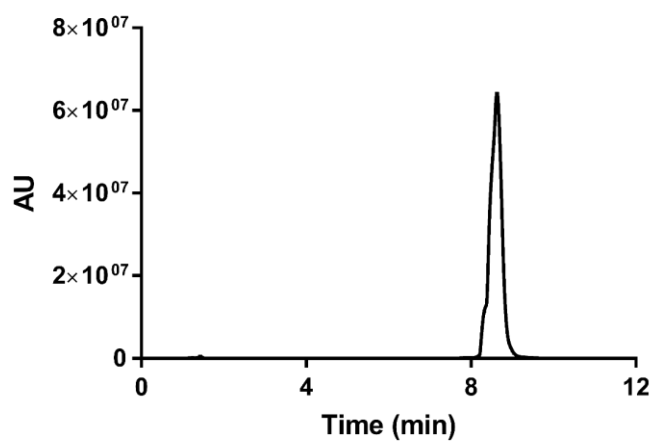
Analytical UV chromatogram from RP-HPLC of purified **4.1** (15-85% ACN/H<sub>2</sub>O, 0.1% TFA, 10 minutes, RT = 9.21 min).



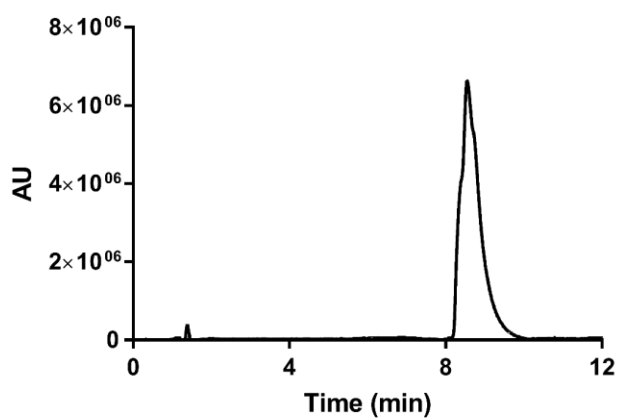
Analytical UV chromatogram from RP-HPLC of purified **4.2** (25-85% ACN/H<sub>2</sub>O, 0.1% TFA, 10 minutes, RT = 7.83 min).



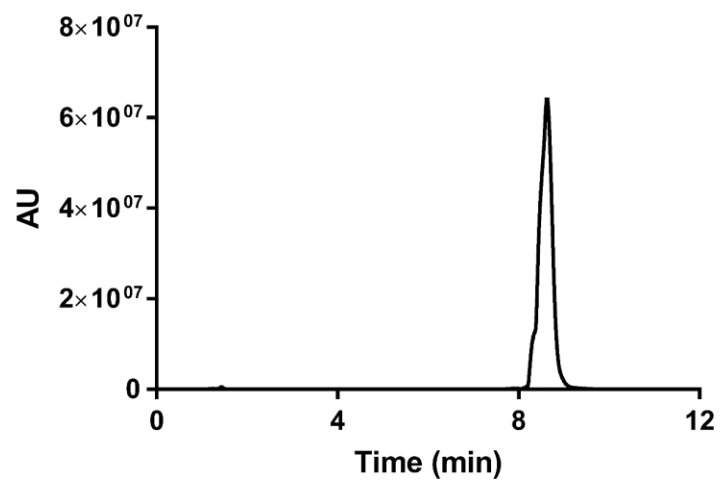
Analytical UV chromatogram from RP-HPLC of purified **4.3** (20-80% ACN/H<sub>2</sub>O, 0.1% TFA, 10 minutes, RT = 8.63 min).



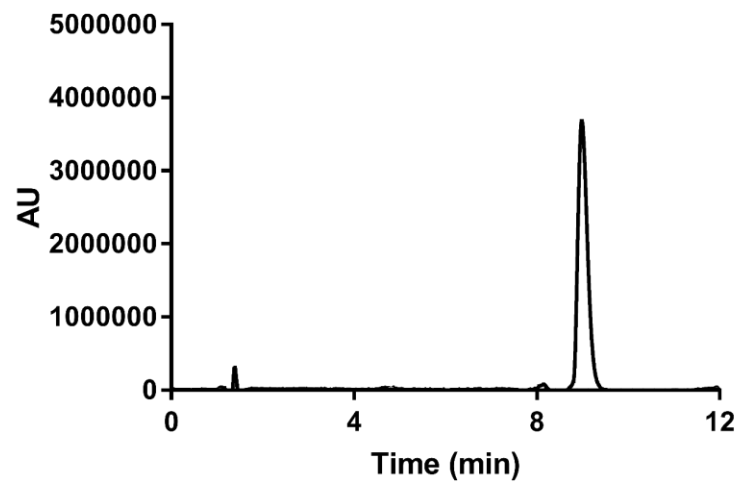
Analytical UV chromatogram from RP-HPLC of purified **4.4** (25-85% ACN/H<sub>2</sub>O, 0.1% TFA, 10 minutes, RT = 8.55 min).



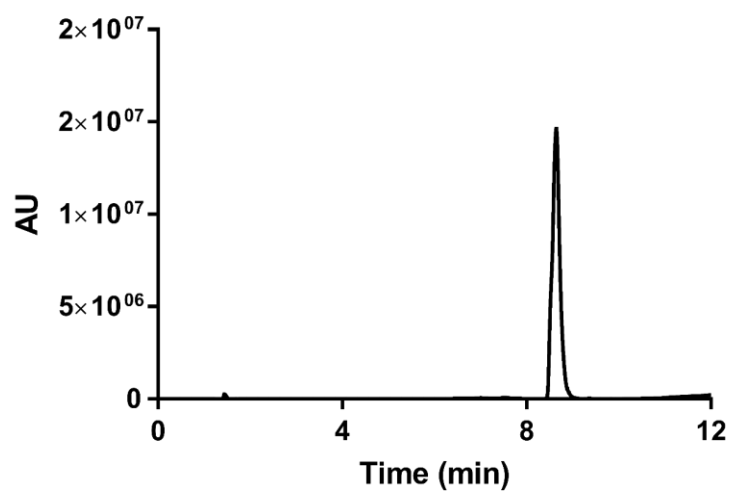
Analytical UV chromatogram from RP-HPLC of purified **4.5** (20-80% ACN/H<sub>2</sub>O, 0.1% TFA, 10 minutes, RT = 8.74 min).



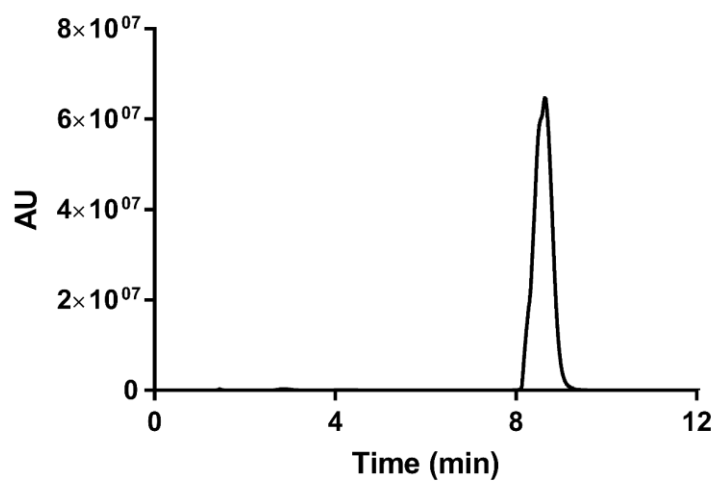
Analytical UV chromatogram from RP-HPLC of purified **4.6** (25-85% ACN/H<sub>2</sub>O, 0.1% TFA, 10 minutes, RT = 8.98 min).



Analytical UV chromatogram from RP-HPLC of purified **4.7** (20-80% ACN/H<sub>2</sub>O, 0.1% TFA, 10 minutes, RT = 8.64 min).



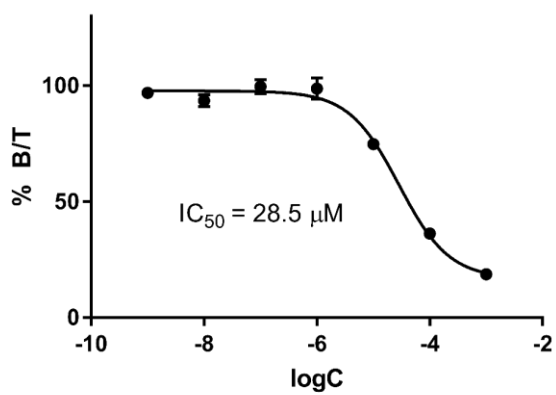
Analytical UV chromatogram from RP-HPLC of purified **4.8** (20-80% ACN/H<sub>2</sub>O, 0.1% TFA, 10 minutes, RT = 8.64 min)



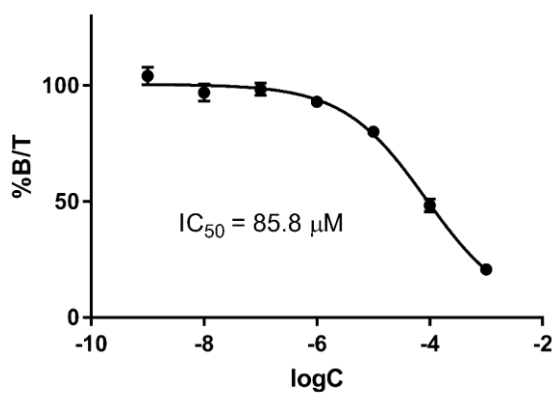


## 6.2 IC<sub>50</sub> Curves for Hit Peptides

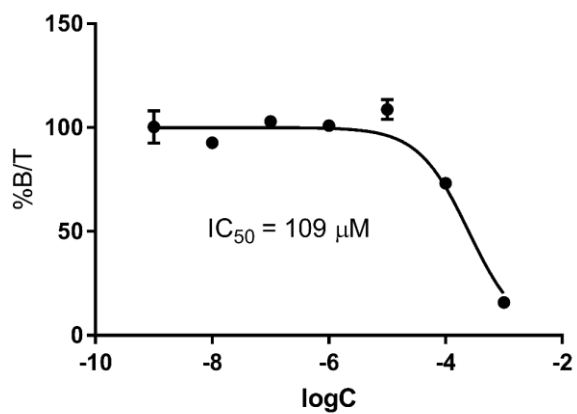
IC<sub>50</sub> curve for 4.1

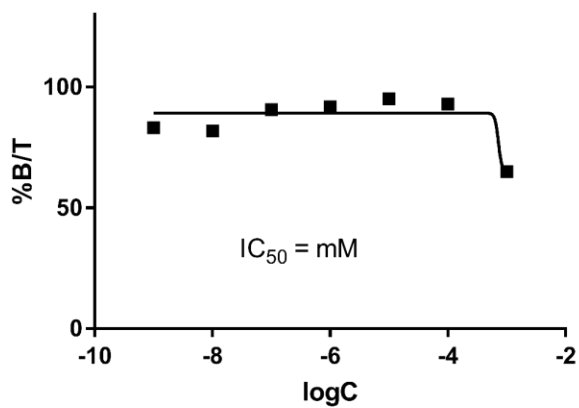
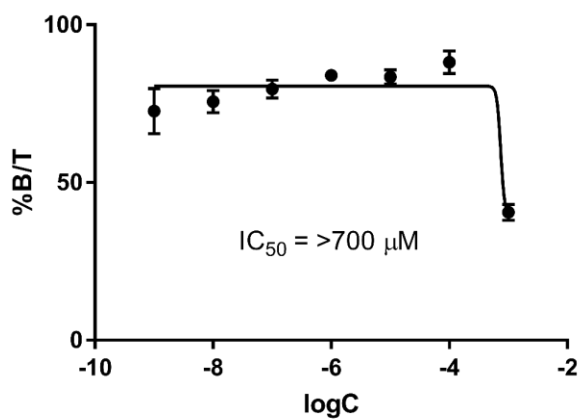
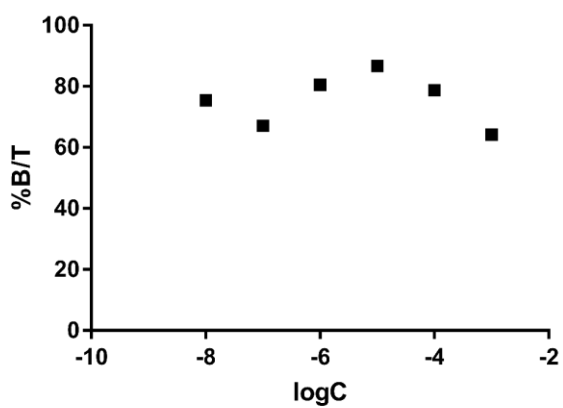


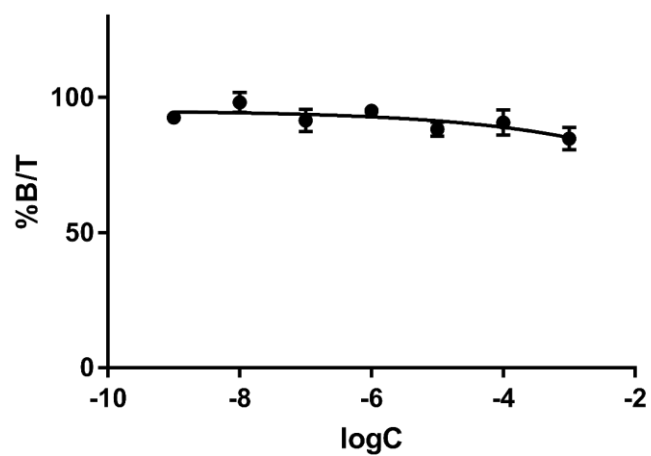
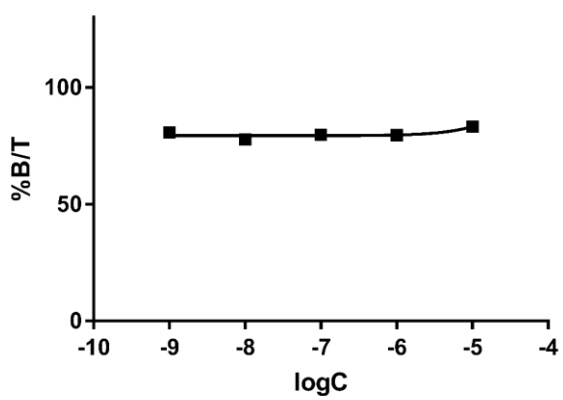
IC<sub>50</sub> curve for 4.2



IC<sub>50</sub> curve for 4.3

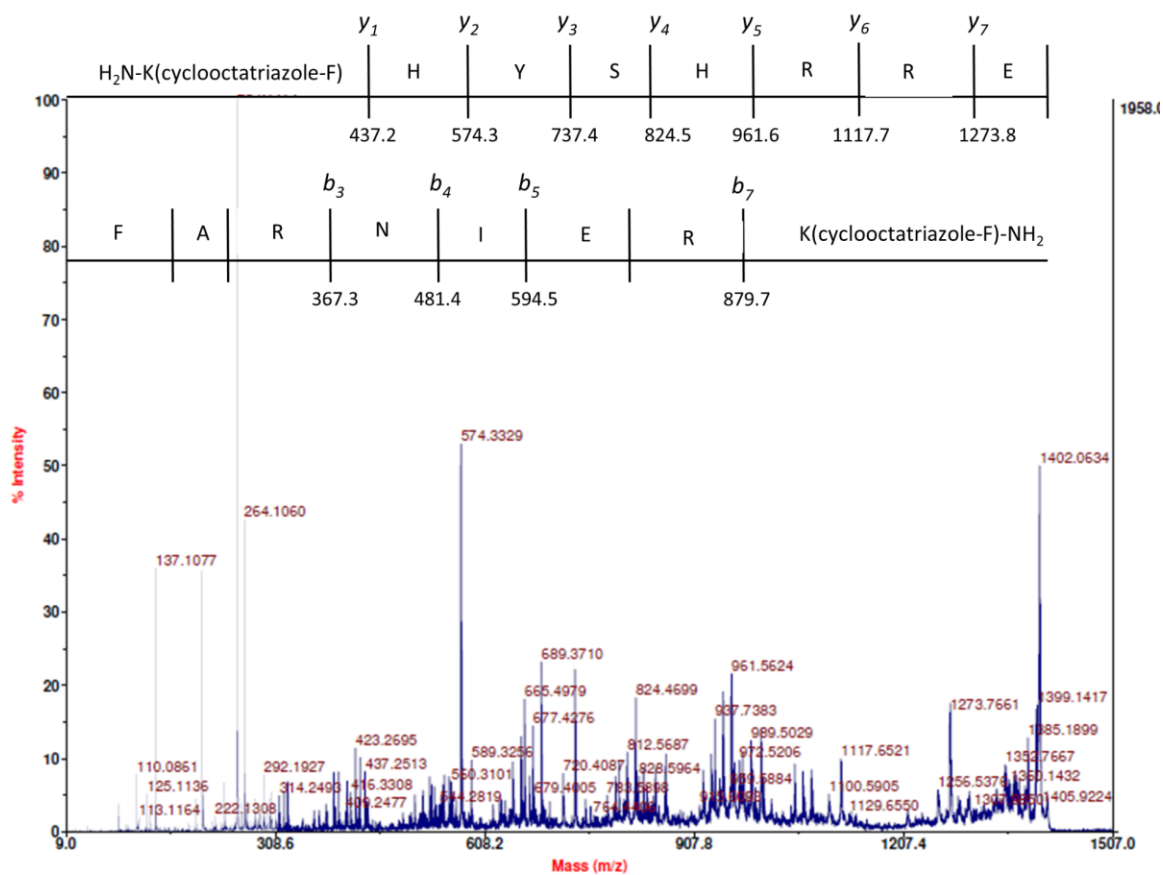


IC<sub>50</sub> curve for 4.4IC<sub>50</sub> curve for 4.5IC<sub>50</sub> curve for 4.6

IC<sub>50</sub> curve for 4.7IC<sub>50</sub> curve for 4.8

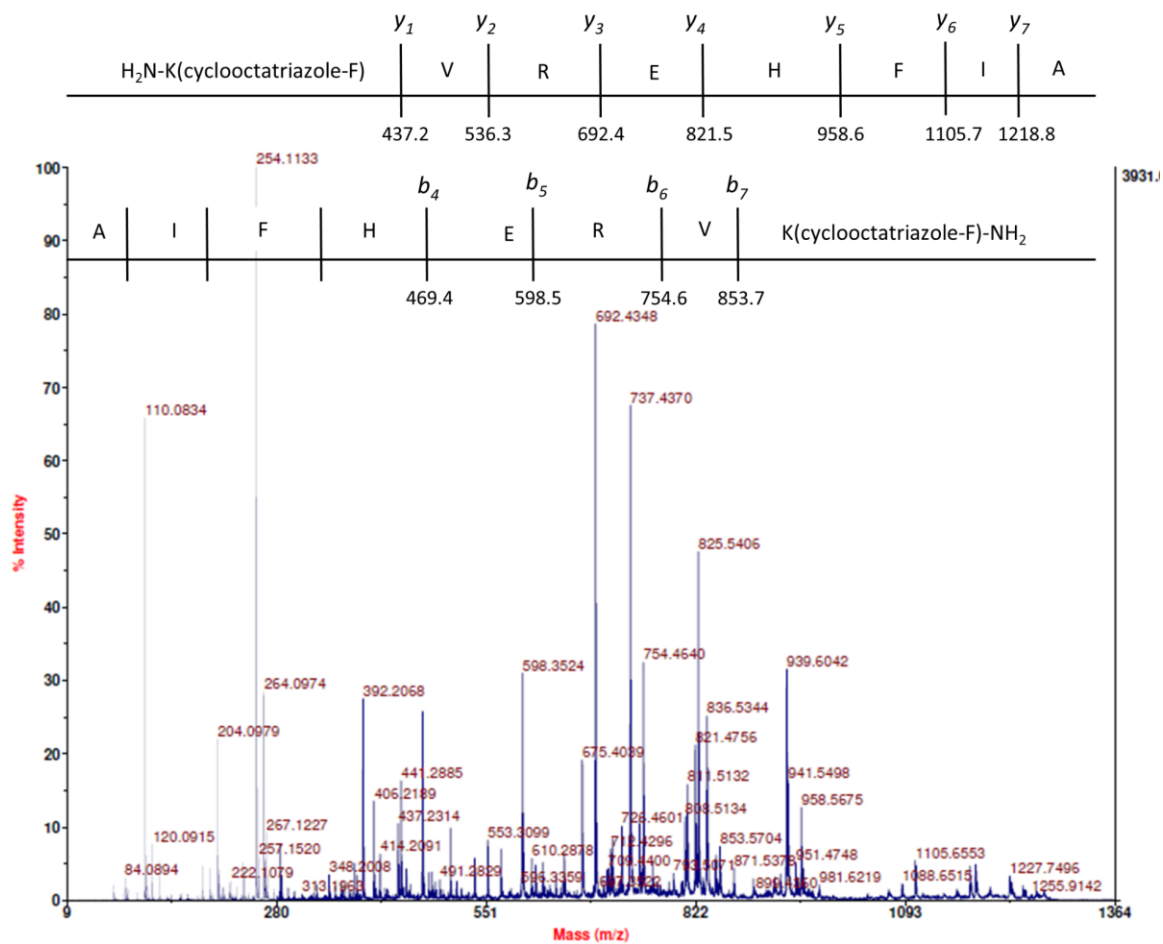
## 6.3 MALDI MS/MS Deconvolution for Hit Peptides

### MALDI MS/MS of **4.1**

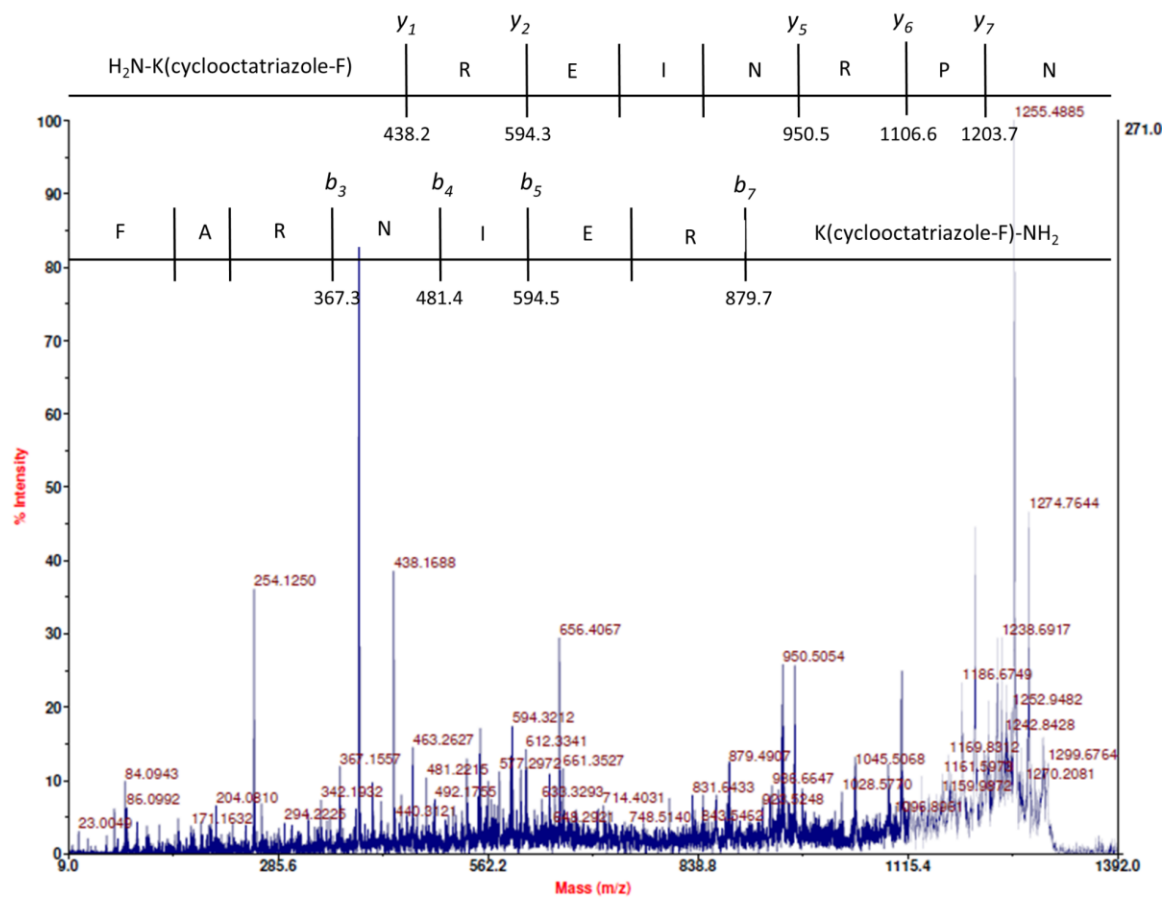


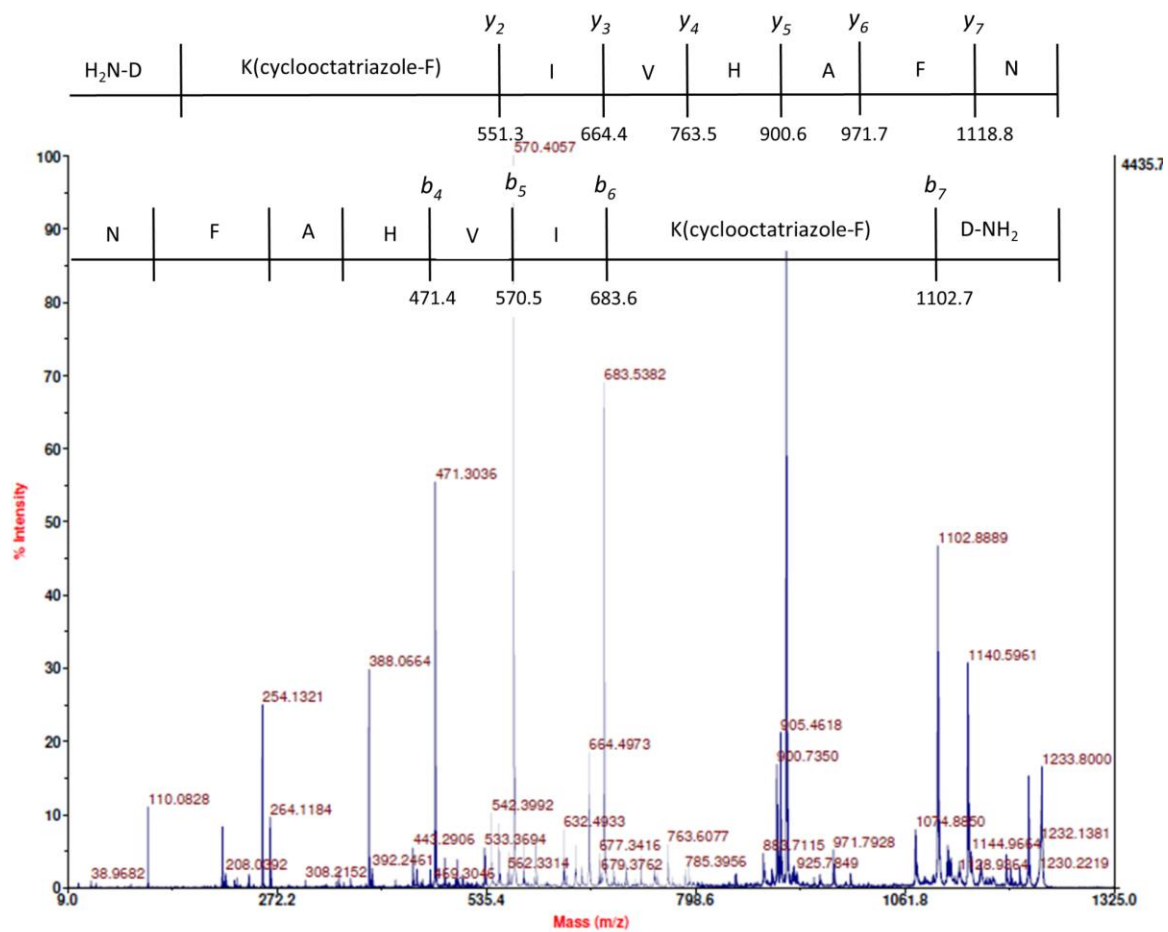


## MALDI MS/MS of 4.4



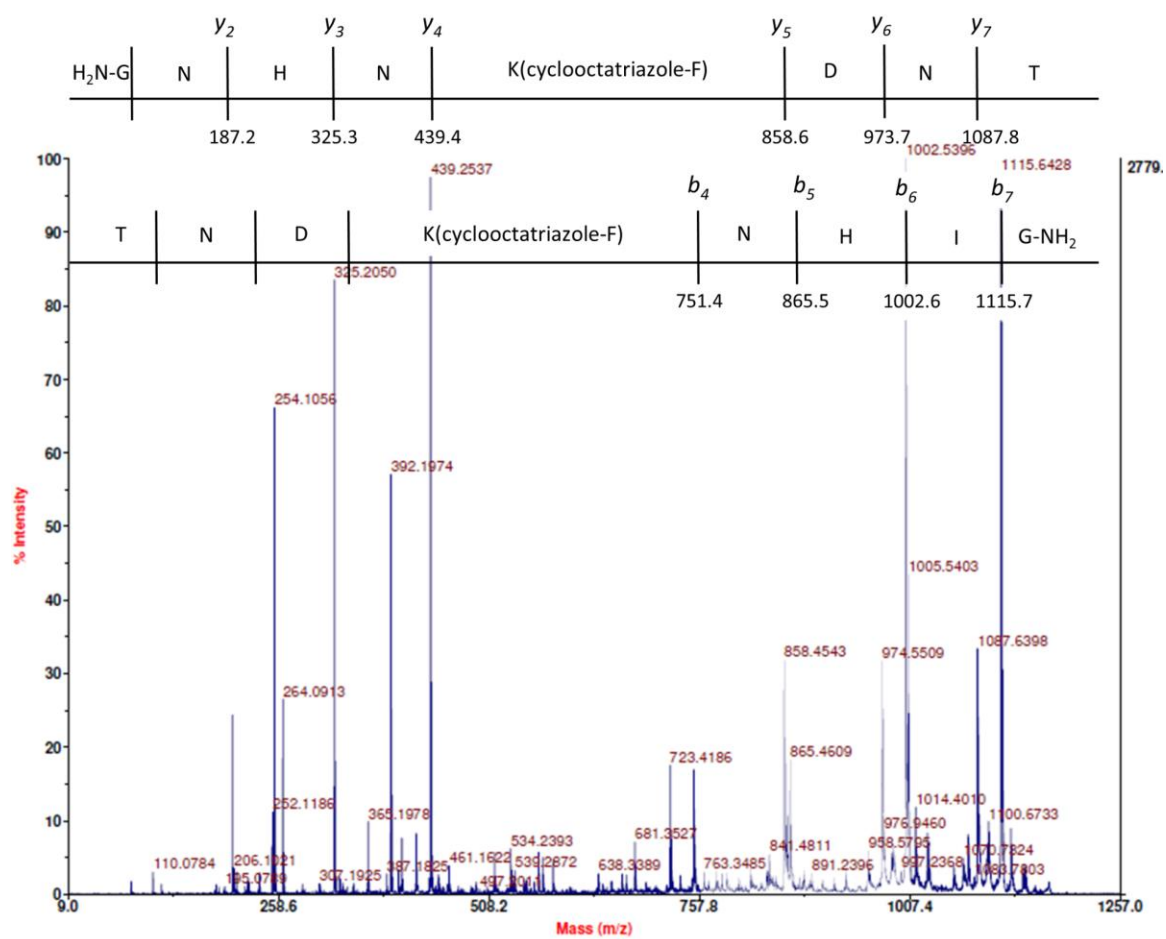
## MALDI MS/MS of 4.5

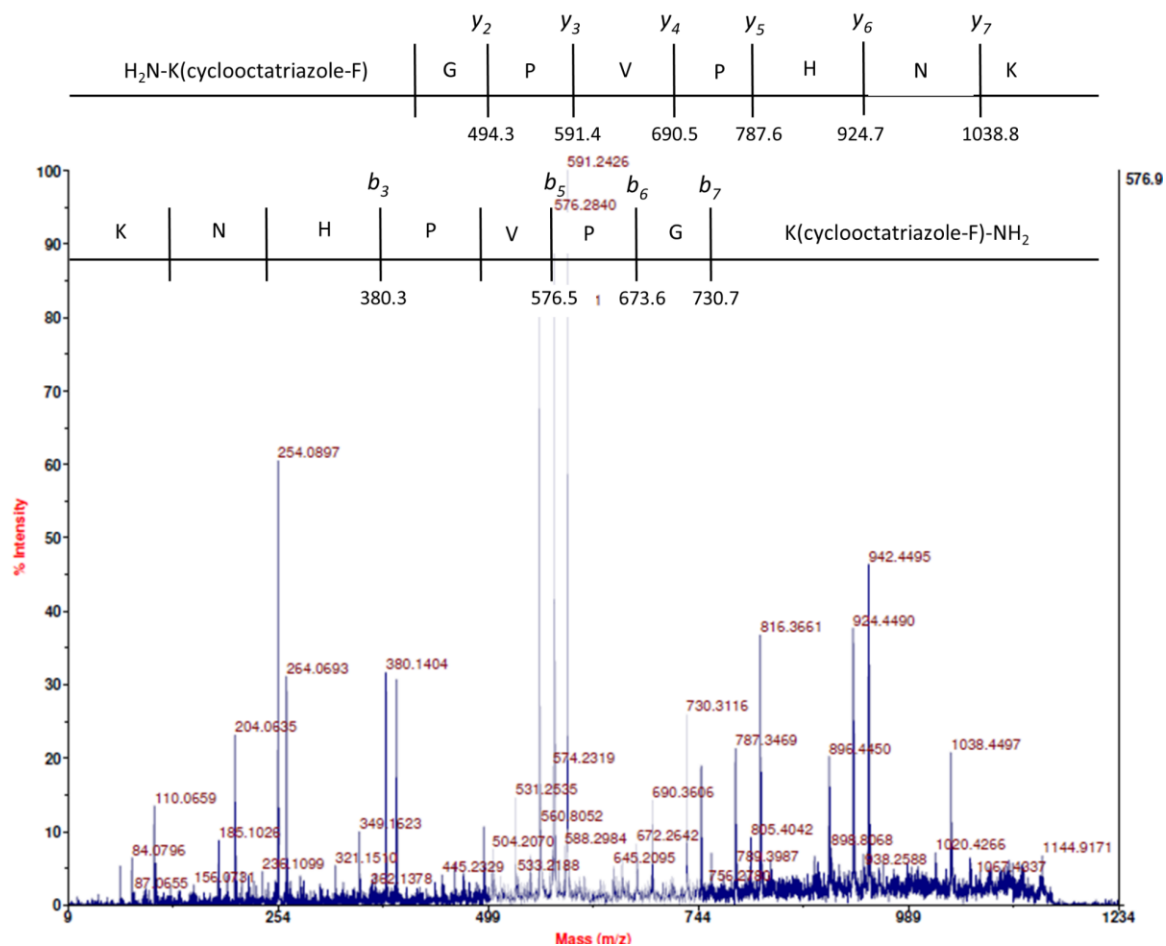


MALDI MS/MS of **4.6**



## MALDI MS/MS of 4.7



MALDI MS/MS of **4.8**

## Curriculum Vitae

### EDUCATION

- 09/14-08/19      **Doctor of Philosophy, Organic Chemistry and Molecular Imaging**  
University of Western Ontario, London, Ontario, Canada
- Supervisor: Dr. Leonard G. Luyt  
Thesis: *Incorporation of Fluorine into Peptides and Peptide OBOC Libraries through Copper-free Click Chemistry for the Development of Radiopharmaceuticals*
- 09/09-04/13      **Honours Bachelor of Science, Chemistry**  
***Certificate in Medicinal Chemistry***  
Dalhousie University, Halifax, Nova Scotia, Canada
- Supervisor: Dr. D. Jean Burnell  
Thesis: *Trapping of the Cationic Intermediate of the Nazarov Intermediate by Pyrrole and by Thiophenes*

### HONOURS and AWARDS

- 2019              J. Peter Guthrie Conference Travel Award
- 2019              Society of Radiopharmaceutical Sciences ISRS 2019 Travel Bursary Award
- 2019              Molecular Imaging Graduate Program Travel Bursary
- 2018              Society of Radiopharmaceutical Sciences TERACHEM 2018 Travel Bursary Award (Education & Research Foundation for Nuclear Medicine and Molecular Imaging)
- 2018              Molecular Imaging Graduate Program Travel Bursary
- 2017              Society of Radiopharmaceutical Sciences ISRS 2017 Bursary Award
- 2017              Molecular Imaging Graduate Program Travel Bursary
- 2016              Oncology Research and Education Day Poster Award
- 2013-2019      Western Graduate Research Scholarship

### PUBLICATIONS

- Turnbull, W. L.; Yu, L.; **Murrell, E.**; Milne, M.; Charron, C. L.; Luyt, L. G. A dual modality  $^{99m}\text{Tc}/\text{Re(I)}$ -labelled T140 analogue for imaging of CXCR4 expression. *Org. Biomol. Chem.*, **2019**, 17, 598-608.
- **Murrell, E.**; Kovacs, M. S.; and Luyt, L. G. A Compact and Synthetically Accessible Fluorine-18 Labelled Cyclooctyne Prosthetic Group for Labelling of

- Biomolecules by Copper-Free Click Chemistry. *ChemMedChem*. **2018**, 13, 1625-1628.
- Simpson, E. J.; Gobbo, P.; Bononi, F. C.; **Murrell, E.**; Workentin, M. S.; and Luyt, L. G. Bombesin-functionalized water-soluble gold nanoparticles for targeting prostate cancer. *Journal of Interdisciplinary Nanomedicine*. **2017**, 2, 174–187.
  - Turnbull, W. L.; **Murrell, E.**; Bulcan-Gnirss, M.; Luyt, L. G. A Study of  $^{99m}\text{Tc}/\text{Re}$ -Tricarbonyl Complexes of 4-Amino-1,8-Naphthalimides. *Dalton Transactions* [Under Revision]

## PUBLISHED ABSTRACTS

- **Murrell, E.**; Luyt, L. G.; A Combinatorial Library of Fluorine-Integrated Peptides for PET Imaging Agent Discovery. 23<sup>rd</sup> International Symposium on Radiopharmaceutical Sciences, **2019**, *J. Labelled CpmDs. Radiopharm.* 62, S219.
- Cho, C.-F.; Ghotmi, Y.; Fadzan, C.; Wolfe, J.; Bergmann, S.; Qu, Y.; **Murrell, E.**; Bononi, F.; Luyt, L.; Chiocca, E. A.; Viapiano, M.; Pentelute, B.; Lawler, S.; BTP-7, A novel peptide for therapeutic targeting of malignant brain tumors. *Neuro-Oncology*. **2018**, 20 (suppl\_6), vi74.
- **Murrell, E.**, Kovacs, M; Luyt, L. A novel fluorine-18 labelled azadibenzocyclooctyne prosthetic group for labelling of biomolecules by copper-free click chemistry. 22nd International Symposium on Radiopharmaceutical Sciences, **2017**, *J. Labelled CpmDs. Radiopharm.* 60, S590.
- Cho, C.-F.; Ghotmi, Y.; Fazden, C.; Wolfe, J.; Bononi, F.; **Murrell, E.**; Luyt, L.; Viapiano, M.; Pentelute, B.; Chiocca, E. A.; Lawler, S. Novel peptide homing to glioma-specific isoform of brevicane selectively targets malignant brain tumors. *Neuro-Oncology*. **2017**, 19(suppl\_6), vi62-vi63.

## OTHER CONFERENCE ABSTRACTS

- **Murrell, E.**; Luyt, L. G.; Discovery of new CXCR4-Targeted PET Imaging Agents from a Combinatorial Library of Fluorine-Integrated Peptides. 16<sup>th</sup> Oncology Research and Education Day, June 14, 2019, London, ON, Canada
- **Murrell, E.**; Luyt, L. G.; A Two-Pool Split-and-Mix Synthesis for Incorporating an Imaging Moiety into OBOC Libraries. 102<sup>nd</sup> Canadian Chemistry Conference, June 4 2019, Quebec City, Canada. [Oral Presentation]
- **Murrell, E.**; Turnbull, W. L; Bulcan-Gnirss, M.; Luyt, L. G.;  $^{99m}\text{Tc}/\text{Re}$ -Tricarbonyl Naphthalimide Complexes for Dual Modal Fluorescence/SPECT Imaging Agents. 102<sup>nd</sup> Canadian Chemistry Conference, June 7, 2019, Quebec City, Canada. [Oral Presentation]
- **Murrell, E.**; Turnbull, W. L; Bulcan-Gnirss, M.; Luyt, L. G.; Dual Modal Fluorescence/SPECT Imaging Probes: 4-Amino-1,8-naphthalimide  $^{99m}\text{Tc}/\text{Re}$ -Tricarbonyl Complexes. The Third International Symposium on Technetium and

Other Radiometals in Chemistry and Medicine, September 27, 2018, Bressanone, Italy. [Oral Presentation]

- **Murrell, E.;** Luyt, L. G. Synthesis and Screening of a Combinatorial Library of Fluorine-Integrated Peptides for the Discovery of CXCR4-Targeting PET Agents. 15<sup>th</sup> Oncology Research and Education Day, June 8, 2018, London, ON, Canada.
- **Murrell, E.;** Luyt, L. G. Synthesis and Screening of a Combinatorial Library of Fluorine-Integrated Peptides for the Discovery of Cancer-Targeting PET Agents. Molecular and Cellular Imaging Symposium, May 1, 2018, London, ON, Canada.
- **Murrell, E.;** Kovacs, M. S.; Luyt, L. G. A novel fluorine-18 labelled azadibenzocyclooctyne prosthetic group for click chemistry labelling of biomolecules to create cancer-targeted PET imaging agents. 14<sup>th</sup> Oncology Research and Education Day, June 16, 2017, London, ON, Canada.
- **Murrell, E.;** Luyt, L. G. Incorporation of Fluorine into an OBOC Peptide Library by Copper-Free Click Chemistry for the Discovery of PET Imaging Probes. 100<sup>th</sup> Canadian Chemistry Conference, May 30, 2017, Toronto, ON, Canada. [Oral Presentation]
- **Murrell, E.;** Luyt, L. G. A Fluorine-Containing OBOC Peptide Library for the Discovery of Cancer Imaging Probes. 15<sup>th</sup> Imaging Network Ontario Symposium. March 15, 2017, London, ON, Canada.
- **Murrell, E.;** Luyt, L. G. A Fluorine-Containing OBOC Peptide Library for the Discovery of Cancer Imaging Probes. Imaging Applications in Prostate Cancer Workshop. November 25, 2016, London, ON, Canada.
- **Murrell, E.;** Luyt, L. G. A Fluorine-Containing OBOC Peptide Library for the Discovery of Cancer Imaging Probes. 13<sup>th</sup> Oncology Research and Education Day. June 17, 2016, London, ON, Canada.

## TEACHING EXPERIENCE

- 2018-2019     Mentor, Undergraduate Thesis Research (Marcus Tonogai),  
University of Western Ontario  
*-Re<sup>99m</sup>Tc (I) Tricarbonyl Complexes of Cyclen and Cyclam Derivatives*
- 2017-2018     Mentor, Undergraduate Thesis Research (Mariel Bulcan-Gnirss),  
University of Western Ontario  
*- A Study of the Fluorescent Properties of Rhenium Naphthalimide Complexes*
- 2014-2019     Marking & Laboratory Teaching Assistantships, University of Western Ontario  
Medicinal Chemistry  
Organic Chemistry I: Structure and Spectroscopy  
Organic Chemistry of Biological Molecules  
Organic Chemistry for Life Sciences  
Organic and Biological Chemistry for Food Sciences  
Chemistry: Everywhere and Everything  
Western Integrated Science Program